"Swami Shreeji"

UNIVERSITA' DEGLI STUDI DI TORINO

Dipartimento di Scienze Mediche

DOTTORATO DI RICERCA IN FISIOPATOLOGIA MEDICA

CICLO XXXIII

TESI DI DOTTORATO

Stem cell-derived extracellular vesicles modulate fibrosis in a model of aristolochic acid induced nephropathy

Tutor:

Prof. Maria Felice Brizzi

PhD Candidate**:**

Dr Sharadkumar R Kholia

2017 - 2020

0. Contents

Acknowledgements **1**

Abstract **2**

Original Publications **4**

1. Introduction **5**

1.1 Chronic Kidney Disease 6

1.1.1 Aristolochic acid induced nephropathy 6

1.1.2 Kidney fibrosis 7

1.2 Extracellular vesicles 14

1.2.1 Stem cell derived EVs in regenerative medicine 15

1.3 AIM 18

2. Methodologies **19**

2.1 Eukaryotic Cell lines and Culturing 20

2.1.1 Mesenchymal Stem cells (MSC) 20

2.1.2 Human Liver Stem cells (HLSC) 20

2.1.3 Mouse tubular epithelial cells (mTECs) 21

2.1.4 Mouse kidney cortical fibroblasts (mkCF) 21

2.1.5 MRC5 fibroblasts 21

2.2 Isolation and characterization of EVs 22

2.3 Electron microscopy 24

2.4 Transfection of mkCF cells 24

2.5 AAN *in vitro* model 25

2.6 Fibroblast α-Amanitin assay 25

2.7 AAN *in vivo* model 25

2.8 Total body weight and Kidney function analysis 26

2.9 RNA extraction and qRT-PCR 26

2.10 Renal histological analysis 29

2.11 Preparation of mouse tissue lysates 30

2.12 Immunoblotting 30

2.13 Fireplex miRNA assay 31

2.14 Fibrosis Array and miRnome Array 32

2.15 Bioinformatic Analyses 33

2.16 Statistical Analyses 33

3. Mesenchymal stem cell-derived extracellular vesicles ameliorate kidney injury in aristolochic acid nephropathy 34

3.1 Results 35

3.1.1 Characterization of MSC-EVs 35

3.1.2 MSC-EVs ameliorate AA induced kidney damage 37

3.1.3 MSC-EVs revert AA induced upregulation of pro-fibrotic genes in AAN mice kidneys 41

3.1.4 MSC-EV treatment induced the downregulation of pro-fibrotic genes in fibroblasts *in vitro* 43

3.1.5 MSC-EVs reverse the expression of miRNAs dysregulated in AAN 44

3.2 Discussion 49

3.3 Conclusion 54

4. Human liver stem cell-derived extracellular vesicles prevent aristolochic acid induced kidney fibrosis 56

4.1 Results 57

4.1.1 Characterization of HLSC-EVs 57

4.1.2 HLSC-EVs prevent development of chronic kidney disease 57

4.1.3 HLSC-EVs downregulate pro-fibrotic genes in kidneys of AA treated mice 62

4.1.4 HLSC-EVs downregulate pro-fibrotic genes in fibroblasts *in vitro* 62

4.1.5 Mouse miRNome array 65

4.2 Discussion 71

4.3 Conclusion 76

5. HLSC-EVs alleviate kidney fibrosis by partially interfering with the β-catenin pathway 77

5.1 Results 78

5.1.1 The expression of active β-catenin is reduced in AA mice treated with HLSC-EVs 78

5.1.2 Expression of β-catenin in mouse renal fibroblasts in an AAN model *in vitro* 79

5.1.3 Silencing of β-catenin in mkCF fibrobalsts 80

5.1.4 Gene silencing of β-catenin prevents the molecular activation of fibroblasts in AAN in vitro assay 83

5.1.5 HLSC-EVs could potentially regulates β-catenin through mir29b 84

5.2 Discussion 87

5.3 Conclusion 90

6. References 91

Acknowledgements

First and foremost I would like to thank Bhagwan Swaminarayan and my beloved Gurus HDH Pramukh Swami Maharaj and HDH Mahant Swami Maharaj for their blessings and guidance towards completing this PhD.

I would also like to offer my sincerest gratitude to Prof. Maria Felice Brizzi, the director of my studies, together with Prof. Giovanni Camussi for giving me the opportunity to work under their supervision. Not only did they patiently provide the vision, encouragement and advice necessary for me to progress through the programme and complete my thesis, but also gave me strength and motivation during the uphill moments of this PhD. Their abilities to listen with patience, humility, and enthusiasm to name a few are qualities that are truly inspirational which make them ideal role models to have for a successful career in research. I truly would like to apologies for any inconvenience that I may have caused to them during the course of my PhD.

I would also like to thank Dr Maria Beatrice Sanchez Herrera for her expert guidance, advice and friendship that were essential towards the success of the research project. A most heartfelt thank you to Prof. Bussolati, and all the members of Lab 10/11 for their guidance, advice, motivation, and friendship without which, completing this PhD would have been impossible.

My heartfelt gratitude to: my parents, my sister, and the whole Kholia family for their love, support and blessings which became my inspiration and driving force. Thank you to Prof. Vincenzo Cantaluppi and Prof. Simona Fontana for reviewing my thesis. Last but not least, I would like to apologise to and thank all those who I may have missed out but have played an important role in the successful completion of my PhD. Finally, I would like to dedicate this work to my beloved Guru HDH Pramukh Swami Maharaj, my family and all my friends in ITALY.

"Education is the manifestation of perfection that is already present in man"

HDH Pramukh Swami Maharaj

Abstract

Inadequate therapeutic strategies for the prevention and progression of chronic kidney disease (CKD) remain a major drawback in patient's outcomes and a burden on global health care systems. Alternative therapies therefore need to be developed and implemented to alleviate this burden. Aristolochic acid (AA) nephropathy is a rapidly progressive form of nephrotoxic CKD characterised by inflammation, and tubular damage progressing to interstitial fibrosis. Stem cell derived extracellular vesicles (EVs) have been reported to exhibit therapeutic properties in various pre-clinical disease models including kidney injury. In this study, we aimed to investigate the therapeutic effects and mechanisms of action of mesenchymal stem cells derived EVs (MSC-EVs) and human liver stem cell derived EVs (HLSC-EVs) in a mouse model of aristolochic acid nephropathy (AAN). Immunodeficient NSG mice were injected with HLSC-EVs or MSC-EVs 3 days after the intraperitoneal administration of AA on a weekly basis for 4 weeks. A gradual loss of weight together with deterioration in kidney function was observed in mice injected with AA. Moreover, tubular damage, infiltration of inflammatory cells, and interstitial fibrosis was also observed in these mice. Treatment with HLSC-EVs or MSC-EVs significantly ameliorated functional parameters such as blood urea nitrogen and plasma creatinine. In addition, a significant reduction in tubular necrosis, interstitial fibrosis, and infiltration of inflammatory cells was also observed following EV treatment. At a molecular level, both HLSC-EV and MSC-EV treatment significantly reduced the expression of pro-fibrotic genes *in vivo* and in activated fibroblasts *in vitro.* Bioinformatic analysis of kidney tissue revealed an upregulation of profibrotic genes and miRNAs which were downregulated following HLSC-EV and MSC-EV treatment. Although both MSC-EVs and HLSC-EVs downregulated genes and miRNAs that regulate common pathways activated in kidney injury the profile of the genes and miRNAs between the two were different. This therefore confirmed that both MSC-EVs and HLSC-EVs exhibit similar therapeutic properties but the mechanism of action at a molecular level is different. The expression of β-catenin was

found to be elevated in AA kidneys as well as in activated fibroblasts in vitro. Furthermore, upregulation of β-catenin was significantly reduced following treatment with HLSC-EVs both *in vitro* and *in vivo* at a molecular and protein level. Silencing of β-catenin gene in fibroblasts prevented the upregulation of the pro-fibrotic genes α-SMA and Collagen type 1 after activation with TGF-β1 or AA injured mTECs, therefore confirming the role of Wnt/β-catenin pathway in fibroblast activation. In addition, AA mice kidneys and fibroblasts treated with HLSC-EVs showed elevated levels of miR29b. Treatment of fibroblasts with HLSC-EVs in the presence of α-amanitin, or antimir29b inhibited the upregulation of the miRNA in recipient cells. Furthermore, expression of the β-catenin gene, α-SMA gene, and Collagen type 1 gene was found to be upregulated in these fibroblasts. Taken together this data suggests a novel regulatory HLSC-EV mechanism of action whereby β-catenin is downregulated by miR29b induced directly by HLSC-EVs in fibroblasts in vitro.

Original Publications

i. **Kholia, S.**, Herrera Sanchez, M. B., Cedrino, M., Papadimitriou, E., Tapparo, M., Deregibus, M. C., Bruno, S., Antico, F., Brizzi, M. F., Quesenberry, P. J., & Camussi, G. (2020). Mesenchymal Stem Cell Derived Extracellular Vesicles Ameliorate Kidney Injury in Aristolochic Acid Nephropathy. *Frontiers in cell and developmental biology*, *8*, 188.

ii. **Kholia, S**., Herrera Sanchez, M. B., Cedrino, M., Papadimitriou, E., Tapparo, M., Deregibus, M. C., Brizzi, M. F., Tetta, C., & Camussi, G. (2018). Human Liver Stem Cell-Derived Extracellular Vesicles Prevent Aristolochic Acid-Induced Kidney Fibrosis. *Frontiers in immunology*, *9*, 1639.

1. Introduction

1.1 **Chronic Kidney Disease**

Chronic kidney disease (CKD) is a pathology that affects billions of individuals globally [1]. Currently, treatment for end stage CKD is limited to haemodialysis and kidney transplantation, both of which are restricted to financial restraint and/or availability of donor kidneys [2]. These limitations have been a major drawback in improving patient recovery and therefore become imperative that a solution be found to improve the overall health and well-being of patients with CKD [3].

Damage to the kidney can occur in a variety of ways. For instance nephrotoxins such as cis-platin, Adriamycin, and aristolochic acid can induce damage to the kidneys eventually leading to CKD [4]. Damage to the kidneys can also occur through sepsis or an autoimmune response leading to acute kidney injury which eventually progresses to CKD. Ischemia, and multi organ failure as well as obstruction of the ureter has also been linked to kidney damage leading to CKD [5]. An imbalance between the injury and the compensatory response regardless of source, leads to a maladaptive tissue repair which in turn contributes progression towards CKD and eventually fibrosis [4].

1.1.1 Aristolochic acid induced nephropathy

Aristolochic acids (AA) are a group of toxins that are enriched in plants of the genus *Aristolochia* and *Asarum,* commonly found worldwide [6]. These plants have been regularly used as part of traditional herbal therapy for the treatment of various ailments including weight management [7]. In the early 1990s, various women who were on a similar weight loss regimen, consisting of Chinese herbs, presented with a rapidly progressive form of chronic kidney disease known at that time as Chinese herbal nephropathy (CHN) [7]. Another form of nephropathy, more prominent in the Balkan region of Eastern Europe, hence recognized as Balkan endemic nephropathy (BEN), also exhibited similarities to CHN [8]. Further investigations led to the discovery of AA in the Chinese herbs as the prime cause of CHN.

Meanwhile, the contamination of the weed species *Aristolochia clematitis* (rich in AA) in wheat consumed in the Balkan regions was identified to be the root cause of BEN [7]. As a result, both CHN and BEN are now collectively classified as aristolochic acid nephropathy (AAN) [7].

AAN is a rapidly progressing form of CKD predominantly characterised by tubular damage and atrophy accompanied with interstitial nephritis and extensive fibrosis. In addition, 40% of cases also manifest with urothelial carcinoma due to the DNA adducting properties of AA. Although extensive research has been done over the years to elucidate the underlying mechanisms of AAN, no effective therapeutic regimen is available as of yet [6].

1.1.2 Kidney fibrosis

During tissue injury, various cells of mesenchymal origin are activated as a result of an inflammatory response to initiate tissue healing and regeneration. When there is repeated tissue injury with recurring inflammatory response the healing process is dysregulated leading to the excessive production and accumulation of matrix connective tissue (**Figure 1.1**) [9]. This eventually leads to the replacement of functional tissue with scar tissue ultimately leading to organ dysfunction which is often associated with high morbidity and mortality [9].

In the kidney, fibrosis is considered to be a reliable predictor of prognosis and renal insufficiency. Based on the kidney's histological structure, fibrosis can be divided into three parts. Fibrosis in the glomeruli is known as glomerulosclerosis, in the tubule-interstitium it is known as tubulointerstitial fibrosis and in the kidney vasculature it is known as arteriosclerosis and perivascular fibrosis [10].

Kidney fibrosis can be considered as a very dynamic and converging process that consists of four overlapping phases [11]. During the first phase known as priming, tissue injury instigates an inflammatory response from injured cells whereby cytokines are released that creates a chemotactic

gradient towards the site of injury. This leads to the infiltration of local and systemic inflammatory cells such as lymphocytes, monocytes, macrophages, dendritic cells and mast cells [11]. Although an inflammatory response is vital in response to an injury, non-resolving inflammation is considered to be a major driving force towards the development of fibrosis [12]. The activated inflammatory cells release a plethora of molecules such as cytokines, chemokines, growth factors, reactive oxygen species that lead to further damage [9]. This creates a vicious cycle of tissue damage and inflammation that eventually leads to the build-up of fibrogenic cytokines and growth factors released by both the injured tissue and infiltrating cells of the immune system [11]. The accumulation of profibrotic cytokine pressure primes fibroblasts, epithelial and endothelial cells to undergo phenotypic activation or transition that triggers the process of fibrogenesis [11].

The next two phases of activation and execution follow each other as the upsurge of profibrotic cytokine pressure in the tissue microenvironment causes the activation of matrix producing cells [11]. Even though various different cell types in the kidney interstitium are capable of producing extracellular matrix (ECM) such as tubular epithelial cells following EMT, vascular smooth muscle cells, and resident subset of macrophages, fibroblasts remain the principle generators of ECM proteins such as collagen type 1, type 2 and fibronectin [9]. Fibroblasts in their active form are known as myofibroblasts and often express elevated amounts of α-smooth muscle actin (α-SMA) and release collagen type 1 [12]. Therefore both of these proteins are considered to be markers of fibroblast activation. Historically, myofibroblasts were assumed to have been originated from resident fibroblasts in the kidney interstitium. However, recent research has identified at least five different sources of myofibroblasts usually found in the fibrotic kidney [11]. These include activation of resident interstitial fibroblasts, infiltration of circulating fibrocytes, phenotypic conversion of tubular endothelial and epithelial cells, and differentiation of Pericytes. Regardless of the origin, myofibroblasts remain the main source and depositors of ECM proteins in fibrosis [11].

The execution phase involves myofibroblasts to contribute towards the production of ECM proteins involving a mixture of collagen type 1, 2 and fibronectin [11]. However, the presence of fibrogenic cytokines and molecules such as TGFβ-1, β-catenin, Platelet derived growth factor (PDGF), basic fibroblast growth factor 2 (FGF2), and connective tissue growth factor (CTGF) have been reported to influence the activation of collagen and fibronectin genes through signalling pathways activating their transcription [9]. In addition, there is constant modification of the ECM proteins through biochemical modifications and cross linking that influences the progression of fibrosis from reversible to irreversible [11]. For instance, the enzyme tissue transglutaminase and lysyl oxidase modify the extracellular matrix proteins making them more stiff and resistant to proteolysis [11].

Kidney fibrosis is usually defined as excessive production of ECM which is a very simplistic definition of the process [13]. In reality, various events both at a cellular and molecular level that occur either during or after the process of ECM production influence the progression of fibrosis towards end stage renal disease. In fact, the level of these events such as tubular atrophy, microvascular rarefaction, and tissue hypoxia govern the reversibility and overall outcome of the disease [11].

1.1.2.1 Signalling pathways in fibrosis

Myofibroblasts are considered to be the key cells in the pathophysiology of fibrosis with a variety of stimuli that could trigger their activation [14]. In order to develop anti-fibrotic therapies it is important to understand the signalling pathways involved in the activation of myofibroblasts and the general process of fibrosis. Several signalling pathways have been linked to play a role in the development and progression of kidney fibrosis [15].

The most commonly known and widely studied pathway in fibrosis is the TGF-β canonical pathway [15]. In homeostatic conditions, TGF-β is located in the extracellular matrix in an inactive form associated with latency

associated peptide (LAP) and latent TGF-β binding protein (LTBP) known as large latent complex (LLC). In the presence of stimuli, TGF-β is cleaved from the LLC allowing it to bind to two type I and two type II receptors. This initiates signal propagation leading to phosphorylation of regulatory Smad proteins (Smad2/3) downstream [16] (**Figure 1.1D**). Upon phosphorylation, Smad2/3 together with the co-activator Smad4 migrates to the nucleus where they localize to specific Smad-binding elements (SBE) to regulate activation of target genes such as PAI1, COL1A1, CCN2 among others) [16] (**Figure 1.1D**).

In the setting of CKD, injured cells of the kidney parenchyma together with the influx of inflammatory cells increases the level of TGF-β therefore dysregulating the pathway causing it to activate target genes mainly involved in myofibroblast activation, production of extracellular matrix, as well as endothelial to mesenchymal transition (EMT) [16]. Despite an increased level of experimental work in the literature, the underlying mechanism of fibroblast activation is incompletely understood. Simply because both activation as well as inhibition of Smad proteins have been shown to activate fibrosis, and a total inhibition of the TGF-β signalling cascade does not completely abrogate the fibrotic response, therefore suggesting the involvement of other signalling mechanisms in the activation of fibroblasts and fibrosis [15].

The Wnt/β-catenin signalling cascade is an evolutionary conserved, highly complex pathway that has also been implicated to play a role in kidney injury and repair [17]. The dual role of promoting repair/regeneration or aiding the progression of AKI to CKD depends on the magnitude and duration of its activation [18]. The Wnt family includes a group of lipid modified glycoproteins that are secreted upon activation. At least 19 members of the Wnt family have been identified in mammals considered to be important in the development of the kidney [18]. Once secreted, Wnt proteins interact with the Frizzled (Fzd) family of receptors and co-receptors known as low-density lipoprotein receptor-related protein-5 or 6 (LRP-5/6) in target cells triggering the activation of Disheveled (Dsh/Dvl). At this point, the signalling branches

into the canonic β-catenin-dependent pathway and the non canonic β-catenin independent pathway [17].

In the canonical pathway, phosphorylation of LRP leads to the activation of Dsh/Dvl which in turn inhibits the ubiquitination activity of the β-catenin destruction complex composed of Dvl, axin, adenomatous polyposis coli (APC), glycogen synthase kinase 3 (GSK3), and casein kinase 1 (CK1) ultimately leading to the dephosphorylation of β-catenin [18] (**Figure 1.1D**). This active non-phosphorylated form of β-catenin than translocates to the nucleus where it binds to T-cell factor/lymphoid enhancer-binding-factor-1 (TCF/Lef-1) transcription factors to promote the transcription of target genes [18] (**Figure 1.1D**).

Over the years many studies have reported the involvement of the canonical WNT/ β-catenin pathway in fibrogenesis of various tissues including the kidneys [17, 18]. For instance, experimental models that overexpressed WNT ligands exogenously or sustained the accumulation of β-catenin in the nucleus suggest that the canonical pathway is enough to trigger the fibrogenic programme in fibroblast [19]. Moreover, prolonged activation of Wnt/β-catenin in vivo via expression of Wnt1 post AKI accelerates progression of the disease to CKD whereas inhibition of the signalling pathway prevented AKI-CKD progression [18]. Several preclinical models have also reported the involvement of Wnt/β-catenin pathway in the development of the CKD. For instance, in a model of unilateral ureteral obstruction (UUO) which is characteristic of progressive interstitial fibrosis, He et al observed an upregulation of Wnt family ligands, Fzd receptor and accumulation of active β-catenin as in the cytoplasm and nuclei of renal tubular epithelial cells which correlated with the upregulation of numerous β-catenin target genes [20]. Moreover, delivery of Wnt antagonist DKK-1 gene reduced the levels of active β-catenin significantly, ameliorating the upregulated target genes such as collagen type 1 and fibronectin [20]. There is therefore sufficient evidence to support the involvement of the β-catenin

pathway in the progression of kidney fibrosis. However, the involvement of this pathway in the progression of AAN remains to be elucidated.

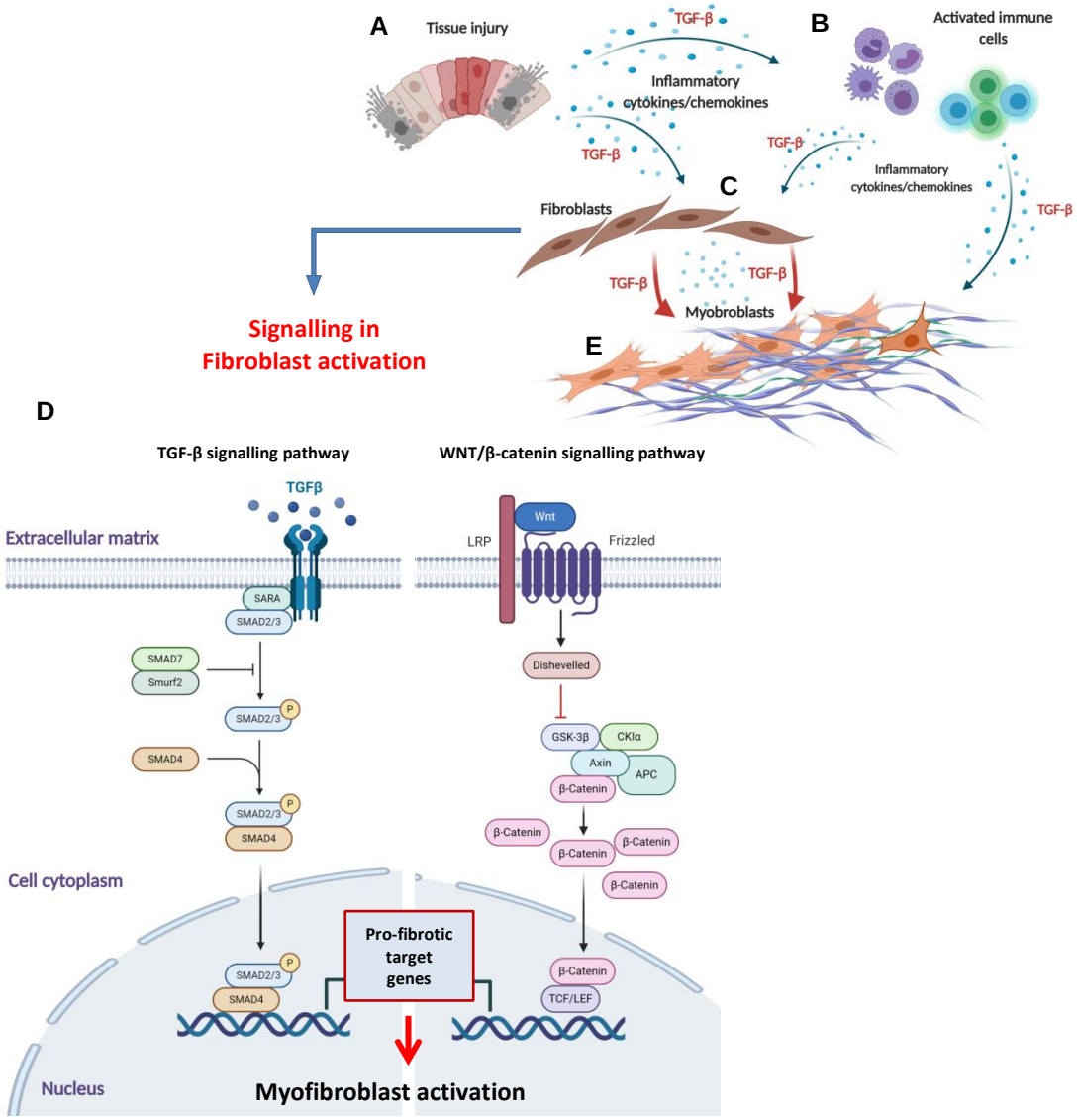

Figure 1.1. Signalling pathways involved in fibrosis. Damaged tissues release inflammatory cytokines and chemokines systemically and locally (**A**), which inturn lead to the activation and migration of the immune cells to the area of damage (**B**). The activated immune cells together with cells from damaged tissue release more cytokines and chemokines including TGF-β which activates infiltrating/resident fibroblasts (**C**). Pro-fibrotic signalling pathways including TGF-β and Wnt/β-catenin pathways are activated in these fibroblasts due to the presence of their respective ligands (**D**). Phosphorylation of SMAD2/3 proteins by TGF-β, and accumulation of active β-catenin due to Wnt activation leads to their nuclear translocation where they activate transcription of pro-fibrotic genes which leads to myofibroblast activation and excessive production of extracellular matrix (**E**).

1.2 **Extracellular vesicles**

Over the past decade, a new paracrine mechanism of cell to cell communication has to come to light. Once considered to be cell debris, extracellular vesicles (EVs) have become the centre stage of research in various fields of biology. These heterogeneous vesicles are composed of a lipid bilayer that encapsulates the biologically active cargo within mainly composed of nucleic acids, and complex proteins. The lipid bilayer protects the cargo from degradation when delivered to recipient cells locally or systemically through the blood or lymphatic system [21]. EVs can be classified into two major types known as microvesicles or exosomes. Due to their overlapping phenotype and size distribution they are collectively known as extracellular vesicles [22]. Microvesicles are released by the outward budding of the cell membrane through a process of shedding and are between 100 to 200 nm in size. They differ from apoptotic bodies and pre-apoptotic microvesicles which are also shed from the plasma membrane but are much larger in size and limited to cells exposed to injury [23].

Exosomes on the other hand are a more homogenous group of vesicles much smaller in size ranging from 30-150 nm. They are generated through the endosomal membrane invagination of endosomes eventually know as multi-vesicular bodies (MVBs) within the cell [24]. Although various mechanisms of exosome biogenesis have been suggested, the endosomal sorting complex required for transport (ESCRT) pathway together with ceramide and tetraspanins remains to be the most well characterised mechanism of formation and release [21]. MVBs are eventually trafficked towards the internal part of the plasma membrane. The high cholesterol content of MVBs together with Rab proteins such as Rab7 and SNARE complex (soluble N- ethylmaleimide- sensitive fusion attachment protein receptor) facilitates the fusion of MVBs with the plasma membrane leading to the releasing of exosomes in the extracellular environment [21].

As both microvesicles and exosomes have the potential of influencing target cells physiologically and or pathologically, a lot of research has been generated on EVs as a whole, apart from some groups that focus more on either microvesicles or exosomes.

As EVs are released by almost all the cells in the body, their influence has been attributed to play both a physiological and or pathological role depending on the source. Based on this principle, EVs from different stem cell types have been investigated in various models tissue pathologies [21].

1.2.1 Stem cell derived EVs in regenerative medicine

Stem cells are undifferentiated cells that have the capability to self-renew, form identical clones and differentiate into different cell lineages. They are usually classified on the basis of their ability to differentiate. Embryonic stem cells have the ability to differentiate in to the three primordial germ layers and therefore are totipotent [25]. Adult stem cells on the other hand are classified as multipotent or unipotent and are located in various tissues of children, adolescents and adults. Although both types of stem cells have therapeutic and regenerative capacities, the ethical issues surrounding the use of embryonic stem cells make adult stem cells a preferable option for use in regenerative medicine [21]. Although many studies have reported adult stem cells from various organs to be effective as alternative therapeutic options, their ability to form malignancies due to their undifferentiated nature has hampered their progression into clinical applications [26].

Stem cell derived EVs have generated huge interest over the years due to the similar stem cell like properties they exhibit without the danger of forming malignancies. Various studies have reported the regenerative properties of stem cell derived EVs in particular those derived from mesenchymal stromal cells (MSCs) in various models of human pathology including kidney disease [27]. For instance, Bruno et al reported that MSC-EVs improved the recovery of damaged tubular cells by promoting proliferation and inhibiting apoptosis in a glycerol induced mouse model of acute kidney injury (AKI) [28].

Interestingly a similar effect was observed when injecting MSC cells in the same model of AKI therefore confirming EVs to exhibit similar effects to the cells of origin [28]. In another study by Alzahrani et al, EVs derived from MSCs were able to alleviate the disease in a rat model of renal ischemia reperfusion injury [29]. In addition, exosomes that were isolated from MSCs preconditioned to melatonin were even more effective indicating a way of enhancing the therapeutic effect of EVs even further [29]. MSC-EVs have also been reported to be effective in toxin related AKI. In a lethal model of cis-platin induced AKI in mice, a single dose of MSC-EVs improved survival, kidney function and morphology but did not prevent tubular injury and amelioration of BUN and creatinine [30]. On the other hand, a multi-dose regimen of MSC-EVs further improved survival of mice and after 21 days renal histology and function was at near normal levels [30]. This therefore indicates that the efficacy and effectiveness of MSC-EVs increases in a dose dependent manner. Apart from AKI, MSC-EVs have been shown to be effective in models of CKD as well. For instance, Grange et al reported that in a murine model of diabetic nephropathy, an improvement in renal function and a reversal of fibrosis was observed following treatment with MSC-EVs [31]. In other models of CKD involving 5/6 nephrectomy [32] and unilateral ureter obstruction [33], administration of MSC-EVs was effective in reducing glomerulosclerosis and fibrosis.

The human liver stem cells (HLSC) are another type of stem cell population found to be resident in the liver. Discovered in our lab in 2004, HLSCs also exhibit mesenchymal and embryonic markers, and have the potential to differentiate into several subtypes of cells [34]. Over the years, we have shown these cells to display remarkable therapeutic properties from contributing towards regeneration of liver parenchyma in a mouse model of acetaminophen-induced liver injury [34, 35], to the improvement of renal morphology and function in a model of AKI [36]. HLSC-EVs like their cellular counterpart have also shown to exhibit regenerative properties. For instance, in a glycerol induced mouse model of AKI, HLSC-EVs were able to ameliorate kidney function by improving blood urea and creatinine levels, as

well as reducing hyaline cast formation, and tubular necrosis. An enhancement in tubular cell proliferation was also observed [36]. In a diabetic nephropathy model of CKD, a similar effect was observed upon treatment with HLSC-EVs whereby there was an improvement in functional parameters such as blood urea and creatinine, reduction in kidney fibrosis, and improvement in overall renal morphology [31].

1.3 **AIM**

Chronic kidney disease has become a major health care problem due to a high risk of accelerated cardiovascular disease and death. Those who survive to progress to end stage renal disease are restricted to dialysis and renal transplantation the availability of which is limited to specific parts of the world. In addition, AAN a rapidly progressive form of CKD has become a common occurrence in south Asia, and the Balkan region of Europe. With no effective therapeutic regimen available as of yet, It is imperative that an alternative be found to alleviate this problem to improve general health and wellbeing of patients with CKD

Stem cell based therapies have been suggested and have shown to be effective in pre-clinical models of kidney disease, however ethical concerns in combination with side-effects associated with cell transplantation have prevented their progression to human clinical application. Stem cell derived EVs have recently come to light and have been proven to exhibit similar therapeutic properties to their cell counterparts. Although extensive research has been reported on MSC-EVs in CKD, very few studies have been done on HLSC-EVs and CKD and no studies have been performed to understand the effects of stem cell derived EVs in AAN.

The aim of this work was therefore to investigate the effects of MSC and HLSC derived EVs in an in vivo CKD model of AAN and identify/elucidate the biologically active molecules and molecular mechanisms by which stem cell derived EVs exert their anti-fibrotic and regenerative effects.

Data on MSC-EVs and HLSC-EVs together with the mechanism of action of HLSC-EVs are reported and discussed separately.

2. Methodologies

2.1 Eukaryotic Cell lines and Culturing

2.1.1 Mesenchymal Stem cells (MSC)

Human bone marrow MSCs purchased from Lonza (Basel, Switzerland) were cultured in mesenchymal stem cell basal medium (MSCBM, Lonza) supplemented with the accompanied bullet kit as per manufacturer's instructions. Cells were sub-cultured after 15 days following thawing from passage one and then after every seven days for successive passages. Characterisation was performed by flowcytometry for the expression of typical mesenchymal markers (CD44, CD105, CD73, and CD90) as described previously [28]. EVs were isolated from cells until passage six.

2.1.2 Human Liver Stem cells (HLSC)

HLSCs were isolated from human cryopreserved normal adult hepatocytes (Lonza, Basel, Switzerland) as described before [36]. Briefly, hepatocytes were cultured in Hepatozyme-SFM medium (Lonza, Basel, Switzerland) for 2 weeks to allow majority of the hepatocytes to die. The surviving population of cells were cultured in α-MEM/EBM-1 (3:1) (Lonza, Basel, Switzerland) supplemented with L-glutamine (5 mM), HEPES (12 mM, pH 7.4), penicillin (50 IU/ml), streptomycin (50 µg/ml) (all from Sigma, St. Louis, MO, USA) and 10% foetal calf serum (FCS) (Invitrogen, Carlsbad, CA, USA). Cells were expanded, characterised and cryo-preserved as described previously [36].

HLSCs were positive for mesenchymal stem cell markers, but not hematopoietic and endothelial markers as described before [36]. In addition, they were positive for human albumin, alpha-fetoprotein, resident stem cell markers such as vimentin and nestin, and negative for CD34, CD117 and cytokeratin 19 oval cell markers as reported previously [36]. Embryonic stem cell markers such as nanog, oct4, sox2 and SSEA4 were also positively expressed in HLSCs. Stemness of HLSCs was confirmed by endothelial, osteogenic, and hepatic differentiation under appropriate culture conditions as described earlier [36].

2.1.3 Mouse tubular epithelial cells (mTECs)

mTECs isolated from kidneys of healthy female C57 mice (as described previously in our lab [28]) were cultured in Dulbecco's modified essential medium (DMEM) supplemented with L-glutamine (5 mM), penicillin (50 IU/ml), streptomycin (50 µg/ml) and 10% FCS. Cells were sub-cultured every other day with splitting to a ratio of 1:3 at a cell confluence of 90%.

2.1.4 Mouse kidney cortical fibroblasts (mkCF)

mkCFs were isolated from the kidneys of healthy male CD1 mice using a modified protocol described by Grimwood and Masterson (18). Briefly, cortical sections of kidneys from CD1 mice were minced and plated on gelatin coated petridishes and incubated at 37°C for 72 hrs in DMEM high glucose supplemented with L-glutamine (5 mM), penicillin (50 IU/ml), streptomycin (50 µg/ml), 10 ml HEPES and 20% FCS. The medium was replaced after 72 hrs and cultures allowed to grow for 10-14 days until a 75% confluent monolayer of fibroblast like cells was formed. Cells were further expanded and characterized for fibroblast lineage. Media was changed twice weekly to maintain cultures.

Fibroblasts were characterised through a series of inclusion/exclusion criteria according to their distinctive biochemical and morphological characteristics as reported previously [37]. Cells were positive for established mesenchymal markers such as: vimentin and α-SMA, as well as fibroblast specific protein 1 (FSP1) a marker of fibroblasts [38]. In addition, expression of the endothelial/epithelial cell marker pan-cytokeratin was found to be negative, together with minimal expression of desmin (smooth muscle cell marker) therefore confirming no contamination from these cells [37].

2.1.5 MRC5 fibroblasts

The human foetal lung fibroblast like cell line MRC5 PD 19 (purchased from Sigma, St. Louis, MO, USA) was adopted for the isolation of EVs as a negative control for in vivo studies. Briefly, cells were cultured in DMEM low

glucose supplemented with L-glutamine (5 mM), HEPES (12 mM, pH 7.4), penicillin (50 IU/ml), streptomycin (50 µg/ml) and 10% FCS. At a confluency of 90%, cells were starved overnight in serum free RPMI. The supernatant was collected and subjected to EV isolation as mentioned below.

2.2 **Isolation and characterization of EVs**

EVs were obtained from supernatants of HLSCs ($2x10^6$ cells/T75 flask), MSCs ($1x10^6$ cells/T150 flask), or MRC5 human fibroblasts cultured in serum free, phenol free Roswell Park Memorial Institute Medium (RPMI) (Euroclone S.p.A, Italy) for 18 hrs. Viability of cells at the time of supernatant collection was 98% as confirmed by Trypan blue exclusion. Briefly, supernatants were centrifuged at 3000 *g* for 15 min at 4°C, followed microfiltration using a 0.22 µm vacuum filter unit (Millipore, USA), for the removal of cell debris and apoptotic bodies. This was followed by ultracentrifugation at 100,000 *g* for 2 hrs at 4°C (Beckman Coulter Optima L-90 K, Fullerton, CA, USA). The pellet of EVs obtained was resuspended in RPMI supplemented with 1% dimethyl sulfoxide (DMSO) and stored at -80°C until use. Further purification of EVs was performed by iodixanol (Optiprep, Sigma, St. Louis, MO, USA) floating density separation protocol modified from the one described by Kowal *et al.* [39] to accommodate for larger centrifugation volumes. Briefly, EVs acquired through ultracentrifugation were resuspended in 500µl of 60% iodixanol supplemented with 0.25M sucrose. One ml of 30%, 15%, and 5% iodixanol working solution was layered sequentially above the EV/60% iodixanol suspension and the final volume adjusted to 10 ml with saline solution. The tubes were ultracentrifuged at 350,000 *g* for 1 hr at 4°C without brake in an Optima L-100K ultracentrifuge (Beckman Coulter) equipped with Type 90Ti rotor. The 15%, 30%, and 60% fractions were recovered, diluted in PBS and re-ultracentrifuged at 100,000 *g* for 1 hr at 4°C. The pellet obtained was resuspended in PBS/1% DMSO for subsequent studies. EVs were mainly detected in the 15% fraction as determined by the Nanosight LM10 system (NanoSight, Wiltshire, UK). EVs isolated from the 15% fraction were used for experiments.

For HLSC-EV internalization experiments, EVs were labelled with 1μM Dil dye (Thermo Fisher Scientific, Waltham, MA, USA) as described before [40]. Briefly, purified EVs were resuspended in PBS together with 1μM Dil dye and ultracentrifuged for 1 hr at 4°C. The pellet of EVs obtained was washed once by ultracentrifugation and resuspended in PBS/1%DMSO for use in experiments.

Characterisation of EVs was performed by cytofluorimetric analyses. HLSC-EVs were positive for the typical mesenchymal surface markers characteristic of HLSCs such as CD29, CD44, CD73, and CD90 as well as the exosomal markers CD81 and CD107 as described before [36]. A further characterisation was performed by electron microscopy showing the presence of vesicles ranging between 40-100nm. Western blot analyses of EV protein also confirmed the presence of classical exosomal markers such as CD63, CD81, and TSG101 as described previously [36].

For MSC-EVs, the expression of surface markers was evaluated using the human cytofluorimetric bead-based MACSPlex exosome kit (Miltenyi Biotec, Germany) according to manufacturer's protocol. Briefly, three independent MSC-EV preparations consisting of approximately $1x10^9$ MSC-EVs/ preparation were diluted in MACSPlex buffer (MPB) to a final volume of 120 μl in a 1.5 ml microcentrifuge tube. This was followed by the addition of 15 μl of MACSPlex exosome capture beads (containing a cocktail of 39 different exosomal marker epitopes). The EVs on capture beads were counterstained by adding 5 μl of APC-conjugated: anti-CD9, anti-CD63, and anti-CD81 detection antibodies to each of the tubes and incubating for 1 hr at room temperature in the dark on an orbital shaker at 450 rpm. Post incubation, the beads were washed once with 1 ml of MPB at 3,000 *g* for 5 min, followed by a longer washing step by incubating the beads in 1 ml of MPB on an orbital shaker (as before) for 15 min. After this step, the beads were centrifuged at 3,000 *g* for 5 min and the supernatant was carefully aspirated leaving a

residual volume of 150 µl per tube for acquisition. Flow cytometric analysis was performed using the Cytoflex flow cytometer (Beckman Coulter, Brea CA, USA) whereby approximately 5000-8000 single bead events were recorded per sample. The median fluorescence intensity (MFI) for all 39 exosomal markers were corrected for background and gated based on their respective fluorescence intensity as per manufacturer's instructions.

Quantification and size distribution of purified EVs was determined by Nanosight (NanoSight, Wiltshire, UK) equipped with a 405 nm laser. Briefly, EV preparations were diluted (1:200) in sterile saline solution and analyzed by the Nanoparticle Analyses System using the NTA 1.4 Analytical Software as described previously [36].

2.3 **Electron microscopy**

Transmission electron microscopy was performed by loading HLSC-EVs onto 200 mesh nickel formvar carbon coated grids (Electron Microscopy Science) for 20 min. This was followed by fixation in a 2.5% glutaraldehyde/2% sucrose solution. Following repeated washings in distilled water, samples were negatively stained with NanoVan (Nanoprobes, Yaphank) and examined by a Jeol JEM 1010 electron microscope (Joel, USA).

2.4 **Transfection of mkCF cells**

mkCF cells were transfected with validated mouse β-catenin (CTNNB1) siRNA or negative control siRNA 1 (Ambion, Inc., Austin, TX) at a final concentration of 20 nM in the presence of HiPerfect transfection reagent (Qiagen), as per the manufacturer's instructions. After transfection, the cells were harvested at 72 h for RNA analysis and after 7 days for protein and RNA analysis. All experiments were performed in triplicate.

2.5 **AAN *in vitro* model**

In order to study the effects of stem cell derived-EVs on cortical renal fibroblasts, an *in vitro* model of AA-induced fibrosis was set-up. Briefly, $1.5x10^4$ mTECs pre-seeded in a 24 well cell culture inserts (1.0µm pore) (Thermo Fisher Scientific) were exposed to 100µM of AA for 4 hrs. Post incubation, cells were washed and co-cultured with mkCF cells ($2x10^4$ cells pre-seeded 24 hrs prior to the co-culture) for 5 days at 37°C. For selected experiments, fibroblasts co-cultured with AA exposed mTECs were treated with HLSC-EVs (50,000 EVs/cell) or MSC-EVs (75,000 EVs/cell). For some experiments, fibroblasts co-cultured with AA exposed mTECs were treated with HLSC-EVs together with 200 nM of antimiR-29b or antimiR-SCR in the presence of HiPerfect transfection reagent for the duration of the assay. After 5 days of incubation, mkCFs were analyzed for fibrotic gene expression by qRT-PCR. Fibroblasts co-cultured with healthy mTECs served as controls.

In order to study the mechanism of action and pathways activated, in vitro assays treated with HLSC-EVs were subjected to both RNA and protein isolation using the Norgen all in one isolation kit (Norgen Biotek, Canada) as per manufacturer's protocol.

2.6 **Fibroblast α-Amanitin assay**

In order to elucidate whether HLSC-EVs transferred or induced the transcription of miR29b in mkCF following treatment, cells were treated with the transcription inhibitor α-Amanitin. Briefly, $2x10^4$ mkCF cells/well pre-seeded in a 24 well plate were treated with 10 ng/ml of TGFβ-1 in the presence or absence of HLSC-EVs (50,000 EVs/cell) in the presence or absence of 50 µg/ml of α-amanitin for 6 h at 37°C. Post incubation, RNA was extracted from the cells and analysed for miR29b expression.

2.7 **AAN *in vivo* model**

Animal studies were conducted in accordance with the National Institute of Health Guidelines for the Care and Use of Laboratory Animals. All

procedures were approved by the Ethics Committee of the University of Turin and the Italian Health Ministry (authorization number: 766/2016-PR). AAN was induced by injecting male NOD/SCID/IL2Rγ KO (NSG) mice (bred at the animal facility in the Molecular Biotechnology Centre) (6/8 weeks old; n=12) with 4mg/kg of AA (Santa Cruz Biotechnology, Santa Cruz CA, USA) on a weekly basis for 4 weeks intraperitoneally. HLSC-EVs (n=9) or MSC-EVs (n=9) or fibroblast derived EVs (Fibro-EVs; as negative control; n=5) at a concentration of $1x10^{10}$ EVs/ml/mouse or vehicle alone (n=5; as control) were injected 3 days after AA administration intravenously on a weekly basis. After 4 weeks of treatments, mice were sacrificed and subjected to multi-parameter analyses as mentioned below. Five animals injected with PBS instead of AA served as controls. NSG immunodeficient mice were adopted for this study to prevent an immunogenic reaction during repeated administration of EVs.

2.8 **Total body weight and Kidney function analysis**

Body weight of mice was recorded to assess the general health of mice on a weekly basis prior to AA injections and at the end of the experiment just before sacrificing. Kidney function of mice from all experimental groups was evaluated by measuring blood plasma creatinine after sacrifice using a colorimetric microplate assay based on the Jaffe reaction (Quantichrom Creatinine Assay, BioAssay systems, Hayward, CA, USA) as per manufacturer's protocol. Blood urea nitrogen (BUN) was measured by direct quantification of plasma urea with a colorimetric assay kit according to the manufacturer's protocol (Quantichrom Urea Assay, BioAssay Systems, Hayward, CA, USA).

2.9 **RNA extraction and qRT-PCR**

Total RNA was isolated from cells using TRIzol™ (Ambion, Thermofisher) followed by RNA extraction using the miRNeasy mini kit (Qiagen, Venlo, The Netherlands) according to the manufacturer's protocol. Briefly, mouse renal tissue was resuspended in 1 ml of TRIzol™ solution (Ambion, Thermofisher)

in microcentrifuge tubes and homogenised in a Bullet blender (Next Advance Inc, NY, USA) at a speed of 8 rpm for 3 min using 3.2 mm size zirconium beads. The tubes were then placed on a tube rotator at 4°C for 30 min, followed by centrifugation at 12,000 *g* for 15 min at 4°C. Supernatant was transferred to clean tubes and subjected to RNA isolation using the miRNeasy mini kit (Qiagen, Frederick, MD, USA), according to the manufacturer protocol. For the isolation of RNA from cells, 700 µl of TRIzol™ solution was added to the cells in the wells and incubated for 10 min on a shaker. The mixture was then transferred to 1.5 ml RNAse free tubes and subjected to RNA isolation using the miRNeasy mini kit (Qiagen, Frederick, MD, USA), according to the manufacturer protocol. Total RNA was quantified using the NanoDrop2000 spectrophotometer (Thermo Fisher, Waltham, MA, USA) and either used immediately or stored at -80°C until further use.

Total RNA from HLSC-EVs was extracted using the All-in-one purification kit (Norgen, Biotek Corp) as per manufacturer's protocol. Isolated RNA was quantified using the NanoDrop2000 spectrophotometer (Thermo Fisher Scientific) and either used immediately or stored at -80°C until further use.

cDNA was synthesised by retro-transcribing 200 ng of total RNA using the High Capacity cDNA reverse transcription kit (Thermo Fisher, Waltham, MA, USA), according to the manufacturer's protocol. qRT PCR was performed using the StepOnePlus RT-PCR machine (Thermo Fisher, Waltham, MA, USA) in 20 µl reactions with Power SYBR Green PCR Master Mix (Thermo Fisher, Waltham, MA, USA) and specific oligonucleotide primers (**Table 1**) (MWG-Biotech, Eurofins Scientific, Brussels, Belgium). Data were analysed using ΔΔCt method with *Gapdh* as endogenous control.

Validation of the expression of specific miRNAs obtained from the Fireplex assay by ABCAM, was performed as follows. Total RNA was isolated from 10 (8 µm) formalin fixed parafilm embedded (FFPE) sections (n=3/condition) using the RecoverALL™ Total Nucleic acid isolation kit for FFPE (Thermo Fisher, Waltham, MA, USA) according to the manufacturer's protocol. The total RNA from each mouse (200 ng of input RNA) was reverse transcribed,

using the miScript Reverse Transcription Kit (Thermo Fisher, Waltham, MA, USA) and the cDNA was subjected to RT-PCR, to validate the miRNAs of interest. Experiments were performed in triplicate using 3 ng of cDNA for each reaction as described by the manufacturer's protocol (Qiagen). The following miRNAs were screened in all mice conditions: miR-132-5p, miR-342-3p, and miR-214-3p with RNU6b as endogenous control.

For some experiments RNA from in vivo mouse tissue and in vitro fibroblasts from AAN in vitro assay were subjected to miRNA analysis whereby cDNA was reverse transcribed from RNA using the miSCript Reverse Transcription kit as mentioned above. The cDNA was subjected to RT-PCR analysis to assess the expression of miR-29b-3p with RNU6b as endogenous control.

Gene	Primer Sequence 5'-3'
m_*Col1a1* Forward	ATC TCC TGG TGC TGA TGG AC
m_*Col1a1* Reverse	ACC TTG TTT GCC AGG TTC AC
m_*Tgfb1* Forward	CGA AAG CCC TGT ATT CCG TCT
m_*Tgfb1* Reverse	GCA ACA ATT CCTGGC GTT ACC
m_*α-Sma* Forward	CTG ACA GAG GCA CCA CTG AA
m_*α-Sma* Reverse	CAT CTC CAG AGT CCA GCA CA
m_*Ltbp1* Forward	GGA GCC CGA AGT GGT AAC AG
m_*Ltbp1* Reverse	GAA TAG TTG AAA CCC CTG GGG
m_*Gapdh* Forward	TGT CAA GCT CAT TTC CTG GTA TGA
m_*Gapdh* Reverse	TCT TAC TCC TTG GAG GCC ATG T
hsa-miR-132-5p	TAA CAG TCT ACA GCC ATG GTC G
hsa-miR-342-3p	TCT CAC ACA GAA ATC GCA
hsa-miR-214-3p	ACA GCA GGC ACA GAC AGG
hsa-miR-29b-3p	TAG CAC CAT TTG AAA TCA GTG TT
hsa-RNU6b	CGC AAG GAT GAC ACG CAA

Table 1. List of Primers used for qRT-PCR

2.10 **Renal histological analysis**

Paraffin embedded renal tissues were cut in 5 μm-thick sections and stained with haematoxylin and eosin (for tubular damage and hyaline cast formation), or Masson's Trichrome (for interstitial fibrosis) (Bio-Optica, Milan, Italy), according to the manufacturer's protocols. Assessment of tubular necrosis was performed by analysing 10 non-overlapping cortical fields/section at a magnification of 400x (high power field, HPF) using ImageJ software. Quantification of interstitial fibrosis was performed by measuring collagenous fibrotic areas stained in blue (sections stained with Masson's Trichrome) in 10 random cortical fields/section from images taken at a magnification of 200x, using multiphase image analysis with ImageJ software version 1.49s [41].

Immunohistochemical staining was performed as follows. Briefly, 5 μm sections were deparaffinised, hydrated, and subjected to antigen-retrieval. Endogenous peroxidase was removed using 5% H_2O_2. Sections were blocked with 3% BSA/PBS and then incubated with antibodies of interest: proliferating cell nuclear antigen (PCNA) (1:400, Santa Cruz Biotechnology), α-smooth muscle actin (α-SMA) (1:100, Ab7817, Abcam), S100A4 (Fibroblast specific protein 1 (FSP-1)) (1:500, Ab41532, Abcam), or CD45 (1:500, Ab10558, Abcam), overnight at 4℃. The following day, after two washes with PBS-tween 0.01%, the sections were incubated with secondary horse radish peroxidase antibody (1:1000, Pierce, Rockford, IL, USA) for 1 hr at room temperature. Sections were then developed with diaminobenzidine (DAB) (Dako, Carpinteria, CA, USA), counterstained with haematoxylin, and analysed via microscopy.

For sections that required immunofluorescence staining, the slides were blocked with 3% BSA/PBS for 30 min following antigen retrieval, permeabilised in 0.2%Triton-X100/PBS for 6 min at 4℃ and then incubated with the primary antibodies of interest: anti-CD45 (1:100, Biorbyt, San Francisco CA, USA), anti-S100A4 (FSP-1) (1:100, Ab41532, Abcam, Cambridge, MA, USA), anti-collagen 1 (1:100, Ab21286, Abcam), anti-α-

SMA (1:100, Ab7817, Abcam), platelet derived growth factor receptor beta (PDGFRβ, 1:50, Ab32570, Abcam), and anti-non phospho active β-catenin (1:100, 8814s, Cell signalling technologies) overnight at 4℃. The respective alexa fluor fluorescence secondary antibodies (1:1000) were incubated with sections for 1 hr at room temperature. Following three washes, the sections were stained with DAPI and mounted with Fluorescent mounting media and analysed via microscopy. Sections labelled only with secondary antibody served as controls.

In order to evaluate changes in cell death, kidney tissue sections were stained for DNA fragmentation using terminal deoxynucleotidyl transferase dUTP nick end labelling (TUNEL) according to the manufacturer's protocol (Roche, United Kingdom). Cell death was quantified by averaging the number of TUNEL-positive nuclei in 8 random cortical fields/section, from images taken at a high magnification (400x), using ImageJ software as mentioned above.

2.11 **Preparation of mouse tissue lysates**

Mouse renal tissue was resuspended in 1 ml of RIPA lysis buffer containing phosphatase inhibitor cocktail 2 (1:100, P5726, Sigma), phosphatase inhibitor cocktail 3 (1:100, P0044, Sigma), Phenylmethanesulfonyl fluoride (PMSF, 1:100, 93482, Sigma), and protease inhibitor (1:100, P8340, Sigma) in microcentrifuge tubes and homogenised in a Bullet blender (Next Advance Inc, NY, USA) at a speed of 8 rpm for 3 min using 3.2 mm size zirconium beads. The tubes were then placed on a tube rotator at 4°C for 30 min, followed by centrifugation at 12,000 *g* for 15 min at 4°C. The total protein concentration was determined using the Bradford method and then subjected to SDS-PAGE analysis.

2.12 **Immunoblotting**

To separate proteins which were denatured by SDS according to their molecular masses, SDS polyacrylamide gel electrophoresis (SDS-PAGE) of

30 µg total protein was performed on 4-20% gradient mini PROTEAN TGX stain-free precast gels (4568094, BIO-RAD). Proteins were transferred onto Nitrocellulose membranes (IB23001, Invitrogen) using the iBlot 2 gel transfer device (IB21001, Invitrogen). Non-specific binding sites were blocked with 5% bovine serum albumin (BSA) in tris-buffered saline supplemented with 0.1% Tween-20 (TBS-T) for 1 hr at room temperature on a shaker. The blots were than incubated with the primary antibodies of interest overnight at 4ºC on a shaker. The primary antibodies used include: anti-β-catenin (1:1000, Ab16051, Abcam), anti-non phospho active β-catenin (1:500, 8814s, Cell signalling technologies), and anti-GAPDH (1:3000, Ab37168, Abcam) that served as loading control. Appropriate HRP-conjugated secondary antibodies (1:3000, Sigma) were applied for 1 hr at room temperature on a shaker. Protein detection was done using ECL substrate (170-5061, BIO-RAD) and chemiluminescence detected using the ChemiDoc Touch imaging system (BIO-RAD). Relative densitometry analysis was performed using the image lab ver 6.0.1 (BIO-RAD).

2.13 **Fireplex miRNA assay**

The FirePlex® multiplex miRNA allows a high-throughput analysis of up to 65 literature validated peer-reviewed miRNA targets, involved in kidney injury, by flow cytometry and efficient analysis with the FirePlex Analysis Workbench Software. In order to evaluate the regulation of miRNAs specifically involved in kidney injury, formalin fixed paraffin embedded tissue slices (in duplicate) from mice treated with AA (n=3), AA mice treated with MSC-EVs (n=5), and healthy mice (n=3) were provided to Abcam to perform the assay specific to kidney injury (kidney toxicity panel, ab219508, Abcam) as a service. The samples were processed as per the published protocol. Briefly, FFPE samples were mixed with 36 µL Digest Buffer, 20 µL water and 4 µL Protease Mix and incubated at 60°C for 45 min with shaking. For each sample run, FirePlex Particles (35 µL) were added to a well of a 96-well filter plate and filtered. Twenty-five µL Hybe Buffer was added to each well followed by 1 ng of total RNA. The plate was incubated at 37°C for 1 hr with

shaking. After two washes with 1× Rinse A, 75 µL of 1× Labelling Buffer was added per well. The plate was further incubated at room temperature for 1 hr with shaking. After two washes with 1× Rinse B and one wash with 1× Rinse A, a catch plate was added to the vacuum manifold and the filter plate put under constant vacuum. 65 µL of 95°C RNAse-free water was added twice to each well to elute the ligated sample. 30 µL of this melt off was added to a clean PCR plate and mixed with 20 µL PCR master mix. The mixture underwent 32 cycles of PCR amplification. 60 µL of Hybe Buffer was then added back to each well of the original particles followed by 20 µL of the PCR product, and the plate was incubated at 37°C for 30 min with shaking. After two washes with 1× Rinse B and one with 1× Rinse A, 75 µL of 1× Reporting Buffer was added per well and the plate was incubated at room temperature for 15 minutes on a shaker. Post incubation, the plate was washed twice with 1× Rinse A, and then 175 µL of Run Buffer was added to each well. The samples were then scanned on an EMD Millipore Guava 6HT flow cytometer (MilliporeSigma, Germany) and the Flow cytometry quantification data was analysed with the FirePlex™ Analysis Workbench software (Abcam, Cambridge, MA) whereby, the Fluorescence intensity values across all samples were normalized using the geNorm algorithm.

2.14 **Fibrosis Array and miRnome Array**

In order to elucidate the regulation of pro-fibrotic genes in mice treated with AA in the presence or absence of HLSC-EVs, total RNA extracted from kidneys of experimental mice were analysed using the Fibrosis RT^2 Profiler PCR array (PAMM-120Z, Qiagen) as per manufacturer protocol. Analyses were performed using the online software provided by the manufacturer with global normalization. A total of three mice per experimental group were subjected to array analyses. Furthermore, total RNA from the same mice was subjected to miRNA analyses using the QuantiMir^{TM} mouse miRNome microRNA profiler array (RA670A-1, Systems Biosciences, Palo Alto, CA, USA) according to manufacturer protocol. In addition, total RNA from fibroblasts from the *in vitro* experiments were subjected to miRNA analyses

using the QuantiMir^{TM} mouse miRNome microRNA profiler array. Only selected miRNAs upregulated or downregulated by HLSC EVs following AA treatment in mice (*in vivo*) were assessed.

2.15 **Bioinformatic Analyses**

Data from the Fireplex miRNA assay were further analysed using FirePlex® Analysis Workbench Software version 2.0 (Abcam) Fireplex Analysis Workbench software (Abcam). Gene target prediction from both the FirePlex assay and the miRnome array was performed with miRWalk 3.0 considering only miRNAs targeting the 3'UTR sequence and a score above 0.95 [42]. Panther Classification System online software was used for pathway enrichment analysis [43]. Only pathways with a minimum number of five genes were considered in the classification and biological processes of selected genes showing a p value <0.05 were considered as significantly enriched.

2.16 **Statistical Analyses**

Data analyses were performed using GraphPad Prism 6.0. Results are expressed as mean ± standard deviation (SD) or standard error of the mean (SEM) where indicated. Statistical analyses were performed by employing: student's *t* test, one way analyses of variance (ANOVA) or two-way ANOVA with a multi comparison test where appropriate. A p value of <0.05 was considered statistically significant.

3. Mesenchymal stem cell-derived extracellular vesicles ameliorate kidney injury in aristolochic acid nephropathy

3.1 **Results**

3.1.1 Characterization of MSC-EVs

EVs were evaluated for typical expression markers using the MACS multiplex bead-based flow cytometry assay described recently [44, 45]. The assay involves incubating EVs with a cocktail of 39 different bead populations, each representing a typical exosomal surface antigen (37 markers and 2 isotypic controls). EVs bound to beads are counterstained with a cocktail of APC conjugated detection antibodies of commonly used exosome markers anti-CD9, anti-CD63, and anti-CD81 and analysed by flow cytometry. Data analysis revealed that EVs were positive for the typical MSC markers such as CD29, CD44, CD49e, CD105, CD146, as well as for the exosomal positive tetraspanins CD9, CD63 and CD81 (**Figure 3.1A**). In addition, the EVs were negative for the endothelial marker CD31 and epithelial marker CD326, therefore confirming them to be of mesenchymal origin (**Figure 3.1A**). Furthermore, Nanosight analysis revealed the size of EVs to be in the typical range of 30-300 nm, which was further confirmed by transmission electron microscopy (**Figure 3.1B, C**). Western blot analysis showed that EVs were positive for CD63 and negative for the cell cytoplasmic marker GM130 (**Figure 3.1D**).

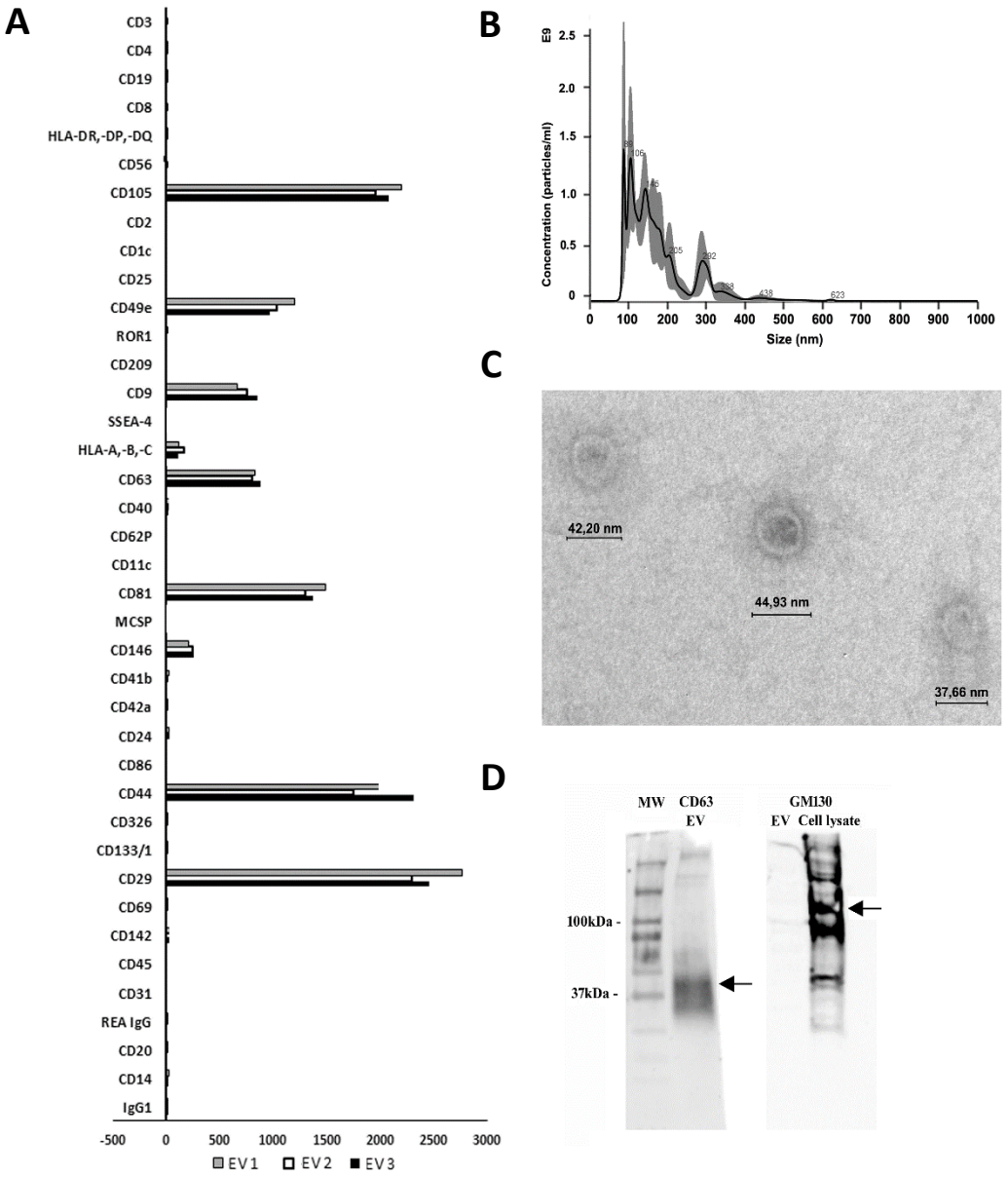

Figure 3.1. Characterization of MSC-EVs. (A). Multiplex bead-based flow cytometry assay was used to characterize MSC-EV surface antigens. 39 multiplexed populations of dye-labeled antibody-coated capture beads containing established exosomal markers were incubated with MSC-EVs and analysed by flow cytometry. Experiments were performed with 3 different samples. **(B)** Nanoparticle tracking analyses showing the size distribution and quantity of MSC-EVs purified by differential ultracentrifugation. **(C)** Representative transmission electron microscopy showing MSC-EVs (original magnification 150,000X). **(D)** Representative Western blot analysis of the exosomal marker CD63 (30-60 kDa) in MSC-EVs and negatively stained for GM130 (130 kDa) (MSC lysate was used as positive control).

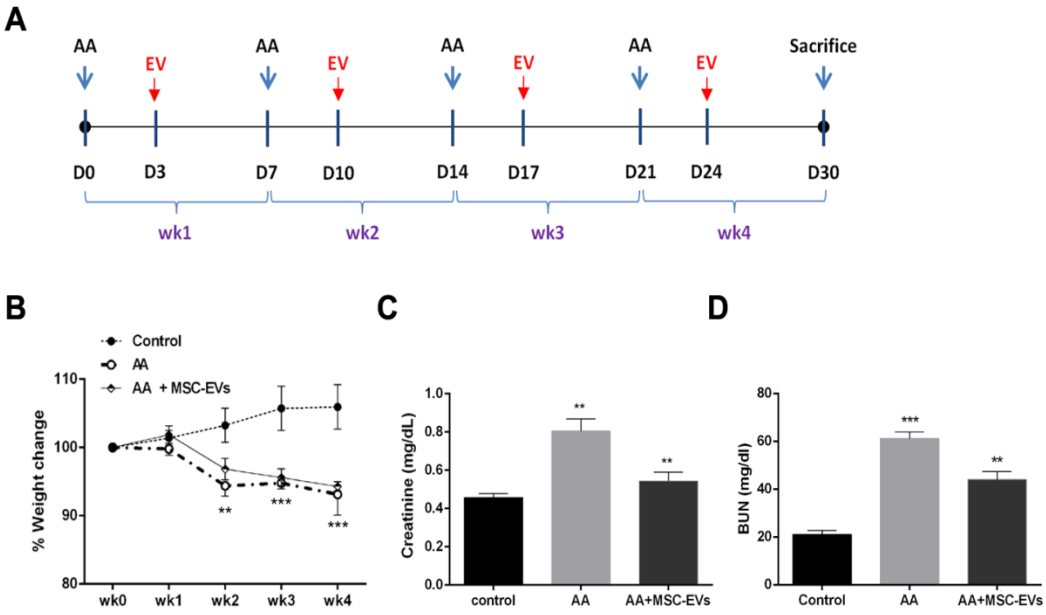

Figure 3.2. Induction of nephropathy in NSG mice by aristolochic acid intoxication. (A) Schematic representation of the experimental design for aristolochic acid nephropathy (AAN) *in vivo* showing the days of administration of AA or Human bone marrow mesenchymal stem cell-derived extracellular vesicles (MSC-EVs) for 4 weeks (wk). **(B)** Mice body weight was measured weekly before AA injections for 4 weeks. The body weight is represented as percentage weight change. A two-way analyses of variance (ANOVA) was performed with Bonferroni's multi comparison test; Data are expressed as mean ± SEM of seven mice per group. **p and ***p < 0.001 AA vs control. **(C)** Plasma creatinine and **(D)** BUN levels in mice treated with vehicle alone or mice injected with AA or AA mice injected with MSC-EVs (n=7 mice per group). **p< 0.001 AA vs control and AA+MSC-EVs vs AA. Data are expressed as mean ± SEM; a one way ANOVA with Bonferroni's multi comparison test was performed.

3.1.2 MSC-EVs ameliorate AA induced kidney damage

Weight loss is considered to be one of the main macro symptoms of AAN. Therefore, we monitored the total body weight of each mouse on a weekly basis prior AA administration (**Figure 3.2A**). Mice injected with AA lost weight significantly from week 2 onwards compared to healthy mice (**Figure 3.2B)**. Treatment with MSC-EVs, post AA administration, did not ameliorate the loss of weight induced by AA throughout the course of the pathology (**Figure 3.2B**). As a parameter of kidney function, the plasma creatinine and BUN levels were also evaluated in all mice groups at sacrifice. Data analysis revealed a significant increase in plasma creatinine and BUN levels of mice

injected with AA compared to healthy controls (**Figure 3.2C, D**). In contrast, AA mice treated with MSC-EVs had significantly reduced levels of both plasma creatinine and BUN in comparison with mice injected with AA alone (**Figure 3.2C, D**).

Immunohistochemical analyses were performed to evaluate the morphological changes of kidney tissue from all the experimental groups. Kidney tissue of mice that had been injected with AA alone had a severe damage of the proximal tubules, formation of hyaline casts, and development of interstitial fibrosis, compared to healthy controls (**Figure 3.3A, B**). On the other hand, mice that received treatment with MSC-EVs had a significant amelioration in kidney damage, whereby there was a marked reduction in tubular necrosis (H&E staining) and interstitial fibrosis, as observed by Masson's trichrome staining (**Figure 3.3A, B**). This was further confirmed by the histological score (obtained by quantifying tubular necrosis and interstitial fibrosis in kidney sections from all experimental groups) whereby, mice inoculated with MSC-EVs significantly reduced the number of necrotic tubules, and interstitial fibrosis compared to AA injured mice (**Figure 3.3C, D**). Furthermore, assessment of proliferation and apoptosis through PCNA/TUNEL staining showed a significant increase in PCNA positive cells (**Figure 3.4A**) and a decrease in TUNEL positive apoptotic cells **(Figure 3.4B**) in AA mice treated with MSC-EVs compared to mice injected with AA alone.

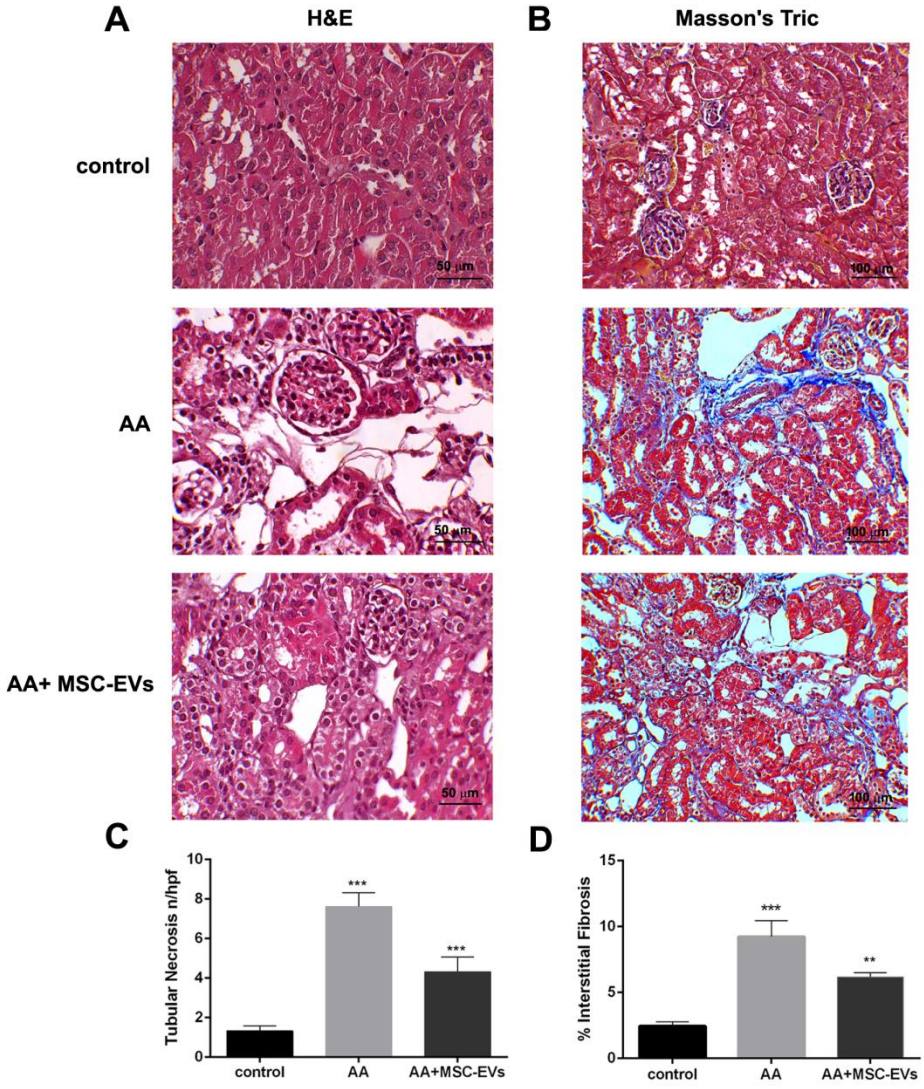

Figure 3.3. Histological analyses of AAN *in vivo* model. (A) Micrographs representing H&E stained renal tissue from healthy mice injected with the vehicle alone (control), or mice injected with AA, or AA mice treated with MSC-EVs. Original magnification at 400X**. (B)** Micrographs representing Masson's trichrome stained renal sections from control, AA or MSC-EV treated AA mice. The blue stain is collagen fibres signifying interstitial fibrosis. Original magnification at 200X. **(C)** Histological score of tubular necrosis in AAN mice experimental groups. Mice treated with AA had significantly high levels of tubular necrosis, which was reduced, on treatment with MSC-EVs. Data represent mean ±SEM of tubular necrosis observed under high power field (original magnification: 400X). A one way ANOVA with Bonferroni's multi comparison test was performed. ***p<0.001 AA vs control or MSC-EV vs AA. **(D)** Histological quantification of interstitial fibrosis in AAN mice experimental groups by multiphase image analysis of 10 fields per section. Data represent mean ±SEM; A one way ANOVA with Bonferroni's multi comparison test was performed. ***p<0.001 AA vs control, ** p<0.01 MSC-EV vs AA.

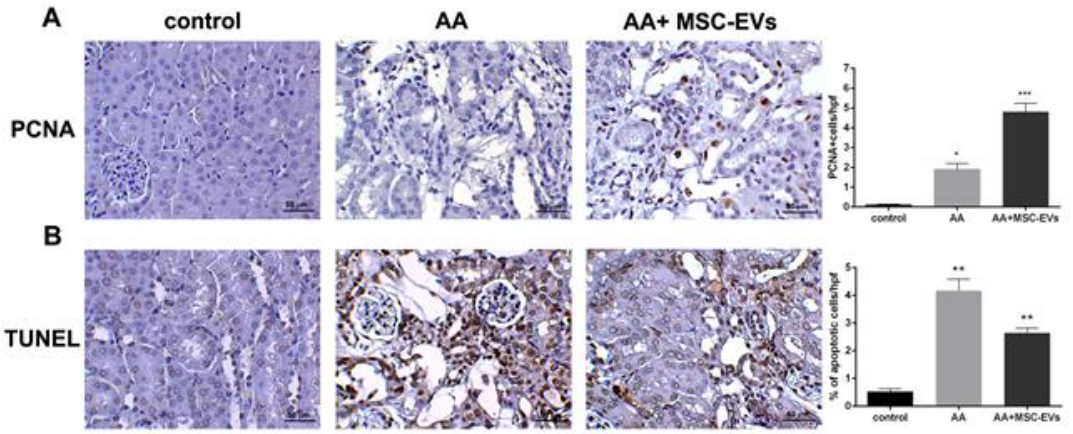

Figure 3.4. Representative micrographs of PCNA and TUNEL stained renal tissue. **(A)** Proliferating cell nuclear antigen (PCNA) staining of control, AA, or AA mice treated with MSC-EVs. Histological score of PCNA positive cells in AAN mice experimental groups observed under high power with an original magnification of 400X. An increase in PCNA positive cells was observed in MSC-EV treated mice renal tissue. Data represent mean ±SEM. A one way ANOVA with Bonferroni's multi comparison test was performed. *p<0.01 AA vs control, or ***p<0.05 MSC-EVs vs AA. **(B)** TUNEL staining of control, AA, or AA mice treated with MSC-EVs. Histological score of % of apoptotic cells (by TUNEL staining) in AAN mice experimental groups observed under high power with an original magnification of 400X. A decrease in TUNEL positive cells was observed in MSC-EV treated mice renal tissue. Data represent mean ±SEM. A one way ANOVA with Bonferroni's multi comparison test was performed. **p<0.01 AA vs control, or **p<0.05 MSC-EVs vs AA. Original magnification at 400X.

Activation of fibrogenic cells, as assessed by α-SMA staining, was found to be significantly elevated in mice injected with AA compared to healthy controls (**Figure 3.5A**). Interestingly, this elevation was significantly reduced in AA mice treated with MSC-EVs as evaluated by morphometric analyses (**Figure 3.5A**). Infiltration of FSP-1 positive cells, and CD45 positive inflammatory cells was also assessed through staining with their respective antibodies. Mice treated with AA had a significantly higher presence of both FSP-1 and CD45 cells compared to healthy controls (**Figure 3.5B, C**). In contrast, treatment of AA mice with MSC-EVs significantly reduced the infiltration of FSP-1 and CD45 positive cells (**Figure 3.5B, C**). This was further confirmed by histological score analyses which revealed a significant difference between the three experimental groups, exhibiting an ameliorating effect of MSC-EVs (**Figure 3.5B, C**). Pericytes are perivascular cells that

migrate to the interstitium and differentiate into myofibroblasts during renal interstitial fibrosis. The presence of pericytes/myofibroblasts was therefore assessed through PDGFrβ/α-SMA co-staining. Data analyses revealed a significant rise in PDGFrβ/α-SMA positive cells in the kidney interstitium following AA induced injury compared to healthy controls (**Figure 3.5D**). However, AA mice treated with MSC-EVs had significantly lowered levels of PDGFrβ/α-SMA positive cells compared to AA mice (**Figure 3.5D**).

3.1.3 MSC-EVs revert AA induced upregulation of pro-fibrotic genes in AAN mice kidneys

Real time PCR of kidney tissue from the experimental mice groups revealed that mice treated with AA alone had significantly elevated levels of the pro-fibrotic genes: alpha Smooth muscle actin (*α-Sma*), Collagen 1a1 (*Col1a1*) and Transforming Growth Factor beta 1 (*Tgfb1*) (**Figure 3.6A, B, C**) compared to healthy controls. However, AA mice, that had received MSC-EVs, exhibited significantly lower levels of all three pro-fibrotic genes (**Figure 3.6A, B, C**) in comparison with AA injured mice. Furthermore, we also evaluated the regulation of the gene Latent-Transforming Growth Factor beta-binding protein 1 (*Ltbp1*), that codes for the LTBP1 protein, involved in the activation of TGFβ1. Mice treated with AA had significantly upregulated levels of the *Ltbp1* gene which was found to be significantly downregulated in AA mice treated with MSC-EVs (**Figure 3.6D**).

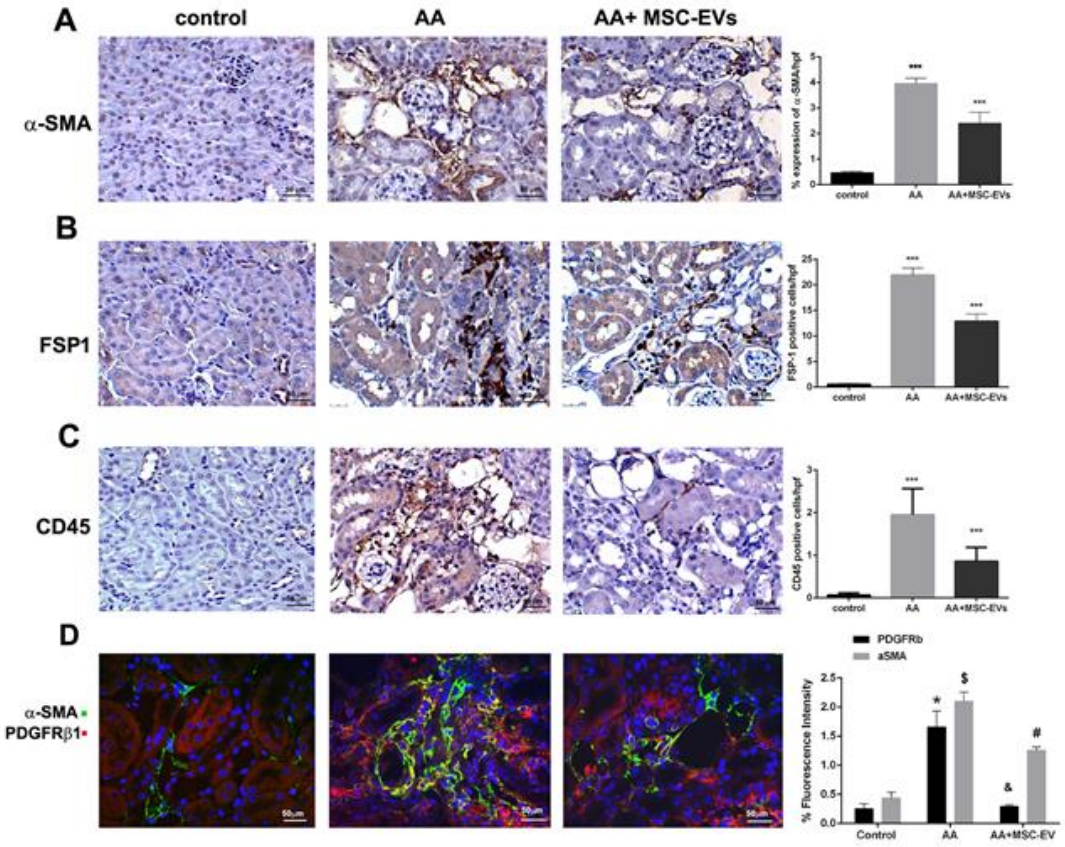

Figure 3.5. Immunohistological staining of kidneys from mice treated with AA. Kidney paraffin-sections from healthy mice, or mice treated with AA, or AA mice treated with MSC-EVs were stained for α-SMA **(A)**, FSP-1 **(B)** or CD45 **(C)** to identify presence of active fibroblasts and inflammatory cell infiltration (original magnification: x400). **(D)** PDGFRβ/α-SMA staining was also performed to identify pericyte/myofibroblast transition in the renal interstitium of kidney paraffin-sections from AAN mice experimental groups (original magnification: 400X). The histograms represent the quantification of cells positive for the relative immunostaining in mouse kidney paraffin-sections from AAN mice experimental groups. Data represent mean ±SEM of the fluorescence intensity or cells positive per high power field measured from 10 images taken at random from six samples per treatment. ***p<0.001 AA vs control or MSC-EV vs AA. A one way ANOVA with Bonferroni's multi comparison test was performed.

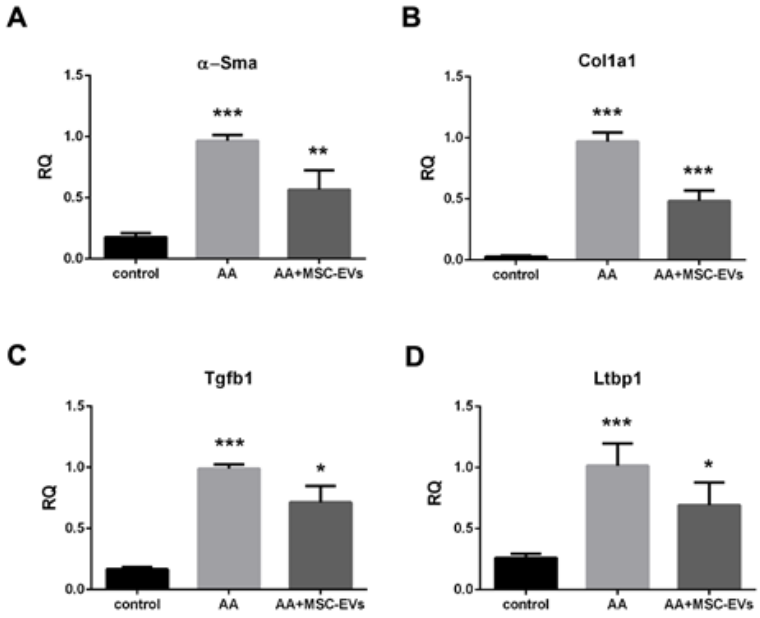

Figure 3.6. MSC-EVs downregulate pro-fibrotic genes in mice treated with AA. Gene expression levels of *α-Sma* **(A)**, *Col1a1* **(B)**, *Tgfb1* **(C),** and *Ltbp1* **(D)** in mice treated with vehicle alone (control), or mice treated with AA, or AA mice treated with MSC-EVs. Data show mean ±SEM of n=7 samples per treatment. ***p<0.001 AA vs control, *p<0.05, **<0.01, ***p<0.001 MSC-EV vs AA. A one way ANOVA with Bonferroni's multi comparison test was performed.

3.1.4 MSC-EV treatment induced the downregulation of pro-fibrotic genes in fibroblasts *in vitro*

In order to elucidate the role of MSC-EVs on activated renal fibroblasts, an *in vitro* model in which AA injured mTECs were co-cultured with kidney fibroblasts in a transwell system (**Figure 3.7A**). Analyses of pro-fibrotic genes in renal fibroblasts revealed a significant increase in α-*Sma, Tgfb1, Col1a1* expression in fibroblasts exposed to mTECs pre-treated with AA **(Figure 3.7B).** Following treatment with MSC-EVs, this upregulation of pro-fibrotic genes was significantly reduced **(Figure 3.7B),** therefore confirming the direct effect of MSC-EVs on activated fibroblasts.

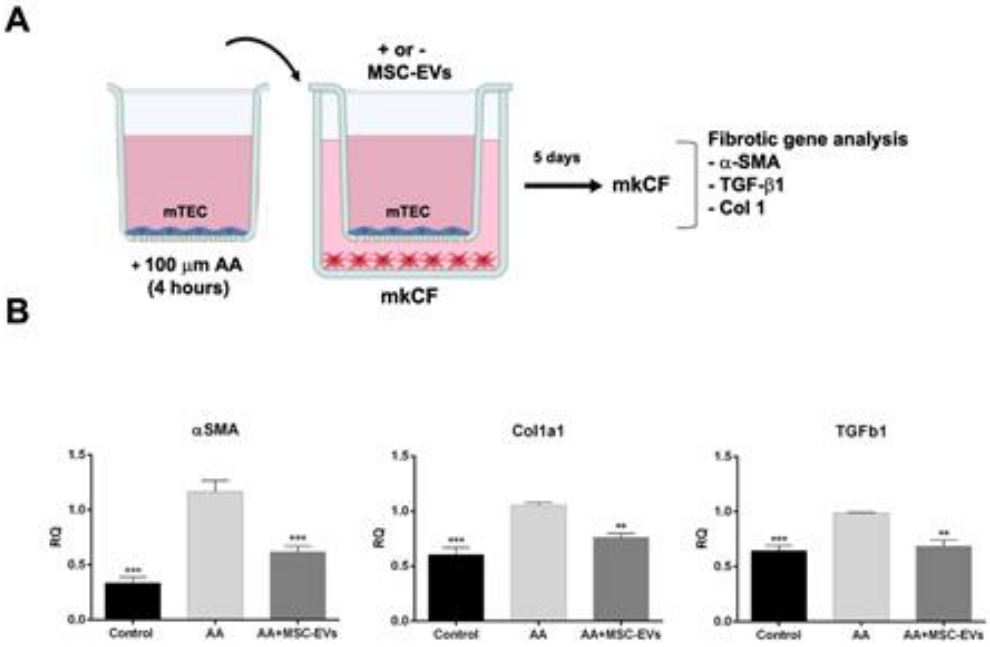

Figure 3.7. MSC-EVs downregulate pro-fibrotic genes in kidney cortical fibroblasts in an *in vitro* model of AAN. (A) An illustration depicting the AAN in vitro assay whereby: mTECs treated with or without AA for 4 hrs were co-cultured with mouse fibroblasts (mkCF) in the presence or absence of MSC-EVs (75,000 EVs/cell) for 5 days at 37̊C. **(B)** Gene expression analyses revealed an upregulation of the profibrotic markers: *α-sma, Tgfb1,* and *Col1a1* in mkCFs co-cultured with AA treated mTECs. The expression levels of all three pro-fibrotic genes were reduced significantly following treatment with MSC-EVs. The data represents the mean ±SEM of three independent experiments performed in quadruplicate. **p<0.01 vs AA, ***p<0.001 vs AA. A one way ANOVA with Bonferroni's multi comparison test was performed.

3.1.5 MSC-EVs reverse the expression of miRNAs dysregulated in AAN

miRNAs have been reported to play a crucial role in the regulation of genes involved in kidney injury [46]. Furthermore, it has also been very well established that EVs can influence the regulation of nucleic acids such as miRNAs by transduction or horizontal transfer to recipient cells or tissue [24, 47, 48]. The regulation of miRNAs by MSC-EVs, following AA injury in mice, was evaluated using the mouse Fireplex miRNA assay. Out of the 65 miRNAs analysed, 13 were found to be significantly dysregulated in mice injured with AA and 36 were found to be significantly regulated following treatment with MSC-EVs (**Figure 3.8A**). The comparison of miRNAs between AA and AA+MSC-EV groups, revealed ten to be commonly

regulated. Among them, seven were significantly downregulated following MSC-EV treatment (**Figure 3.8B, C**), whereas three miRNAs were upregulated with respect to AA treated mice and healthy controls (**Figure 3.8B, D**). Three out of the 7 miRNAs were validated through RT-PCR (**Figure 3.8E).**

We further analyzed the seven miRNAs (**Figure 3.8C**) downregulated by MSC-EVs to identify the genes and pathways regulated by them. The list of predicted target genes identified through Mirwalk (data not shown), was further analyzed via Panther gene ontology software online. Ninety nine pathways were predicted to be linked to miRNA targeted genes out of which the top 37 pathways were selected based on a cut off of >5 genes/pathway and the relevance of the pathway in kidney injury (**Table 3.1**). Furthermore, analyses on validated pathways revealed the regulation of 14 pathways **(Table 3.2).** Interestingly, the majority of pathways identified have been implicated in various pathological processes such as fibrosis, inflammation, and apoptosis, all of which are considered to be hallmarks of CKD.

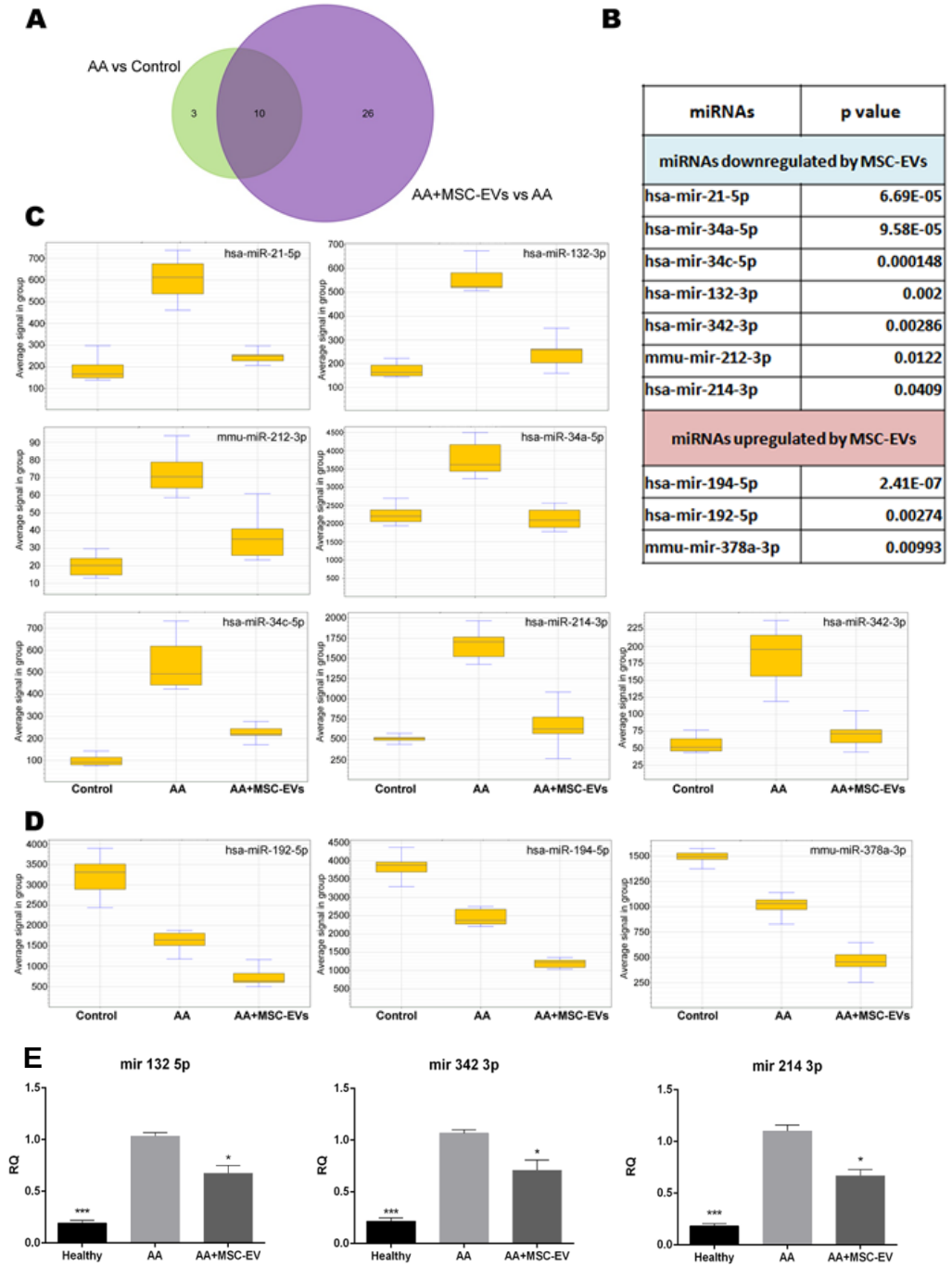

miRNAs	p value
miRNAs downregulated by MSC-EVs	
hsa-mir-21-5p	6.69E-05
hsa-mir-34a-5p	9.58E-05
hsa-mir-34c-5p	0.000148
hsa-mir-132-3p	0.002
hsa-mir-342-3p	0.00286
mmu-mir-212-3p	0.0122
hsa-mir-214-3p	0.0409
miRNAs upregulated by MSC-EVs	
hsa-mir-194-5p	2.41E-07
hsa-mir-192-5p	0.00274
mmu-mir-378a-3p	0.00993

Figure 3.8. FirePlex miRNA assay. miRNAs regulated in kidney toxicity were detected in paraffin kidney sections in mice from all experimental groups (n=3 per group). **(A)** Venn diagram comparing the miRNAs reguated by AA and by MSC-EVs in the AAN model. Thirteen miRNAs were dysregulated in AA intoxicated mice with respect to control mice and 36 in AA mice treated with MSC-EVs. Ten miRNAs were found to be common between the two groups. **(B)** List of the ten modified miRNAs common between AA mice and AA mice treated with MSC-EVs. **(C)** Box plots representing the miRNAs that were upregulated in mice injured with AA and downregulated following treatment with MSC-EVs **(D)** Box plots representing the miRNAs that were common between AA mice and AA mice treated with MSC-EVs but not downregulated. **(E)** Three out of the seven miRNAs were validated by RT-PCR.

Pathways predicted by PANTHER online meta-analyses	No of genes involved
Wnt signalling pathway (P00057)	138
Inflammation mediated by chemokine and cytokine signalling pathway (P00031)	94
Angiogenesis (P00005)	91
Cadherin signalling pathway (P00012)	77
Integrin signalling pathway (P00034)	73
PDGF signalling pathway (P00047)	71
EGF receptor signalling pathway (P00018)	69
FGF signalling pathway (P00021)	58
TGF-beta signalling pathway (P00052)	53
Apoptosis signalling pathway (P00006)	52
p53 pathway (P00059)	44
Interleukin signalling pathway (P00036)	42
Endothelin signalling pathway (P00019)	40
T cell activation (P00053)	39
Ras Pathway (P04393)	35
B cell activation (P00010)	33
Oxidative stress response (P00046)	31
VEGF signalling pathway (P00056)	29
Toll receptor signalling pathway (P00054)	26
PI3 kinase pathway (P00048)	24
Notch signalling pathway (P00045)	24
Interferon-gamma signalling pathway (P00035)	23
FAS signalling pathway (P00020)	15
Hypoxia response via HIF activation (P00030)	14
GABA-B receptor II signalling (P05731)	13
p53 pathway by glucose deprivation (P04397)	13
Histamine H1 receptor mediated signalling pathway (P04385)	13
Heterotrimeric G-protein signalling pathway-rod outer segment phototransduction (P00028)	11
Hedgehog signalling pathway (P00025)	11
General transcription regulation (P00023)	11
JAK/STAT signalling pathway (P00038)	10
Beta3 adrenergic receptor signalling pathway (P04379)	10
Glycolysis (P00024)	10
DNA replication (P00017)	9
Angiotensin II-stimulated signalling through G proteins and beta-arrestin (P05911)	8
Cell cycle (P00013)	7
P53 pathway feedback loops 1 (P04392)	6

Table 3.1. Panther gene ontology pathway analyses. Predicted pathways regulated by miRNAs downregulated by MSC-EVs in AA mice**.** The top 37 pathways have been selected on the basis of number of genes involved in kidney injury.

Pathways validated by PANTHER online meta-analyses	N of genes involved
Angiogenesis (P00005)	12
Apoptosis signalling pathway (P00006)	10
Integrin signalling pathway (P00034)	10
PDGF signalling pathway (P00047)	9
CCKR signalling map (P06959)	9
TGF-beta signalling pathway (P00052)	8
Gonadotropin-releasing hormone receptor pathway (P06664)	8
p53 pathway (P00059)	7
p53 pathway feedback loops 2 (P04398)	7
Inflammation mediated by chemokine and cytokine signalling pathway (P00031)	6
FGF signalling pathway (P00021)	6
FAS signalling pathway (P00020)	6
EGF receptor signalling pathway (P00018)	6
Oxidative stress response (P00046)	6

Table 3.3. Panther pathway enrichment analyses on validated target genes of differentially expressed miRNAs in AA mice treated with MSC-EVs.

3.2 **Discussion**

The current study reveals the ability of MSC-EVs to inhibit the progression of kidney injury in a CKD murine model of AAN. Following MSC-EV treatment, AA mice showed an overall improvement in kidney function, as reflected by a significant reduction of blood creatinine, and BUN levels. In addition, changes in kidney morphology were also observed whereby tubular necrosis and interstitial fibrosis were significantly reduced and renal regeneration propagated. Furthermore, a marked reduction in inflammatory cells, myofibroblasts, and pericytes was also observed following MSC-EV treatment.

Over the last decade, the notion of stem-cell derived EVs, as an alternative therapeutic strategy for tissue regeneration, has evolved tremendously. In particular MSC-EVs, which are the most extensively studied stem cell derived EVs in various experimental disease models [26]. For instance, in the classical CKD model of ureter urinary obstruction (UUO), intravenous administration of MSC-EVs not only improved renal function in a span of two weeks, but also alleviated tubular injury and interstitial fibrosis [33]. Interestingly, in a porcine model of renovascular disease (RVD), a more diverse model of CKD, a single dose of MSC-EVs alleviated renal inflammation through the regulation of pro and anti-inflammatory cytokines contributing to recovery [49].

MSC-EVs from other sources have also been demonstrated to be effective. For instance, MSC-EVs from urine not only increased the significant proliferation of glomerular endothelial cells but also reduced apoptosis of podocytes and tubular epithelial cells in a rat model of diabetic nephropathy [50]. Similar regenerative effects were also observed by Nagaishi et al whereby in a similar mouse model of diabetic nephropathy, administration of MSC exosomes under the renal capsule, resulted in anti-apoptotic effects and general improvement of renal morphology [51].

More recently, our group reported the therapeutic effects of multiple sources of stem-cell derived EVs, in a mouse model of streptozotocin induced diabetic nephropathy [31]. Elevated levels of plasma creatinine, BUN, and albumin/creatinine excretion were significantly reduced to near normal levels in diabetic mice following treatment with EVs from MSCs and HLSCs. In addition, we also observed a significant improvement in kidney morphology as well as a reduction in fibrosis both at a protein and molecular level in mice treated with both the EV types [31].

Comparative miRNA expression analysis between both EV types revealed the enrichment of some common and uncommon miRNAs that were associated with pro-fibrotic gene regulation. These findings further supported anti-fibrotic effects of MSC-EV, observed in a curative model of CKD [31].

Our aim was therefore to evaluate the effect of MSC-EVs in the current AAN model of CKD, identify the molecular and histological changes following EV treatment and elucidate the underlying molecular mechanisms for the anti-fibrotic and regenerative effects observed.

The pathogenesis of CKD frequently presents with a dysfunction of the local parenchyma in the form of tubular and glomerular damage. This ultimately leads to necrosis and formation of hyaline casts [26]. In this state of kidney injury, a correlation between loss of renal function (elevated levels of BUN and plasma creatinine) and loss of body weight has often been observed in various experimental models of AAN [30, 31, 52-54]. In the current study, administration of AA increased tubular damage and necrosis, as well as blood creatinine and BUN. A gradual loss of total body weight was also observed, in AA mice over the course of the experiment. Treatment with MSC-EVs reduced blood BUN and creatinine levels and ameliorated tubular necrosis. However, no significant improvement in body weight was observed in mice treated with MSC-EVs.

Following an insult, various inflammatory, fibrotic, and reparative processes are activated concurrently to promote regeneration and repair. However,

dysregulation of these processes can increase infiltration of inflammatory and pro-fibrotic cells causing impairment in tissue regeneration leading to fibrosis [55]. Renal fibrosis is a progressive form of tissue scarring and a hallmark of CKD prominently featured in AAN. Majority of patient cases with AAN, described in the literature, link fibrosis accompanied with interstitial inflammatory infiltrates to chronic kidney failure [56-58]. In addition, various experimental models of AAN also describe fibrosis, as a common feature instigated by an amalgamation of infiltrating inflammatory cells and activation of resident fibroblasts to myofibroblasts [59, 60].

Pozdzik et al reported the accumulation of activated fibroblasts confirmed by their positive expression of vimentin and α-smooth muscle, in the renal interstitium of rats injected with AA [60]. A similar event was confirmed by Huang *et al* [53] in their mouse model of AAN, whereby FSP-1 positive cells were observed in the kidneys of AA treated mice. In addition, infiltration/activation of fibroblasts was accompanied by the influx of CD45 positive inflammatory cells, activated mononuclear cells and cytotoxic T cells [53, 60]. In our model of AAN, an influx of inflammatory cells (CD45 positive cells) together with myofibroblast activation (cells positive for FSP-1, and α-SMA staining) was also observed in the renal interstitium of mice exposed to AA. Interestingly, mice that received treatment with MSC-EVs, showed a significantly lower expression of CD45 positive cells, FSP-1 and α-SMA positive myofibroblasts. As NSG mice lack an adaptive immune system due to their genetic background [61], we speculate that, the CD45 positive cells are likely to be part of the innate immune system and partly the cause of the severe kidney injury observed in these mice following AA injection. To explore the role of the adaptive immune system, mice with an intact immune system need to be used. However, as the MSC-EVs used in this study were of human origin, immunodeficient mice had to be used to avoid an immune reaction related to xenogeneic material. Overall, our data indicate that MSC-EVs attenuate the innate immune response ameliorating AA induced kidney injury.

Pericytes have also been implicated to play a role in fibrosis as they are considered to be a major source of myofibroblasts in interstitial fibrosis [14]. These perivascular cells rich in PDGFRβ mainly provide support to the vasculature under physiological conditions. However, during a renal pathological insult, they tend to migrate towards the renal interstitium and undergo transition into myofibroblasts expressing α-SMA [14]. In the current model, mice exposed to AA had significantly elevated levels of pericyte/myofibroblast transitioned cells as reflected by cells positive for PDGFRβ/α-SMA. This positivity was significantly reduced in mice that received MSC-EVs. Interstitial fibrosis is normally initiated at a molecular level following upregulation of pro-fibrotic genes such as *α-Sma*, *Col1a1*, and *Tgfb1.* These genes act as molecular witches that govern the process of fibrosis. Molecular analysis of mouse kidney tissue as well as fibroblasts exposed to AA invitro, revealed a significant downregulation of these genes following MSC-EV treatment therefore indicating a potential mechanism of action of EVs at a molecular level. In addition to this, a marked increase in proliferating cells, as evaluated by PCNA staining and a significant reduction in apoptotic cells evaluated by TUNEL staining, indicates that both the anti-fibrotic and regenerative mechanisms of action occur simultaneously following treatment with MSC-EVs which has also been observed in other models of CKD [31, 62].

TGFβ-1 is a major contributor in the pro-fibrotic process leading to the development of scar tissue and eventually end-stage renal disease [7]. Dysregulation of TGFβ-1 has been reported in various experimental models of AAN [63, 64]. In line with these studies, we also observed a significant upregulation of TGFβ-1 at molecular level, in mice damaged with AA. Interestingly, this upregulation was reverted following treatment with MSC-EVs. Moreover, a similar trend was also observed in the expression of the *ltbp1* gene which encodes for the LTBP1 protein, involved in the activation of TGFβ-1. Of note, these data suggest a possible mechanism of action of MSC-EVs in the regulation of TGFβ-1, which itself is a key stone in the progression of inflammation and fibrosis [55, 64].

miRNAs are single stranded non-coding RNA molecules that function as gene silencers and post-transcriptional regulators. Their role in regenerative medicine has been gaining interest over the past decade [65]. Ample studies can be found in the scientific literature reporting the altered expression of miRNAs in renal tissue during the progression of acute and chronic kidney diseases, both in humans and animal models [66]. In addition, miRNAs enriched in EVs, have been shown to exert their biological action by either being directly transferred into recipient cells, or indirectly by influencing the cells genetic content [47, 48]. We therefore, sought to investigate, the miRNA profile in our current model of AAN to identify any significant alterations. Seven miRNAs that were upregulated in AA intoxicated kidneys were downregulated following MSC-EV treatment. Interestingly, these miRNAs have been linked to play a role in kidney fibrosis. For instance, miR21 was first reported by Thum et al [67] to be overexpressed in a fibrosis model of heart failure, which was subsequently followed by studies that demonstrated its involvement in other disease models, including kidney fibrosis [68, 69]. In another study, the upregulation of miR34a was found to be elevated in the interstitium of mouse fibrotic kidneys subjected to UUO injury [70]. miR132-3p and miR214 were identified to be upregulated in various models of kidney diseases associating them with inflammation, apoptosis, myofibroblast activation, and dysregulation of the extracellular matrix [69, 71, 72]. Furthermore, attenuation of these miRNAs through inhibition or silencing ameliorated the various forms of kidney diseases through the downregulation of pathways and processes favouring the progression of injury and fibrosis [69] [73].

Given that these 7 miRNAs were linked to pathology, a meta-analysis was performed to identify their predicted and validated target genes to understand the relative pathological pathways that they could influence. Through online Panther pathway analysis, we identified over 30 predicted pathways out of which some were linked with kidney injury. Amid the pathways identified, the WNT/beta-catenin signalling pathway, chemokine/cytokine pathway, and the TGFβ signalling pathway amongst

others have been reported to play a role in CKD [31, 46, 55, 62]. Moreover, the comparison between miRNAs regulated by MSC-EVs in the current study and HLSC-EVs in our previous study [62], showed no overlap, suggesting that the molecular targets of stem cell derived EVs could differ despite their overall common therapeutic effect. In an earlier study by Collino et al [74], EVs from wild-type MSCs induced morphological and functional recovery of the kidneys in a mouse model of AKI, whereas EVs from drosha-knockdown MSCs that had a global downregulation of microRNAs were ineffective. They showed, through RNA sequencing and gene ontology analysis that genes dysregulated in the kidney post AKI (that mainly influenced pathways related to inflammation, matrix-receptor interaction, among others) were reverted after treatment with wild-type MSC-EVs but not EVs from drosha-knockdown MSCs. Therefore, confirming the contribution of miRNAs enriched in MSC-EVs towards their biological activity. In a recent study by Grange et al [31], molecular analysis of MSC-EVs also revealed the presence of miRNAs involved in the regulation of various inflammatory and pro-fibrotic pathways therefore attributing part of the therapeutic effects to the miRNA content.

Various studies have been performed in our lab to ascertain the active biological molecules responsible for the therapeutic effects observed. For instance, proteomics on MSC-EV fractions performed by Collino et al, revealed the enrichment of cytokines, chemokine receptors (CXCR1 and CXCR6), and interleukins (IL13, IL10, IL 4) that regulate multiple immunomodulatory, and anti-inflammatory pathways [75]. Although, multiple reports have been published dissecting the contents of stem cell derived EVs to ascertain the active content responsible for their biological activity, identifying and proving single and or multiple components responsible for their specific function are still very challenging.

3.3 **Conclusion**

Our data suggest that multiple injections of MSC-EVs not only improved renal function, but ameliorated kidney fibrosis, and tubular necrosis, possibly by attenuating the infiltration of inflammatory cells, reducing the transition of

pericytes and tubular epithelial cells to myofibroblasts, as well as preventing the activation of fibroblasts. Although this work concurs with other works on the therapeutic effects of MSC-EVs, the mechanisms of action through which this effect is achieved still remains to be elucidated.

4. Human liver stem cell-derived extracellular vesicles prevent aristolochic acid induced kidney fibrosis

4.1 **Results**

4.1.1 Characterization of HLSC-EVs

Nanosight analysis revealed the size of EVs mainly detected in the 15% fraction to be in the typical range of 30-300 nm (**Figure 4.1A**) as was confirmed by electron microscopy (**Figure 4.1B**). Western blot analyses confirmed the presence of classical exosomal markers such as CD63, CD81, and TSG101 as described previously (9) (**Figure 4.1C**).

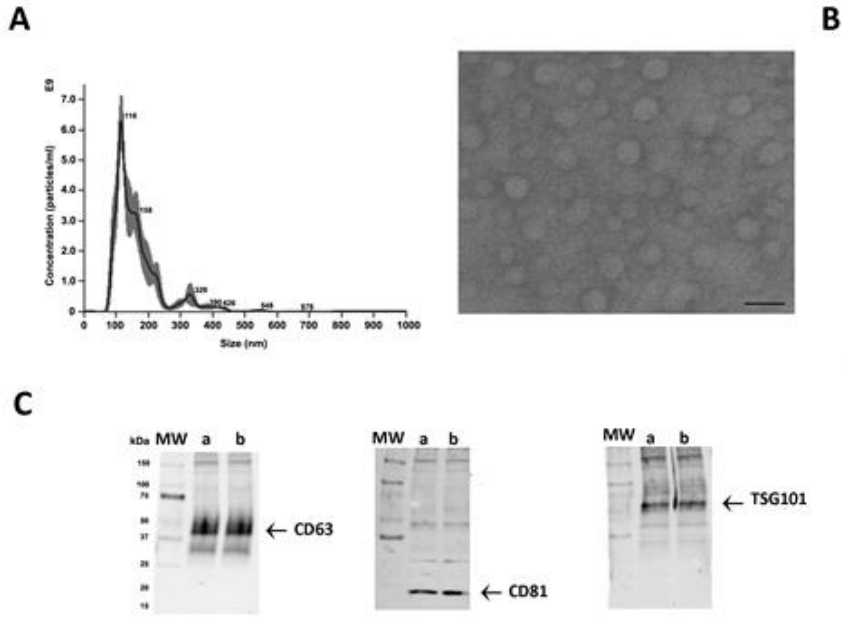

Figure 4.1. Characterization of HLSC-EVs. (A). Nanoparticle tracking analyses showing the size distribution and quantity of HLSC-EVs purified by Iodixanol/sucrose floating (15% gradient). **(B)** Representative transmission electron microscopy showing HLSC-EVs (original magnification x150,000; bar=100nm). **(C)** Western blot analysis confirming the expression of CD63, CD81 and TSG101 in HLSC-EVs purified by; a. differential ultracentrifugation; b. Iodixanol/sucrose floating (15% gradient).

4.1.2 HLSC-EVs prevent development of chronic kidney disease

The body weight of mice measured weekly prior to AA injection (see *in vivo* model schematic, **Figure 4.2A**) was significantly reduced with respect to controls injected with the vehicle alone. The difference in weight was statistically significant after the second injection (week 2) and continued to remain low until sacrificing at week 4 (**Figure 4.2B**). On the other hand, body

weight of AA mice injected with HLSC-EVs increased gradually reaching a significant difference at week 4 compared to mice treated with AA alone. In contrast, mice treated with Fibro-EVs lost more weight compared to mice injected with AA only (**Figure 4.2B**). Serum creatinine levels were significantly increased in AA treated mice at week 4 with respect to controls. In contrast, mice treated with HLSC-EVs had significantly reduced levels of serum creatinine compared to mice treated with AA alone or with Fibro-EVs which served as a negative control (**Figure 4.2C**). Assessment of morphological alterations revealed severe tubular damage in mice injected with AA. The major changes included diffuse degeneration of the proximal tubular epithelium together with hyaline cast formation and tubular necrosis (**Figure 4.3A, D**). However, mice treated with HLSC-EVs had significantly lower number of hyaline casts and necrotic tubules compared to mice injected with AA alone (**Figure 4.3A, D**). The histological score obtained by quantifying tubular necrosis in kidney sections of every experimental group showed a statistically significant increase in AA mice (compared to control mice) and a significant reduction (protection) in mice treated with HLSC-EVs (compared to AA mice) (**Figure 4.3D**). No significant reduction in tubular necrosis was observed in mice treated with Fibro-EVs (**Figure 4.3D**).

Kidney fibrosis, as demonstrated by Masson's trichrome staining, showed an increase in tubular damage and interstitial fibrosis 4 weeks after AA injection (**Figure 4.3B, E**), which was significantly reduced by treatment with HLSC-EVs (**Figure 4.3B, E**). Some reduction of fibrosis was also observed in Fibro-EV treated mice. However, the reduction observed was significantly less effective compared to HLSC-EV treatment.

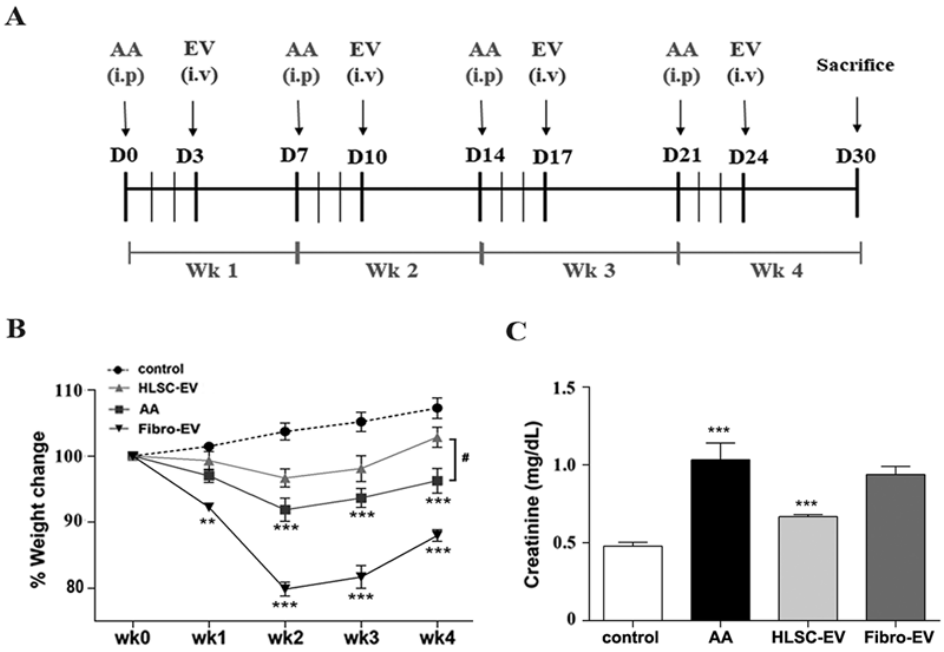

Figure 4.2. HLSC-EVs exhibit antifibrotic effects in AAN *in vivo*. **(A)** Schematic overview of the experimental design for AAN *in vivo* showing the day (D) of administration of AA, HLSC-EVs or Fibro-EV (EV) for 4 weeks (Wk). **(B)** Mice body weight was measured weekly prior to AA injections for 4 weeks and just before sacrifice. The body weight is represented as percentage weight change. A two-way ANOVA was performed with Bonferroni's multi comparison test; Data show mean±SEM of 9 mice per group. ***p<0.001 AA vs control or Fibro-EVs vs control, and #p<0.05 HLSC-EV vs AA. **(C)** Plasma creatinine levels were assessed in mice treated with vehicle alone or mice injected with AA or AA mice injected with HLSC-EVs or Fibro-EVs (n=9 mice per group). ***p<0.001 AA vs control and **p<0.01 HLSC-EV vs AA. Data show mean±SEM; a one way ANOVA with Bonferroni's multi comparison test was performed.

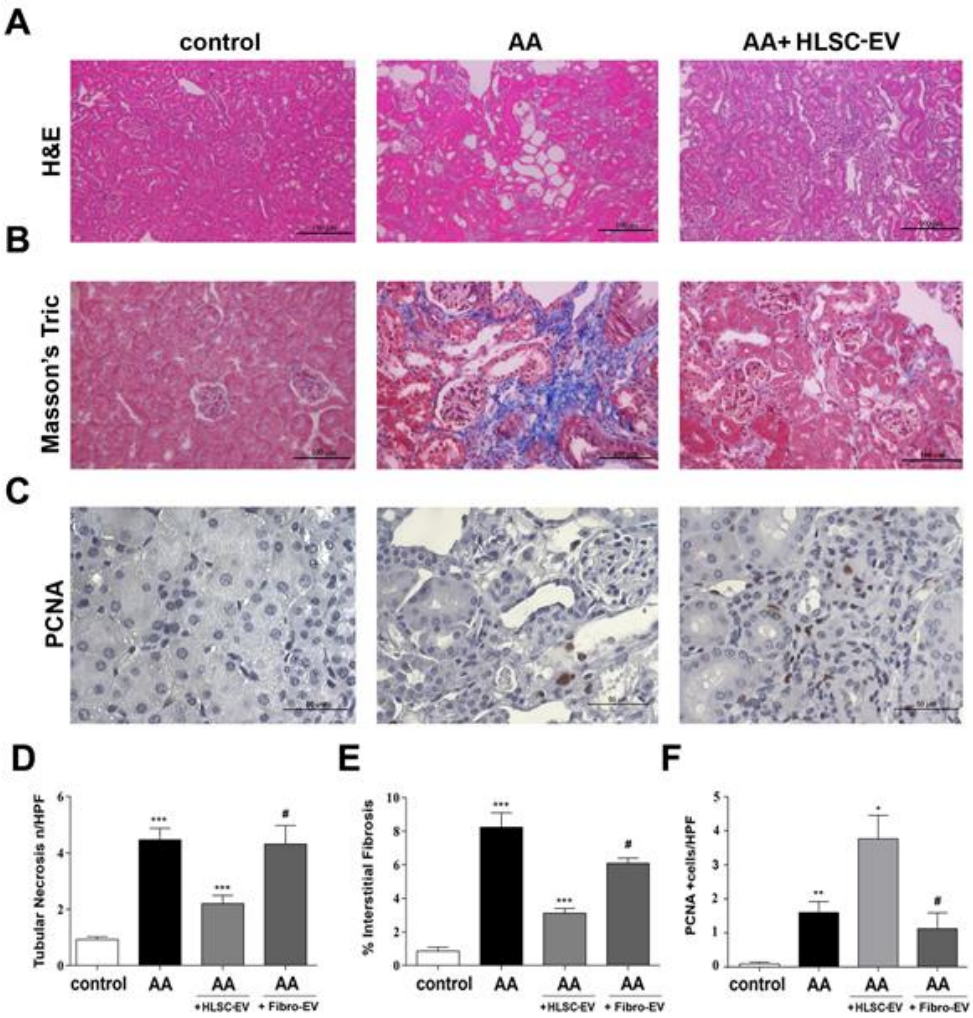

Figure 4.3. Histological analyses of AAN *in vivo* model. (A) Micrographs of H&E stained renal tissue from healthy mice (control), or mice injected with AA (AA), or AA mice treated with HLSC-EVs. **(B)** Micrographs of Masson's trichrome stained renal sections from the AAN mice experimental groups. The blue stain represents collagen fibres (a marker for interstitial fibrosis), Original magnification at x400. **(C)** Micrographs of PCNA stained renal tissue of control, AA, or AA mice treated with HLSC-EVs. Original magnification at x400. **(D)** Histological score of tubular necrosis in AAN mice experimental groups. Mice treated with AA had significantly elevated levels of tubular necrosis which was alleviated on treatment with HLSC-EVs. No significant reduction in tubular necrosis was observed in mice treated with Fibro-EVs. Data represent mean±SD (original magnification: x400). ***p<0.001 AA vs control or HLSC-EV vs AA, #p<0.01 Fibro-EV vs HLSC-EV. **(E)** Histological score of interstitial fibrosis in AAN mice experimental groups by multiphase image analysis of 10 fields per section. Data represent mean±SD; ***p<0.001 AA vs control, ** p<0.01 HLSC-EV vs AA, #p<0.01 Fibro-EV vs HLSC-EV. **(F)** Histological score of PCNA positive cells in AAN mice experimental groups observed under high power with an original magnification of x400. proliferation) Data represent mean±SD. **p<0.01 AA vs control, or Fibro-EVs vs HLSC-EVs, *p<0.05 HLSC-EVs vs AA, #p<0.01 Fibro-EV vs HLSC-EV (n=9 mice per group). A one way ANOVA with Bonferroni's multi comparison test was performed for (**D, E,** and **F**)

PCNA (a marker of cell proliferation) analysis showed a significant increase in PCNA positive cells in AA animals treated with HLSC-EVs but not with Fibro-EVs **(Figure 4.3C, F**).

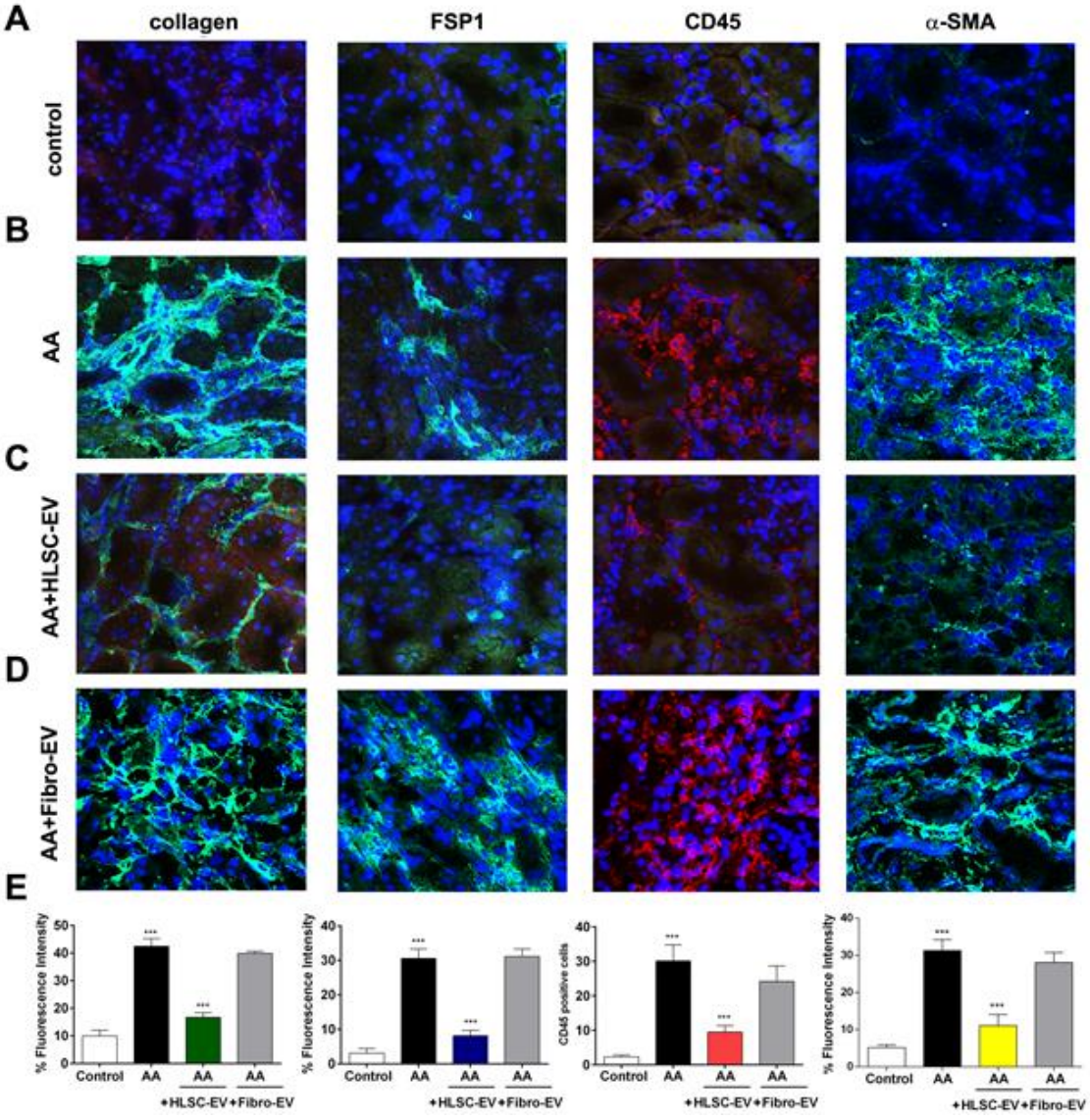

Figure 4.4. Immunofluorescence staining of kidneys from mice treated with AA. Kidney cryo-sections from healthy mice **(A)**, mice treated with AA **(B)**, AA mice treated with HLSC-EVs **(C)** or Fibro-EVs **(D)** were stained for collagen 1a1, FSP-1, CD45, and α-SMA to identify presence of tissue fibrosis, fibroblasts, and inflammatory cells (Original magnification: x200). **(E)** Histograms depicts the fluorescence intensity of collagen, FSP-1, α-SMA and quantification of cells positive for CD45 in mouse kidney cryo-sections from AAN mice experimental groups. Data represent mean±SD of the fluorescence intensity or cells positive per high power field measured from 10 images taken at random from six samples per treatment (n=6 mice). ***p<0.001 AA vs control or HLSC-EV vs AA. No significant differences were observed between AA vs Fibro-EV.

Immunohistochemical staining of kidney cryo-sections showed that mice treated with AA had significantly elevated numbers of CD45, FSP-1 and α-SMA positive cells as well as type 1 collagen deposition compared to controls (**Figure 4.4A, B**). However, on treating mice with HLSC-EVs, expression levels of CD45, FSP-1, α-SMA and Collagen 1 were markedly reduced (**Figure 4.4C**). Morphometric analyses revealed a significant difference between the three experimental groups of animals, showing a protective effect of HLSC-EVs on AA induced injury (**Figure 4.4E**). However, no significant reduction in the expression levels of CD45, FSP-1, α-SMA and Collagen 1 were observed in mice treated with Fibro-EVs (**Figure 4.4D, E**).

4.1.3 HLSC-EVs downregulate pro-fibrotic genes in kidneys of AA treated mice

Kidney tissue obtained from mice treated with AA in the presence or absence of EVs was subjected to RNA isolation. Real time PCR showed mice treated with AA had significantly upregulated levels of the pro-fibrotic genes: *α-Sma* (alpha smooth muscle actin) (**Figure 4.5A**), *Col1a1* (collagen 1a1) (**Figure 4.5B**) and *Tgfb1* (transforming growth factor beta 1) (**Figure 4.5C**). Furthermore, we also observed an upregulation of the gene latent-transforming growth factor beta-binding protein 1 (*Ltbp1*) that codes for the protein (LTBP1) which is responsible for activating TGFβ1 from its latent form (**Figure 4.5D**). In contrast, mice treated with HLSC-EVs had a significant reduction in the expression levels of all three pro-fibrotic genes (**Figure 4.5A, B, C**). In addition a downregulation of *Ltbp1* gene was also observed in mice treated with HLSC-EVs (**Figure 4.5D**). Mice treated with Fibro-EVs showed no significant downregulation of pro-fibrotic genes as well as *Ltbp1* (**Figure 4.5A-D)**.

4.1.4 HLSC-EVs downregulate pro-fibrotic genes in fibroblasts *in vitro*

In order to study the effects of HLSC-EVs on renal fibroblasts, an *in vitro* model was set up whereby mTECs pre-exposed to AA were co-cultured with fibroblasts in a transwell system. A significant rise in *α-Sma*, *Tgfb1*, *Col1a1* expression levels was observed in fibroblasts exposed to mTEC pre-treated

with AA compared to control (**Figure 4.6A, B, C**). This upregulation of pro-fibrotic genes was significantly reduced in the presence of HLSC-EVs, but not Fibro-EVs (**Figure 4.6A, B, C**). Furthermore, internalization of HLSC-EVs by mkCF cells (co-incubation for 6 hrs) was confirmed by z-stack imagery obtained through confocal microscopy (**Figure 4.6C**).

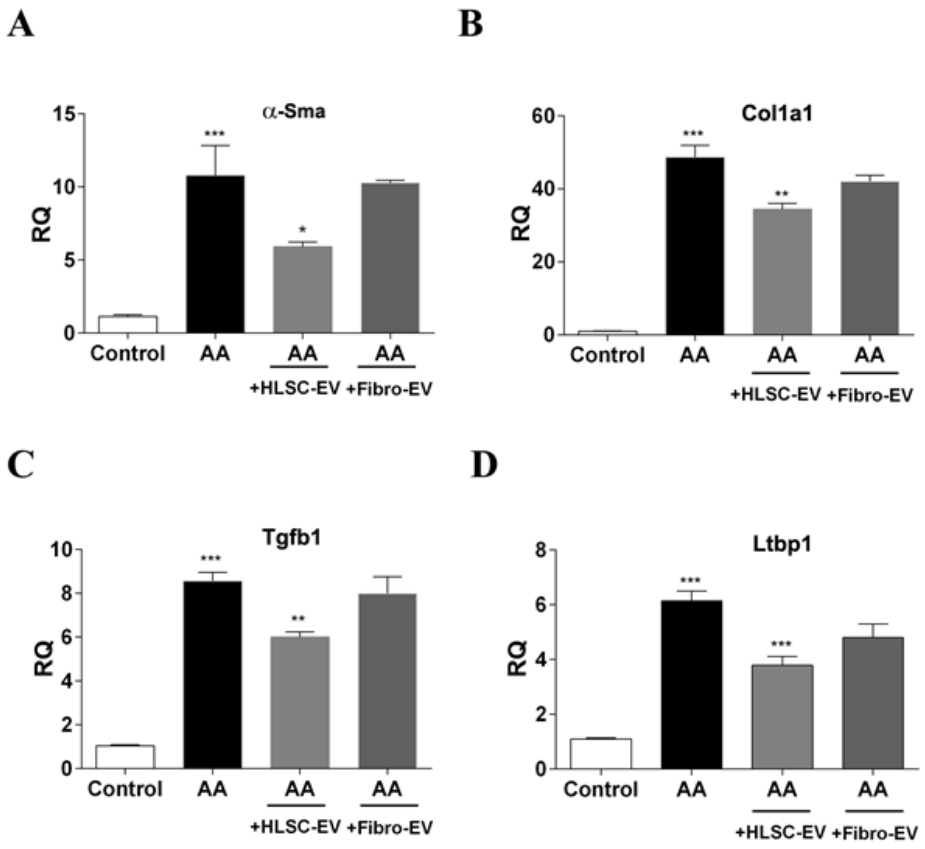

Figure 4.5. HLSC-EVs downregulate pro-fibrotic genes in mice treated with AA. Gene expression levels of *α-Sma* **(A)**, *Col1a1* **(B)**, *Tgfb1* **(C),** and *Ltbp1* **(D)** in mice treated with vehicle alone (control), mice treated with AA, AA mice treated with HLSC-EVs or Fibro-EVs. Data show mean±SD of n=7 mice per treatment. ***p<0.001 AA vs control, *p<0.05, **<0.01, ***p<0.001 HLSC-EV vs AA. No significant differences were observed between AA vs Fibro-EV.

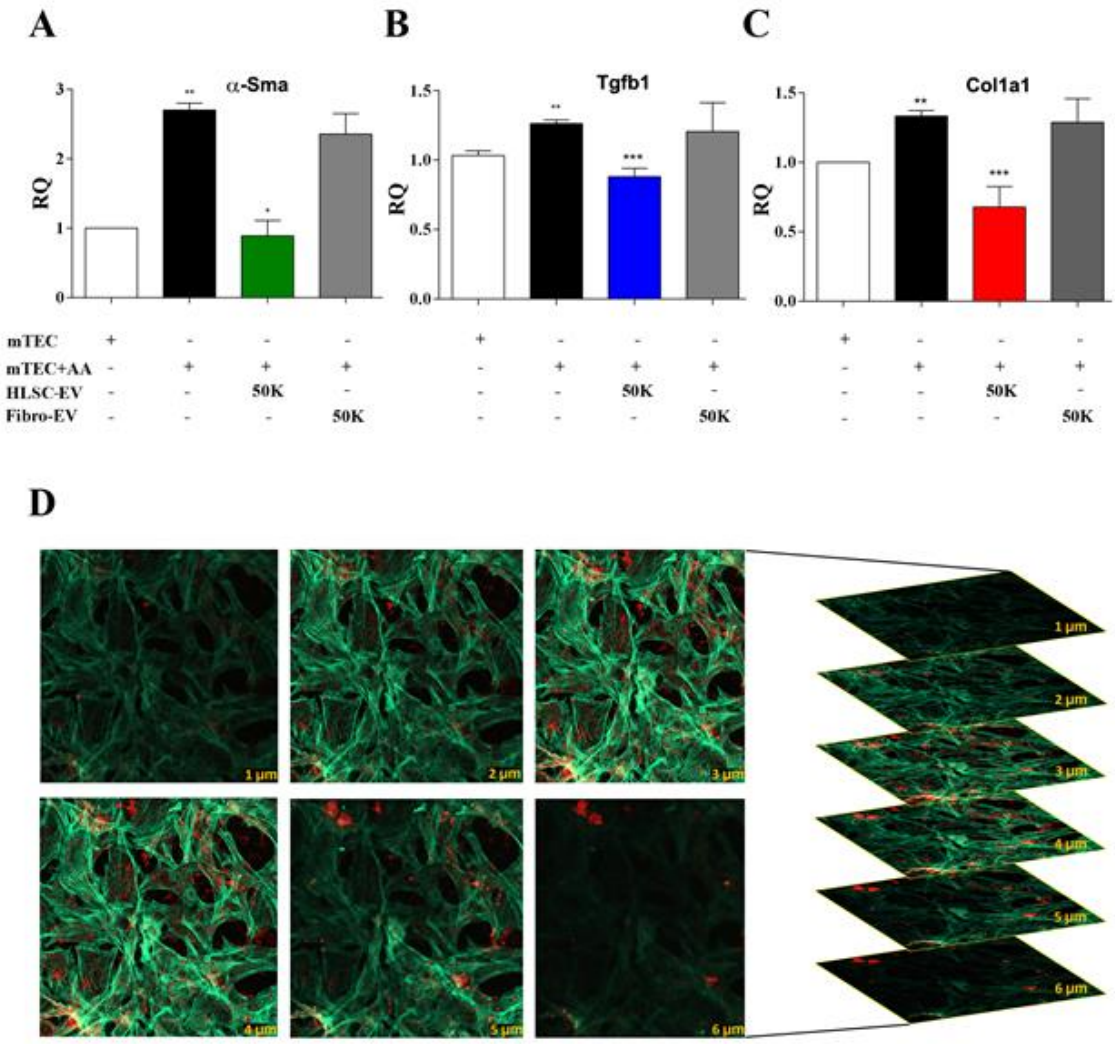

Figure 4.6. HLSC-EVs downregulate pro-fibrotic genes in mouse renal fibroblasts in an *in vitro* model of AAN. mTECs pre-treated with 100µM AA for 4 hrs were co-cultured with mouse fibroblasts in the presence or absence of HLSC-EVs or Fibro-EVs (50,000 EVs/cell) for 5 days at 37°C. Post experimental analyses revealed an upregulation of the fibrotic markers: **(A)** *α-sma*, **(B)** *Tgfb1*, and **(C)** *Col1a1* in fibroblasts co-cultured with AA treated mTECs (AA). Treatment with HLSC-EVs but not Fibro-EVs significantly downregulated all three genes compared to control. The data represent mean±SEM of three independent experiments performed in quadruplicate. *p<0.05, **p<0.01, ***p<0.001 mTEC+AA vs Control, or HLSC-EVs vs mTEC+AA. No significant differences were observed between mTEC+AA vs Fibro-EV. A one way ANOVA with Bonferroni's multi comparison test was performed. **(D)** Representative confocal microscopy depicting the uptake of $1x10^{10}$ DiI dye labelled HLSC-EVs by mouse renal fibroblasts after 6 hrs of co-incubation at 37°C. Z stack analyses shows the presence of EVs within the cytoplasm (phalloidin staining, green) of the cells indicating an effective internalization of vesicles (in red); scale bar=50µm. Data represent one of three experiments performed with similar results.

4.1.5 Mouse miRNome array

In order to analyse the regulation of miRNAs in kidneys of mice treated with AA in the presence or absence of HLSC-EVs, the mouse miRNome miRNA profiling kit was adopted. Analyses of the data revealed, that out of 709 miRNAs analysed, 38 miRNAs were upregulated in AA treated mice (**Table 4.1**) and 109 were downregulated. Furthermore, analysis of AA mice kidneys treated with HLSC-EV treatment revealed a downregulation of 47 miRNAs (**Table 4.1**) and an upregulation of 54 miRNAs.

Comparing the list of miRNAs upregulated in AA mice with the list of miRNAs downregulated on treating the mice with HLSC-EVs, 8 miRNAs were found to be common (**Figure 4.7A**). Furthermore, a comparison was also made to identify miRNAs that were downregulated by AA and upregulated when treating them with HLSC-EVs. The comparison revealed twenty miRNAs to be common between the two groups (**Figure 4.7B**). Expression levels of the 28 miRNAs regulated by HLSC-EVs were verified in fibroblasts from the *in vitro* system. It was observed that out of the 28 miRNAs regulated by HLSC-EVs *in vivo*, 5 were downregulated and 2 upregulated in fibroblasts co-cultured with AA pre-treated mTECs *in vitro* (**Figure 4.7C,D**).

After identifying common miRNAs that inversely correlated between mice treated with AA and AA mice treated with HLSC-EVs, we sought to investigate the genes and pathways that were regulated by these miRNAs. Mirwalk analyses identified over 7000 predicted genes that were regulated by these miRNAs (data not shown). On analysing these genes using Panther gene ontology software online, 141 pathways were linked with the miRNA targeted genes inputted. These pathways were ranked according to the number of genes involved per pathway and the top 36 pathways were selected based on the cut off of **>**5 genes/pathway (**Table 4.2**). Interestingly, out of the pathways identified, quite a few have been implicated in fibrosis including, the WNT signaling pathway, inflammatory cytokine and chemokine pathway, PDGF, FGF and TGFβ signaling pathways (**Figure 4.8A, Table**

4.2). Out of interest, the WNT signaling pathway had the highest number of the predicted miRNA target genes.

mirna upregulated in AA mice		mirna downregulated in HLSCEV mice	
mmu-miR-342-3p	mmu-miR-377-3p	mmu-miR-654-5p	mmu-miR-184-3p
mmu-miR-466e-5p	mmu-miR-375-3p	mmu-miR-296-3p	mmu-miR-154-5p
mmu-miR-466d-5p	mmu-miR-467a-5p	mmu-miR-465a-3p	mmu-miR-138-5p
mmu-miR-466b-3p	mmu-miR-329-3p	mmu-miR-207	mmu-miR-133b-3p
mmu-miR-466a-5p	mmu-miR-294-3p	mmu-miR-409-3p	mmu-miR-101a-3p
mmu-miR-466a-3p	mmu-miR-146b-5p	mmu-miR-542-5p	mmu-miR-30b-5p
mmu-miR-465c-3p	mmu-miR-21a-5p	mmu-miR-325-3p	mmu-miR-26b-5p
mmu-miR-450b-3p	mmu-miR-882	mmu-miR-329-3p	mmu-miR-302a-3p
mmu-miR-467h	mmu-miR-883a-3p	mmu-miR-367-3p	mmu-miR-1b-5p
mmu-miR-34b-3p	mmu-miR-1902	mmu-miR-377-3p	mmu-miR-876-5p
mmu-miR-34b-5p	mmu-miR-1961	mmu-miR-448-3p	mmu-miR-1941-3p
mmu-miR-223-3p	mmu-miR-880-3p	mmu-miR-452-5p	mmu-miR-712-5p
mmu-miR-31-5p	mmu-miR-9-3p	mmu-miR-466h-5p	mmu-miR-741-3p
mmu-miR-466b-3-3p	mmu-miR-10a-3p	mmu-miR-488-3p	mmu-miR-880-3p
mmu-miR-34c-5p	mmu-miR-130b-5p	mmu-miR-504-5p	mmu-miR-1197-3p
mmu-miR-142a-5p	mmu-miR-136-3p	mmu-miR-376c-3p	mmu-miR-9-3p
mmu-miR-190b-5p	mmu-miR-218-2-3p	mmu-miR-302c-3p	mmu-miR-124-5p
mmu-miR-146a-5p	mmu-miR-297c-3p	mmu-miR-297c-5p	mmu-miR-203-5p
mmu-miR-448-3p	mmu-miR-376c-5p	mmu-miR-294-3p	mmu-miR-297c-3p
		mmu-miR-219a-5p	mmu-miR-374b-3p
		mmu-miR-208b-3p	mmu-miR-376b-5p
		mmu-miR-205-5p	mmu-miR-376c-5p
		mmu-miR-201-5p	mmu-miR-433-5p
			mmu-miR-463-5p

Table 4.1: List of miRNAs upregulated in AA mice and downregulated in AA mice treated with HLSC-EVs.

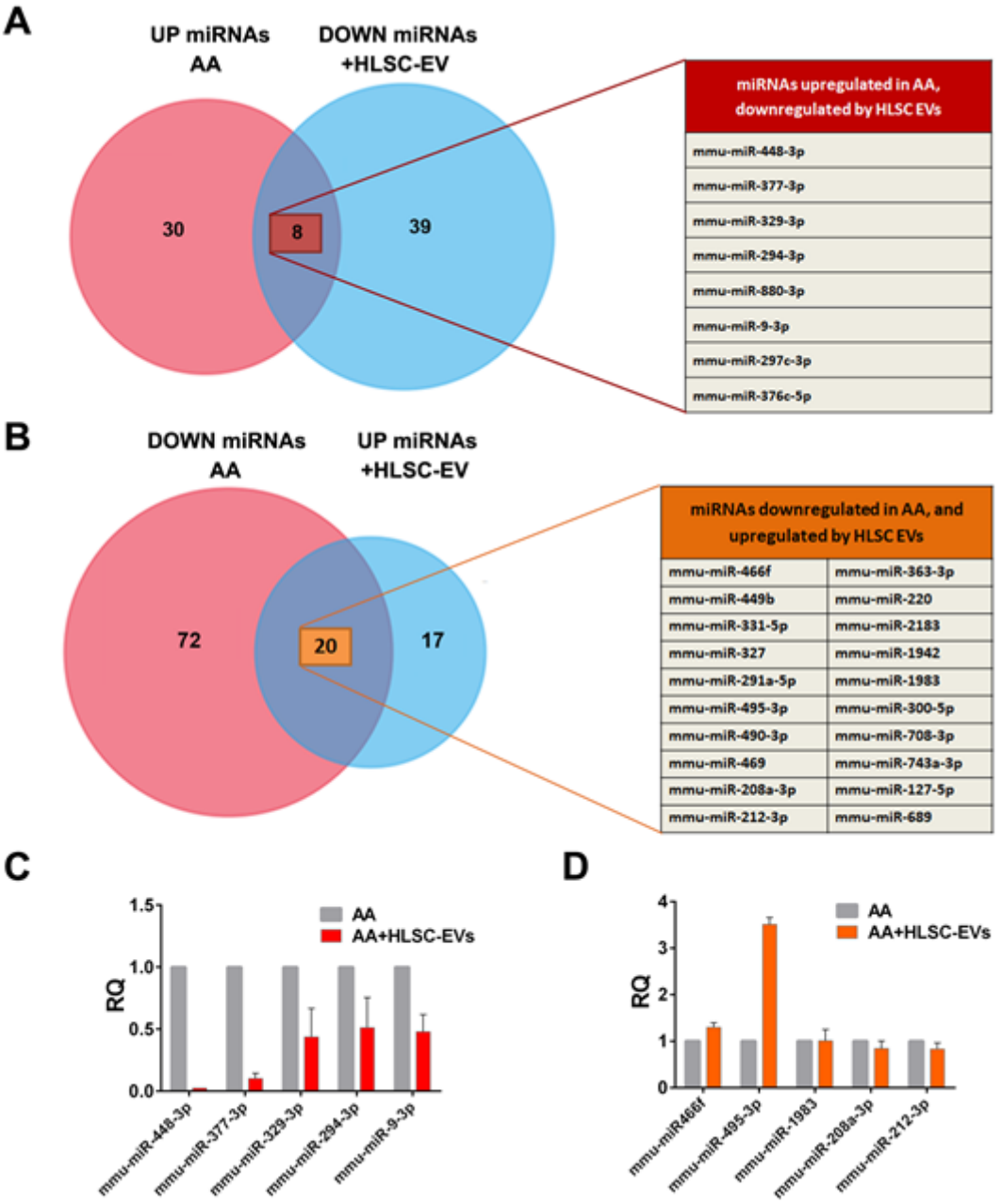

Figure 4.7. Venn diagram comparing miRNAs regulated by HLSC-EV treatment *in vivo* and *in vitro*. (A) 38 miRNAs were upregulated in mice treated with AA and 47 miRNAs were downregulated in AA mice treated with HLSC-EVs. Eight miRNAs were common between the two groups. **(B)** 92 miRNAs were downregulated in mice treated with AA and 37 were upregulated on treating the AA mice with HLSC-EVs. Twenty miRNAs were common between the two groups. n=3 mice/treatment**.** Expression levels of miRNAs regulated by HLSC-EVs *in vivo* were verified in fibroblasts co-cultured with AA pre-treated mTECs. Five were found to be downregulated *in vitro* **(C)**, and two miRNAs upregulated **(D)**. The data represent mean±SEM of three independent experiments performed in quadruplicate.

Pathways predicted by PANTHER online meta-analyses	No of genes involved
Wnt signalling pathway (P00057)	**104**
Inflammation mediated by chemokine and cytokine signalling pathway (P00031)	**70**
Angiogenesis (P00005)	58
Cadherin signalling pathway (P00012)	57
Integrin signalling pathway (P00034)	**53**
PDGF signalling pathway (P00047)	**52**
EGF receptor signalling pathway (P00018)	**43**
FGF signalling pathway (P00021)	**40**
Apoptosis signalling pathway (P00006)	38
Ras Pathway (P04393)	**34**
Endothelin signalling pathway (P00019)	31
T cell activation (P00053)	31
Interleukin signalling pathway (P00036)	**30**
Cytoskeletal regulation by Rho GTPase (P00016)	27
p53 pathway (P00059)	27
TGF-beta signalling pathway (P00052)	**27**
VEGF signalling pathway (P00056)	23
B cell activation (P00010)	21
Oxidative stress response (P00046)	19
p38 MAPK pathway (P05918)	18
Beta1 adrenergic receptor signalling pathway (P04377)	17
Beta2 adrenergic receptor signalling pathway (P04378)	17
PI3 kinase pathway (P00048)	17
Toll receptor signalling pathway (P00054)	17
Dopamine receptor mediated signalling pathway (P05912)	15
Insulin/IGF pathway-protein kinase B signalling cascade (P00033)	13
Hypoxia response via HIF activation (P00030)	12
FAS signalling pathway (P00020)	**11**
Histamine H1 receptor mediated signalling pathway (P04385)	11
Interferon-gamma signalling pathway (P00035)	11
Transcription regulation by bZIP transcription factor (P00055)	11
Angiotensin II-stimulated signalling through G proteins and beta-arrestin (P05911)	10
Insulin/IGF pathway-mitogen activated protein kinase kinase/MAP kinase cascade (P00032)	10
Histamine H2 receptor mediated signalling pathway (P04386)	9
Notch signalling pathway (P00045)	**9**
JAK/STAT signalling pathway (P00038)	**6**

Table 4.2: Panther gene ontology pathway analyses. Pathways regulated by miRNAs downregulated by HLSC-EVs in AA mice**.** Out of 141 pathways identified, 36 pathways have been selected on the basis of number of genes involved. Pathways highlighted in red have been implicated in kidney fibrosis.

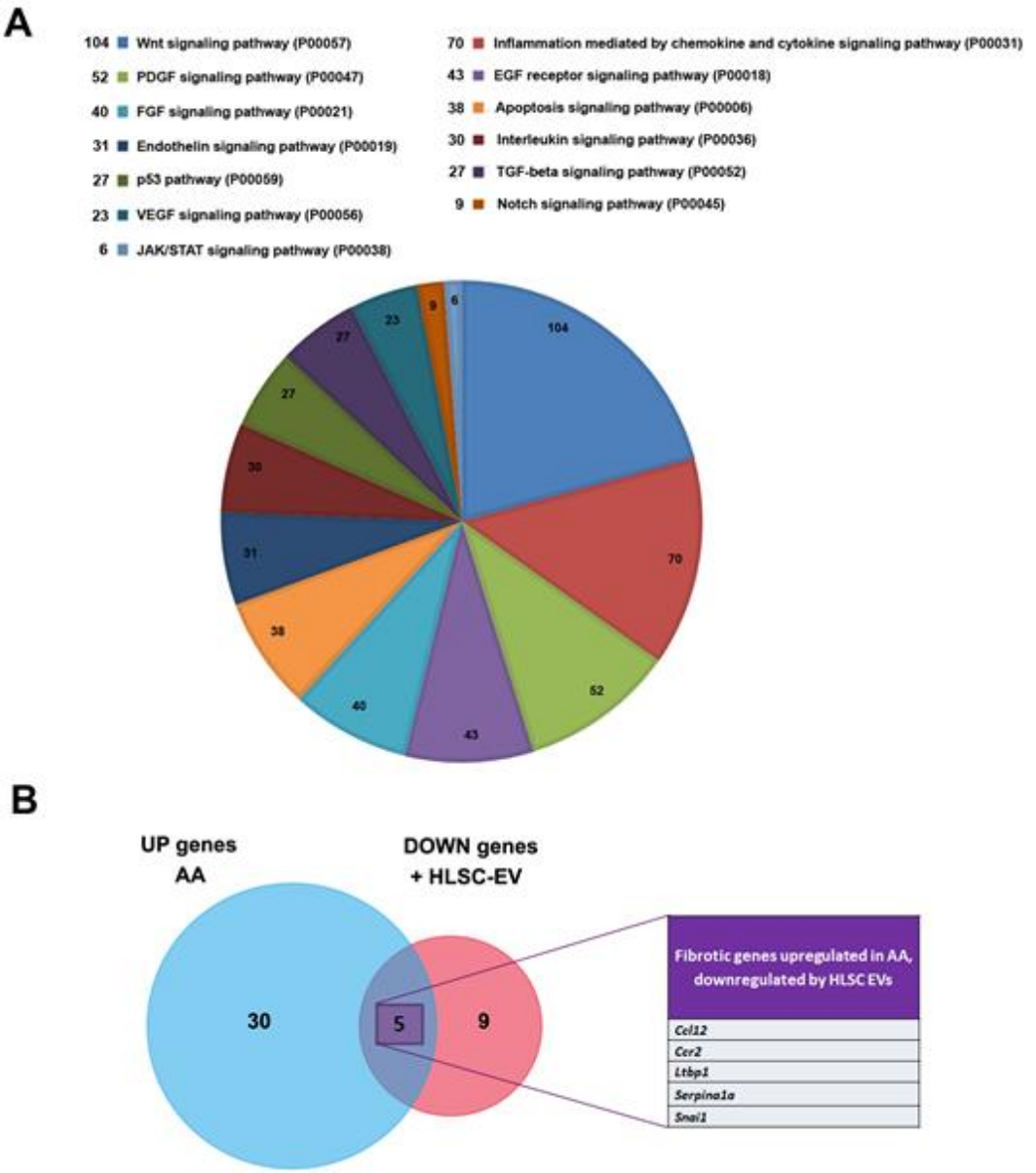

Figure 4.8. Panther pathway analyses of miRNAs regulated by HLSC-EVs and Venn diagram illustrating the pro-fibrotic. (A) Pie chart showing various pathways involved in the process of AA kidney injury as described in Table 2. Pathway analyses of miRNAs regulated by HLSC-EVs in AA mice showed the regulation of WNT signalling pathway, PDGF signalling pathway, FGF and TGFβ signalling pathway. **(B)** Venn diagram of pro-fibrotic regulated in mice treated with AA and in AA mice treated with HLSC-EVs showed 35 genes were upregulated in mice treated with AA and 14 genes were downregulated in AA mice treated with HLSC-EVs out of which 5 genes were upregulated by AA.

In order to understand the regulation of genes involved in fibrosis in the current AAN model, mice treated with AA in the presence or absence of HLSC-EVs were analysed through a Fibrosis RT^2 Profiler PCR array (Qiagen). Out of 84 genes in the array, 35 were found to be upregulated in mice treated with AA and 14 genes downregulated in HLSC-EV treated mice (**Figure 4.8B**, **Table 4.3**). On comparing the genes between the two experimental groups, 5 genes were found to be common (upregulated in AA treated mice and downregulated in HLSC-EV treated mice) (**Figure 4.8B**, **Table 4.3**). All together these results suggest that HLSC-EVs could mediate the progression and development of fibrotic events through the regulation of miRNAs and pro-fibrotic genes.

Genes upregulated in AA mice		Genes downregulated in HLSC-EV mice
Acta2	*Mmp14*	***Ccl12***
Cav1	*Mmp2*	***Ccr2***
Ccl11	*Mmp3*	*Egf*
Ccl12	*Mmp8*	*Fasl*
Ccl3	*Mmp9*	*Ifng*
Ccr2	*Myc*	*Il13*
Col1a2	*Plat*	*Il13ra2*
Col3a1	***Serpina1a***	*Inhbe*
Dcn	*Serpine1*	***Ltbp1***
Edn1	***Snai1***	*Plg*
Grem1	*Tgfb1*	***Serpina1a***
Hgf	*Tgfb2*	*Smad6*
Il1b	*Thbs1*	***Snai1***
Itga2	*Thbs2*	*Stat1*
Itga3	*Timp1*	
Jun	*Timp2*	
Lox	*Tnf*	
Ltbp1		

Table 4.3. Regulation of pro-fibrotic in mice treated with AA and AA treatment plus HLSC-EVs. Thirty five genes were upregulated in mice treated with AA. Fourteen genes were downregulated in AA mice treated with HLSC-EVs. Five genes were common between the two lists (highlighted in red).

4.2 **Discussion**

In the current study, we demonstrate that HLSC-EVs not only avert the development of interstitial fibrosis and tubular necrosis, but also favour renal regeneration in a CKD mouse model of AAN.

Bruno *et al* [28] first reported the beneficial effects of bone marrow MSC derived EVs on acute kidney injury (AKI). They showed that a single intravenous dose of MSC-EVs at the height of the damage was sufficient to alleviate morphological and functional impairment in a glycerol induced model of AKI [28]. Thereafter, several studies have reported the therapeutic role of stem cell derived EVs in different models of AKI. For instance, in a lethal model of cis-platin induced AKI, a single intravenous dose of MSC-EVs improved renal function and morphology, as a result increasing the overall survival rate of injured mice [30]. This effect was further enhanced by the administration of multiple doses of MSC-EVs [30]. In another study, human umbilical cord blood derived MSC-EVs reduced damage in a cis-platin-induced model of AKI both *in vivo* and *in vitro [76]*. Burger *et al.* [77] also observed a similar regenerative and therapeutic effect in their model of AKI, after administration of endothelial precursor cell derived EVs through the jugular vein. These studies and more therefore confirm that MSC derived EVs can exhibit therapeutic effects in various models of AKI regardless of the source or route of administration. Although, ample research has been done over the years on stem cell derived EVs in AKI, studies reporting the effect of EVs in CKD are limited [30, 78]. Nonetheless, one conclusion that can be made from these studies is the potential ability of MSC derived EVs to prevent CKD progression. For instance, in a rat model of ischemia-reperfusion-induced (IRI) chronic kidney injury, Gatti *et al.* showed that MSC-EVs, not only reduced elevated levels of blood urea nitrogen and creatinine but also prevented further progression to fibrosis therefore improving overall kidney function [79]. In a subsequent study, MSC-EVs reduced the infiltration of inflammatory cells by suppressing fractalkine (CX3CL1) in a similar model of IRI [80].

Although single doses of EVs were shown to be effective, multiple doses proved to be even more potent in CKD. For example, several injections of urine derived stem cell EVs prevented apoptosis of podocytes and tubular epithelial cells, and favoured proliferation of glomerular endothelial cells therefore, displaying an overall regenerative effect in a model of Type 1 diabetes [50]. Even though, HLSC-EVs have been shown to promote regeneration and recovery in AKI [36], no studies have been performed investigating their biological activity in CKD. Here we report for the first time the effect of HLSC-EVs in a severe AAN model of CKD in NSG mice.

One of the key features of CKD is loss of kidney function reflected by an abnormal rise in blood creatinine levels as has been reported in various models of CKD including AAN [2, 79, 81, 82]. The findings of the current study are in line with these reports as mice treated with AA had significantly elevated levels of plasma creatinine. In addition, treatment with HLSC-EVs significantly reduced elevated blood creatinine levels therefore confirming the ability of HLSC-EVs to improve renal function as observed previously in our model of AKI [36]. Another key factor in the progression of CKD is inflammation of the interstitium characterized by infiltrating immune and inflammatory cells following injury [7]. Depierreux et al [83] for instance reported the presence of lymphocytic infiltration in biopsies of patients with AAN and, later on this was confirmed by Pozdzik *et al.* [63, 84] both in human patients with AAN as well as in rats whereby an influx of activated mononuclear cells and cytotoxic T lymphocytes was observed in the renal interstitium following exposure to AA. A similar finding was also confirmed in another study, whereby the authors observed infiltration of CD45 positive immune cells in their mouse model of AAN [85]. An infiltration of CD45 positive cells was also observed in the present study thirty days after initiating the damage with AA. We therefore speculate that, these cells are likely to be part of the innate immune system (monocytes and neutrophils) as NSG mice lack lymphocytes and natural killer cells and have defective macrophages and dendritic cells due to their genetic background [61]. Interestingly, AA mice treated with HLSC-EVs had lower counts of CD45

mononuclear cells, therefore suggesting an immune/anti-inflammatory role of these HLSC-EVs not been reported previously in CKD.

Another key feature of CKD and AAN is tubular damage and hyaline cast formation [85-87]. Proximal tubular necrosis together with cast formation was also observed in our model representing the predominant lesions observed. Treatment with HLSC-EVs however, significantly reduced tubular necrosis as well as increased the number of proliferating cells as confirmed by PCNA staining therefore demonstrating regeneration and recovery of damaged renal tissue. Indeed, these tissue healing properties of HLSC-EVs in particular have been reported in an AKI model previously [36]. The observation of similar effects in a model of CKD is novel.

Regardless to the cause of insult, interstitial fibrosis is the final common process that defines CKD and is characterized by the activation of fibroblasts and the progressive accumulation of extracellular matrix mainly collagen [7, 85]. In this study, an increase in the infiltration/activation of fibroblasts in the renal interstitium was observed which correlated with an increase in collagen type 1 in mice exposed to AA. These findings were consistent with what has been reported in other models of AAN [60, 63, 84, 85] in particular Huang *et al.* [85] who also reported an increase in FSP-1 positive cells in a chronic mouse model of AAN. Moreover, treatment with HLSC-EVs significantly reduced the percentage of fibroblasts, as well as collagen deposition in the renal interstitium. A similar result was also observed at a molecular level whereby expression of the pro-fibrotic genes *α-Sma*, *Col1a1*, and *Tgfb1* were significantly reduced in AA mice renal tissue treated with HLSC-EVs. This result was further supported by *in vitro* data whereby HLSC-EVs downregulated the pro-fibrotic genes mentioned above, in renal cortical fibroblasts co-cultured with AA exposed mTECs. This finding, therefore suggests a novel role of HLSC-EVs as mediators of fibroblast activation.

TGFβ is known to play a key role in the developmental process of fibrosis in various models of CKD including AAN [52, 60, 63, 88]. Not only is it involved in the synthesis of ECM, and prevention of its degradation, but also in the

activation of fibroblasts to myofibroblasts [7]. We therefore, investigated the molecular basis of TGFβ signaling that lead to the development of fibrosis, and whether, the healing effect of HLSC-EVs in the current model could be due to the regulation of the genes governed by this pathway. Thirty genes related to fibrosis were identified to be upregulated in mice treated with AA. Some of these genes such as: *Cav1, Dcn, Grem1, Ltbp1, Tgfb1* etc. are part of the TGFβ superfamily including 2 genes (*Jun* and *Myc*) that code for transcription factors involved in the pathway. On the other hand, 14 pro-fibrotic genes in total were identified to be downregulated in mice treated with HLSC-EVs, out of which 5 were initially upregulated in AA mice (Table 2). These 14 genes have been linked with the regulation of various pathways dysregulated during fibrosis including: cytokine and chemokine pathways, growth factors, regulation of the ECM etc.

Out of the five pro-fibrotic genes downregulated by HLSC-EVs, *Ccr2* and *Ccl12* code for inflammatory chemokines that have a receptor ligand relationship and have been implicated in fibrosis. For instance, Moore *et al.* [89] showed that, mice genetically deficient in *Ccr2* gene were protected from lung fibrosis. Furthermore, neutralization of *Ccl12* in wild type mice significantly protected them from FITC-induced lung fibrosis by thwarting the recruitment of fibrocytes [89]. Similarly in another study, the blocking of *Ccr2,* either through gene silencing or inhibitors reduced renal interstitial fibrosis in a UUO mouse model mainly through the downregulation of TGFβ, and collagen type 1 at a molecular and protein level [90] as was observed in our model. Another gene that was downregulated following treatment with HLSC-EVs was snail family zinc finger 1 (*Snai1*). This gene codes for the transcription factor SNAI1 that is very well known to mediate biological processes involved in renal fibrogenesis including EMT of tubular epithelial cells and inflammation [91]. Furthermore, it has also been reported to be upregulated in the kidney tissue of patients with various types of progressive nephropathy [92].

Latent-transforming growth factor beta-binding protein 1 (*LTBP1*) is a gene that codes for the LTBP1 protein. TGFβ is normally secreted as a latent form comprised of three components: the mature TGFβ dimer, the latency associated peptide (LAP), and LTBP [93]. LTBP1 not only facilitates the formation and release of latent TGFβ, but is also involved in the activation of the cytokine. In fact, both TGFβ and LTBP1 were found to be upregulated in patients with idiopathic lung fibrosis [94]. In line with this report, we also observed an upregulation of both *Ltbp1* and *Tgfb1* genes in mice renal tissue exposed to AA. However, following treatment with HLSC-EVs significantly reduced the expression levels of both genes. As LTBP1 is important for the activation of TGFβ, this finding could provide an insight on how HLSC-EVs mediate the downregulation of TGFβ1 particularly in our model of AAN.

MicroRNAs (miRNAs) are small, single strand, non-coding RNAs that regulate gene expression by suppressing or degrading target mRNA at a post-transcriptional level [95]. They have been implicated in various physiological and pathological processes including fibrosis [95]. We therefore investigated the regulation of miRNAs in mice injured with AA and AA mice treated with HLSC-EVs. After identifying the common miRNAs that were inversely correlated between AA mice and mice treated with HLSC-EVs, the genes and pathways that were regulated by these miRNAs were analysed. Online bioinformatics analyses revealed over 7000 genes that were regulated by these miRNAs. Panther pathway analyses linked these genes to 141 pathways out of which the top 36 pathways (ranked according to the number of genes involved per pathway; Table 2) were included in this study. Out of the pathways identified, quite a few have been implicated in fibrosis such as the WNT signaling pathway [17], inflammatory cytokine and chemokine pathways [96], as well as PDGF, FGF, and TGFβ pathways [97]. Through this study, we have shown the ability of HLSC-EVs to exhibit a therapeutic potential by influencing the process of CKD progression at multiple levels. This is mainly attributed to the plethora of biologically active molecules enriched in them that work synergistically inhibiting injury progression as well as simultaneously activating the repair process.

Nonetheless, it is this enrichment of diverse molecules that makes it challenging to dissect the key mechanisms of action that contribute to the therapeutic effects observed.

4.3 **Conclusion**

Taken together, we demonstrate for the first time the therapeutic properties of HLSC-EVs in a model of CKD. We report that multiple doses of HLSC-EVs exhibit regenerative, anti-fibrotic and anti-inflammatory properties in a mouse model of AAN characterized by severe tubular epithelial cell necrosis and interstitial fibrosis. Furthermore, down regulation of pro-fibrotic genes and modulation of miRNAs that regulate the fibrotic pathways could be a mechanism through which HLSC-EVs exert their biological activity. These findings may promote the development of new therapeutic strategies involving HLSC-EVs in CKD.

5. HLSC-EVs alleviate kidney fibrosis by partially interfering with the β-catenin pathway

5.1 **Results**

5.1.1 The expression of active β-catenin is reduced in AA mice treated with HLSC-EVs

As the gene pathway analysis performed on the kidneys of AAN mice experimental groups treated with or without HLSC-EVs revealed the β-catenin signaling pathway from among the signaling pathways regulated by HLSC-EVs, we investigated the expression of active β-catenin which is the primary component of the WNT-β-catenin pathway in the kidneys of these AAN experimental groups.

Immunohistochemical staining of kidney FFPE sections showed that mice treated with AA had significantly elevated levels of active β-catenin compared to healthy controls which was significantly reduced following treatment with HLSC-EVs (**Figure 5.1A and B**). In addition, a similar trend was observed at the molecular level whereby the gene expression of Ctnnb1, which encodes for β-catenin, was upregulated in AA mice compared to healthy controls and was significantly downregulated following treatment with HLSC-EVs (**Figure 5.1C**).

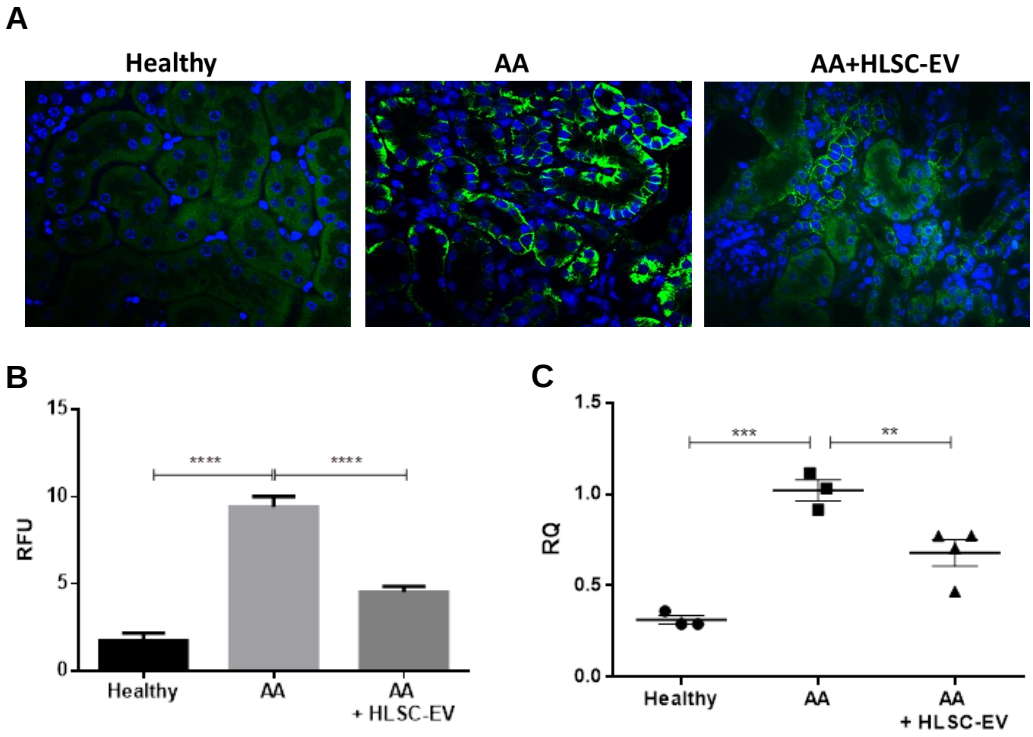

Figure 5.1. β-catenin active is downregulated by HLSC-EVs in AAN. A) Representative micrographs showing the expression of active β-catenin upregulated in mice treated with AA which was significantly downregulated following treatment with HLSC-EVs. (Original magnification: 200X). **B**) Histogram depicting the relative fluorescence intensity of active β-catenin in AAN mice experimental groups. Data represent mean ± SD of the fluorescence intensity per high power field measured from 10 images taken at random from four samples per treatment (n=4 mice). ****p<0.0001 AA vs Healthy and AA vs AA+HLSC-EV. **C**) Gene expression level of *Ctnnb1* (β-catenin) in mouse kidney tissue from AAN mice experimental groups. **p<0.01, ***p<0.001 AA vs Healthy and AA vs AA+HLSC-EV. (n=3 mice for healthy and AA, and n=4 mice for AA+HLSC-EV).

5.1.2 Expression of β-catenin in mouse renal fibroblasts in an AAN model *in vitro*

In order to investigate whether the regulation of β-catenin is one mechanism by which HLSC-EVs mediates fibrosis in renal fibroblasts, we investigated the expression of β-catenin in renal cortical fibroblasts co-cultured with mTECs pre-exposed to AA in a transwell system. Post experimental analysis revealed a significant upregulation of the β-catenin gene Ctnnb1 expression as well as the pro-fibrotic gene α-Sma in fibroblasts exposed to mTECs pre-treated with AA compared to control (**Figure 5.2A, and B**). Following

treatment with HLSC-EVs the upregulation of both the genes was significantly reduced to near normal level (**Figure 5.2A, and B**). A similar trend was also observed at the protein level whereby the expression of both active β-catenin and α-SMA was significantly elevated in fibroblasts exposed to mTECs pre-treated with AA (**Figure 5.2C, and D**). Again, HLSC-EVs significantly reduced β-catenin and α-SMA protein expression (**Figure 5.2C, and D**) therefore confirming that HLSC-EV treatment regulate β-catenin activity in fibroblasts *in vitro*.

5.1.3 Silencing of β-catenin in mkCF fibroblasts

In order to investigate the relevance of β-catenin in the activation of fibroblasts to myofibroblasts, we sought to silence the Ctnnb1 gene that codes for β-catenin using short interfering RNA (siRNA). Briefly, mkCF cells were co-incubated with the transfection complex containing DMEM, HiPerfect transfection reagent and 20nM of Ctnnb1 siRNA for 72 h at 37ºC. In selected experiments, the media was replaced at day three and cells cultured for a further 4 days to assess the efficiency of inhibition by the siRNA for the duration of the AAN in vitro assay. Post experimental analysis revealed a significant downregulation of the Ctnnb1 gene by the respective siRNA after 72 h and 7 days post transfection compared to control siRNA (**Figure 5.3 A**). In addition, a significant inhibition of β-catenin was observed at a protein level 7 days post transfection in fibroblasts transfected with Ctnnb1 siRNA compared to fibroblasts transfected with control siRNA (**Figure 5.3 B**).

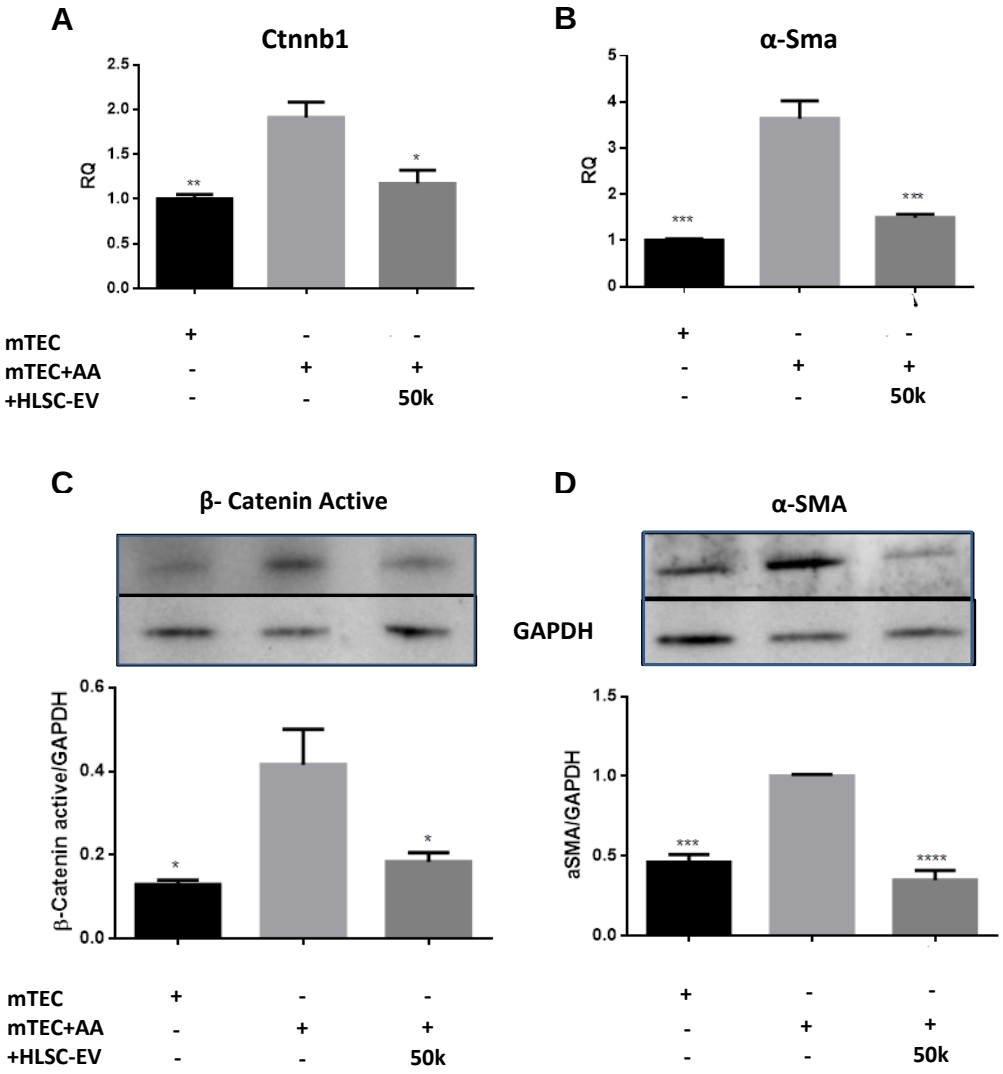

Figure 5.2. HLSC-EVs downregulate β-catenin and pro-fibrotic marker in mkCF in an in vitro model of AAN. mTECs pre-treated with 100 µM AA for 4 h were cocultured with mkCF in the presence or absence of HLSC-EVs. Post experimental analysis revealed an upregulation of the genes Ctnnb1 (β-catenin) **(A)** and the profibrotic marker α-Sma **(B)** in mkCF cells exposed to AA treated mTECs. Treatment with HLSC-EVs downregulated both the genes significantly. Western blot analysis further revealed an upregulation of active β-catenin **(C)** and α-Sma **(D)** at a protein level in mkCF exposed to AA treated mTECs. Treatment with HLSC-EVs significantly downregulated both the proteins significantly. The data represents mean ± SEM of three independent experiments performed in quadruplicate. *p < 0.05, **p < 0.01, ***p < 0.001, **** < 0.0001 vs mTEC+AA. A one-way analyses of variance with Bonferroni's multi comparison test was performed.

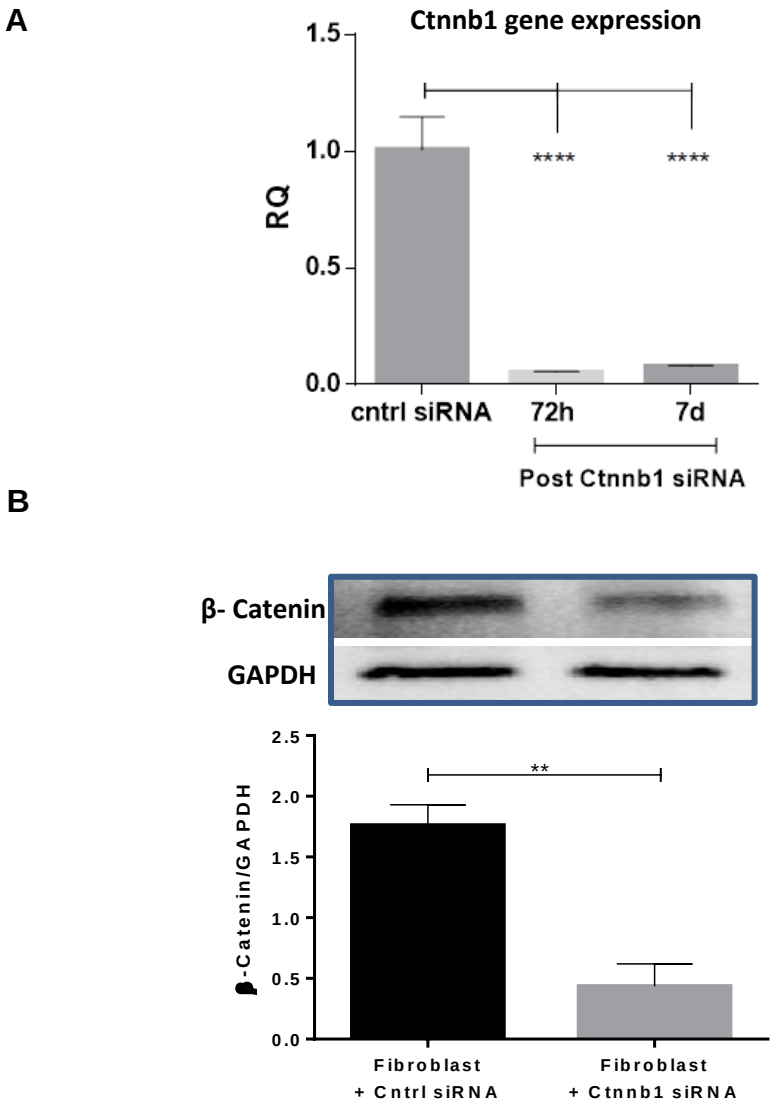

Figure 5.3. Silencing of Ctnnb1 gene in mkCF cells. mkCF cells were transfected with Ctnnb1 siRNA for 72 hours and then cultured for a further 4 days (7d in total post transfection) after which the cells were subjected to molecular and protein analyses. **(A)** RT-PCR analysis revealed a significant inhibition of Ctnnb1 gene 72 hrs and 7 days post transfection compared to control siRNA. **(B)** Western blot analyses revealed a significant donwregulation of β-catenin 7 days post transfection. ** $p < 0.01$, **** $p < 0.0001$ was considered statistically significant. Data represents mean ± SEM of three independent experiments.

5.1.4 Gene silencing of β-catenin prevents the molecular activation of fibroblasts in AAN in vitro assay

In order to investigate the role of β-catenin in the activation of fibroblasts to myofibroblasts as observed in the process of fibrosis, both wild type and mkCF cells silenced for β-catenin were co-incubated with mTECs pre-exposed to AA in a transwell system in the presence or absence of HLSC-EVs for 5 days at 37ºC. Post experimental analysis revealed a significant rise in the expression of the pro-fibrotic genes αSMA and Col1a1 in wild type mkCF fibroblasts which was downregulated following treatment with HLSC-EVs as observed previously (**Figure 5.4 A, and B**).

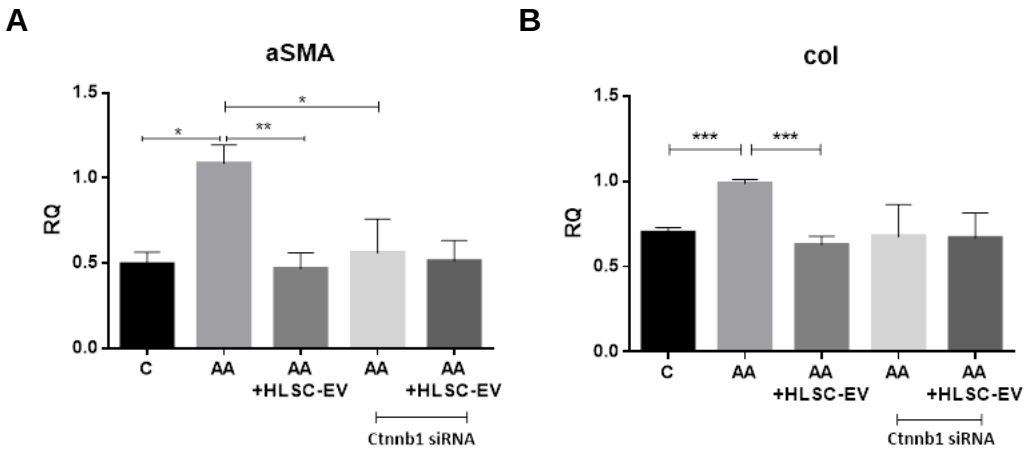

Figure 5.4. Slencing of β-catenin prevents the upregulation of profibrotic genes in fbroblasts *in vitro.* mTECs pre-treated with 100 µM AA for 4 h were cocultured with mkCF or mkCF silenced for Ctnnb1 gene in the presence or absence of HLSC-EVs. Post experimental analysis revealed a significant upregulation of the profibrotic genes: α-Sma **(A)** and Col1a1 **(B)** in fibroblasts exposed to AA treated mTECs which was significantly reduced in the presence of HLSC-EVs. No signifcant upregulation of both profibrotic genes was observed in fibroblast silenced for the Ctnnb1 gene that codes for β-catenin in the presence or absence of HLSC-EVs when compared to control. Data represents the mean ± SD of three independent experiments. A one-way ANOVA with Bonferroni's comparison test was performed. * $p < 0.05$, *** $p < 0.001$ was considered to be statistically significant.

Interestingly, for mkCF fibroblasts silenced for β-catenin, no significant upregulation of both α-Sma and Col1a1 was observed following co-incubation with mTECs pre-exposed to AA. In addition, treatment with HLSC-EVs had no significant effect as well (**Figure 5.2 A, and B**) therefore

confirming the importance of β-catenin in fibroblast activation in an *in vitro* AAN model of fibrosis.

5.1.5 HLSC-EVs could potentially regulates β-catenin through mir29b

In order to elucidate the mechanism by which HLSC-EVs regulates the fibrotic process and in particular β-catenin, we investigated the potential involvement of miR29b. Real time PCR analysis showed a significant upregulation of miR29b in AAN mice kidney tissue treated with HLSC-EVs (**Figure 5.5 A**).

The next step was therefore to investigate if HLSC-EVs directly transferred or induced the transcription of miR29b in recipient cells. It is also very well known in the literature [84] that one of the culprits involved in AAN induced fibrosis is TGFβ1 which is also known to downregulate various anti-fibrotic miRNA such as miR29. Hence, mkCF fibroblasts pre-seeded overnight were treated with TGFβ1 in the presence or absence of HLSC-EVs or in the presence of HLSC-EVs together with the transcription inhibitor α-amanitin for 6 hrs at 37°C. Post experimental analysis revealed a significant downregulation of miR29b in fibroblasts following treatment with TGFβ1 which was significantly increased in the presence of HLSC-EVs (**Figure 5.5 B**). However, treatment of HLSC-EVs in the presence of α-amanitin did not increase the expression of miR29b in fibroblasts (**Figure 5.5 B**) therefore suggesting that HLSC-EVs-mediated miR29b upregulation could be due to induction rather than its horizontal transfer.

In order to understand whether miR29b induced by HLSC-EVs played a role in inhibiting β-catenin and other pro-fibrotic genes such as α-Sma and Col1a1, we performed the AAN in vitro assay. To this end fibroblasts co-cultured with mTECs pre-exposed to AA were co-treated with HLSC-EVs and antimir29b, which is known to inhibit the transcription of miR29b in the cell. Co-treatment with a scramble sequence of antimiR (antimiR SCR) served as control. Post experimental analysis revealed an increase in miR29b expression in fibroblasts following treatment with HLSC-EVs which was

significantly downregulated in the presence of antimir29b. These results further confirmed the contribution of HLSC-EVs in the transcription of miR29b in fibroblasts (**Figure 5.5 C**). No significant downregulation was observed in miR29b in fibroblasts co-treated with HLSC-EVs and antimir SCR (**Figure 5.5 C**). Furthermore, analyzing the expression of the β-catenin gene Ctnnb1 and the profibrotic genes α-Sma and Col1a1 showed some interesting results. Although, treatment with HLSC-EVs significantly downregulated the expression of all three genes in fibroblasts as expected, the presence of antimir29b nullified the effects of HLSC-EVs in downregulating Ctnnb1 (**Figure 5.5 D**). Although a similar effect was observed in the profibrotic genes α-Sma and Col1a1, the inhibition was not as strong as observed with β-catenin. No significant inhibitory effect was observed with antimiR SCR (**Figure 5.5 D**). These data therefore identify miR29b as a potential regulator of β-catenin and a likely mechanism by which HLSC-EVs indirectly impacts on the expression of β-catenin and the other profibrotic genes investigated in our model.

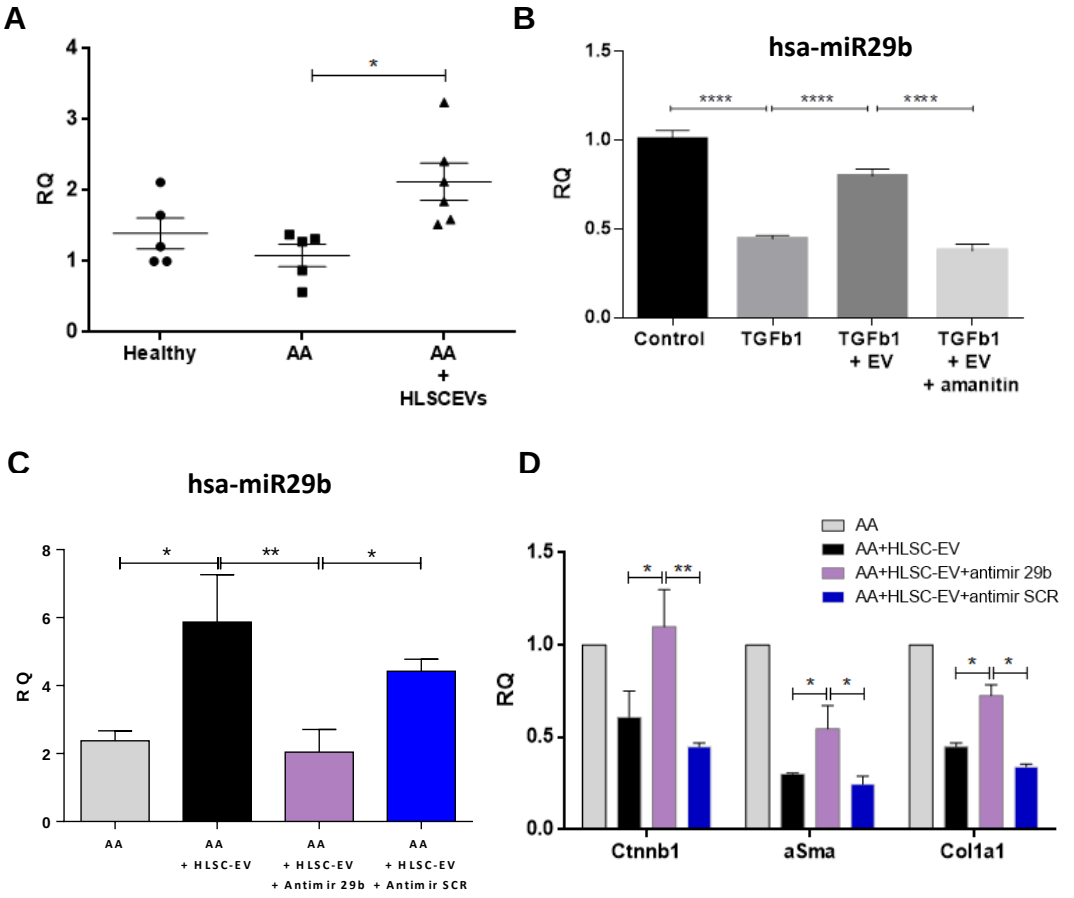

Figure 5.5. HLSC-EVs potentialy regulate β-catenin through miR29b. **A)** The expression of miR29b in AAN mice experimental groups. A significant upregulation of miR29b is observed in AAN mice treated with HLSC-EVs.* p<0.05, (n= 5 mice per group). **(B)** RT-PCR showing the expression of miR29b in fibroblasts treated with TGFb1 alone or TGFb1 with HLSC-EVs, or with TGFb1 with HLSC-EVs in the presence of α-Amanitin for 6 h at 37°C. Post experimental analysis revealed a significant reduction in miR29b following treatment with TGFb1 which was upregulated in the presence of HLSC-EVs. HLSC-EV treatment in the presence of α-Amanitin showed no significant increase in the expression of miR29b therefore confirming HLSC-EVs to induce the transcription of miR29b. ****p<0.0001 was considered statistically significant. **(C)** The expression of miR29b in fibrobroblasts co-cultured with mTECs pre-treated with AA increased following treatment with HLSC-EVs and was significantly reduced in the presence of antimiR29b. *p<0.05, **p<0.01 was considered to be statistically significant. **(D)** The expression of β-catenin and pro-fibrotic genes in fibroblasts co-cultured with mTECs pretreated with AA, in the presence or absence of HLSC-EVs, or HLSC-EVs together with antimir 29b, or HLSC-EVs with antimir SCR. *p<0.05, **p<0.001 were considered to be statistically significant. Data represents mean±SD of three independant experiments.

5.2 **Discussion**

In the last two chapters we have reported the therapeutic effects of both MSC-EVs and HLSC-EVs in a CKD model of AAN. Both EV treatments exhibited anti-inflammatory, anti-fibrotic, and regenerative effects on the kidneys of AAN mice improving overall the kidney function. Various miRNAs and genes were reported to be regulated following EV treatment and bioinformatic analysis performed on the kidney tissues revealed that the Wnt/β-catenin pathway was one of the most expressed from among the predicted pathways regulated by EVs. In this study, we therefore sought to investigate the potential role of the Wnt/β-catenin pathway in the activation of fibroblast and progression of fibrosis in a CKD model of AAN as well elucidate how mechanistically HLSC-EVs regulate this pathway.

The Wnt/β-catenin pathway is an evolutionary pathway involved in regulating a variety of biological processes including organ development, tissue homeostasis and repair as well as in disease pathogenesis [20]. In the kidney, this pathway is mainly involved in nephron formation during mammalian development, and becomes dormant thereafter. However, there is sufficient research to suggest the reactivation of the Wnt/β-catenin pathway often entwined with other signalling pathway during kidney injury. For instance, Dai et al *[98]* have reported the upregulation of the Wnt/β-catenin pathway in glomerular podocytes following injury both *in vivo* and *in vitro.* Through their in vivo Adriamycin nephropathy mouse model, they observed an upregulation of Wnt proteins as well as active β-catenin in the glomeruli of mice treated with Adriamycin. In vitro, they demonstrated that, inhibition of Wnt signalling through DKK1 ameliorated podocytes dysfunction [98]. Surendran et al [99] reported the activation of the Wnt/β-catenin signalling through the upregulation of active β-catenin in renal tubular epithelial and interstitial cells following UUO injury in mice. This was confirmed by He et al (He, Dai et al. 2009), who reported the upregulation of Wnt and Fzd receptors resulting in the accumulation of β-catenin and the activation of its target genes in a similar model of UUO. In addition,

administration of DKK1 gene in vivo reduced the accumulation of β-catenin and attenuated interstitial fibrosis in the kidneys of mice subjected to UUO. In line with these findings, we also demonstrated an increased expression of Ctnnb1 gene (codes for β-catenin) and the active β-catenin in the renal interstitium of mice exposed to AA. Furthermore, treatment with HLSC-EVs significantly reduced the expression of active β-catenin both at a molecular and protein level. This effect was further confirmed in the *in vitro* model of AAN whereby activated fibroblasts treated with HLSC-EVs also expressed significantly lower levels of β-catenin and α-SMA both at a molecular and protein level. This finding therefore identifies a novel mechanism through which HLSC-EVs could interfere with fibrosis.

The importance of β-catenin in the activation of fibroblasts has been extensively documented. For instance, it has been reported that the inhibition of β-catenin signalling prevented the differentiation and activation of lung resident mesenchymal cells into myofibroblasts [100]. In a different study, silencing of the β-catenin gene attenuated TGFβ-1 induced upregulation of α-SMA, collagen type 1 and fibronectin in corneal fibroblasts [101]. A similar effect was observed in our study whereby wild type fibroblasts that were exposed to AA injured mTECs showed a significant upregulation of the pro-fibrotic genes α-SMA and Col1a1 compared to controls. On the other hand, fibroblasts silenced for the Ctnnb1 gene did not show any significant upregulation of both the pro-fibrotic genes when co-cultured with AA injured mTECs. These data therefore confirm the importance of β-catenin in the activation of myofibroblasts regardless of source of fibroblast or mode of injury.

MicroRNAs (miRNA) are a single stranded non coding RNA molecules mainly involved in regulating gene expression [102]. Notably, miRNAs have been increasingly demonstrated to act as key regulators of genes involved in the pathophysiology of various diseases including kidney fibrosis [46, 103]. Evidences from clinical studies and pre-clinical models suggest the anti-fibrotic effects of miR29. There is also growing body of evidence on the role

of the miR29 family, composed of three extremely similar orthologs (miR29a, miR29b, and miR29c) sharing identical seed binding sequence and the ability to bind identical set of target genes [104]. Findings from clinical and pre-clinical studies suggest a role of miR29 in fibrosis. Generally abundant in healthy kidney tissue, several studies have demonstrated a low miR29 expression in different animal models of fibrosis. For instance, Xiao et al [105] observed a downregulation of miR29 in a bleomycin induced model of pulmonary fibrosis, while Qin et al [106] reported a similar downregulation in a UUO mouse model of kidney injury. In line with these results, we also observed a downregulation of miR29b in mice exposed to AA. Moreover, in accordance with the result obtained by Fan et al and Huang et al [107, 108] we also found a downregulation of miR29b expression in fibroblasts *in vitro* treated with TGF-β1. Interestingly, mice that were treated with HLSC-EVs expressed significantly high levels of miR29b compared to AA mice. A similar result was observed in vitro whereby, HLSC-EVs upregulated expression of miR29b in TGF-β1 exposed fibroblasts as well as in fibroblasts exposed to AA treated mTECs. This upregulation of miR29b was inhibited in the presence of the transcription inhibitor α-amanitin as well as in the presence of antiMir29b. These data therefore, confirm the ability of HLSC-EVs to upregulate miR29b primarily through its induction in fibroblasts.

The anti-fibrotic effect of miR29 has been extensively reported. Several studies have shown miR29 to alleviate fibrosis by targeting genes contributing to the ECM [104, 108] ,as well as, by regulating the TGF-β1 signalling pathway downstream [106]. In a recent by study Huang et al [108], it has been shown that miR29c alleviates renal fibrosis *in vivo* as well as inhibits the transition of fibroblasts to myofibroblasts via the Wnt/β-catenin pathway and TMP1. In our *in vitro* model we observed an upregulation of miR29b in fibroblasts exposed to AA injured mTECs following treatment with HLSC-EVs. In addition, a significant downregulation in the Ctnnb1 gene and in the α-SMA and Col1a1 pro-fibrotic genes has been noticed. Of note, in the presence of antimiR29b, the HLSC-EVs effect was abrogated as a significant upregulation of Ctnnb1, α-SMA, and Col1a1 was observed. Taken together

these data suggest that one mechanism by which HLSC-EVs interfere with fibrosis is linked to inhibition of the Wnt/β-catenin pathway and the induction of miR29b both *in vivo* and in fibroblasts *in vitro*. Nonetheless, the mechanism by which HLSC-EVs induce the expression of miR29b driving the inhibition of the Wnt/β-catenin pathway requires further studies.

5.3 **Conclusion**

In the current study we show for the first time, the involvement of the Wnt/β-catenin pathway in the process of fibrosis in a CKD model of AAN. In particular, we have shown the overexpression of β-catenin in AA mice as well as in fibroblasts exposed to AA injured mTECs, and that this effect is rescued after HLSC-EV treatment. Furthermore, we have also shown the upregulation of the anti-fibrotic miR29b following treatment with HLSC-EVs *in vivo* and *in vitro*. Blocking of this miRNA impeded the anti-fibrotic effects of HLSC-EVs and significantly increased the expression of β-catenin and other pro-fibrotic genes in an in vitro model of AAN. Taken together our data suggest a potential involvement of the Wnt/β-catenin pathway in fibrosis and provide evidence for the mechanistic anti-fibrotic action of HLSC-EVs observed in AAN *in vitro* and *in vivo*.

Although the implementation of EVs in CKD as a form of alternative therapy is very lucrative, various hurdles need to be overcome to allow transferring of EV therapy from bench to bedside. These include producing EVs at a large scale in GMP conditions, the pharmacodynamics and pharmacokinetics of EVs, as well as toxicity and host immune reaction to stem cell derived EVs post inoculation.

6. References

1. Coresh, J., et al., *Prevalence of chronic kidney disease in the United States.* JAMA, 2007. **298**(17): p. 2038-47.

2. Sun, D., et al., *Therapeutic effects of human amniotic fluid-derived stem cells on renal interstitial fibrosis in a murine model of unilateral ureteral obstruction.* PLoS One, 2013. **8**(5): p. e65042.

3. Shea, M.K. and S.L. Booth, *Vitamin K, Vascular Calcification, and Chronic Kidney Disease: Current Evidence and Unanswered Questions.* Curr.Dev.Nutr., 2019. **3**(9): p. nzz077.

4. Kurzhagen, J.T., et al., *AKI: an increasingly recognized risk factor for CKD development and progression.* J Nephrol, 2020. **33**(6): p. 1171-1187.

5. Rabe, M. and F. Schaefer, *Non-Transgenic Mouse Models of Kidney Disease.* Nephron, 2016. **133**(1): p. 53-61.

6. Han, J., et al., *Systematic Overview of Aristolochic Acids: Nephrotoxicity, Carcinogenicity, and Underlying Mechanisms.* Front Pharmacol., 2019. **10**: p. 648.

7. Jadot, I., et al., *An Integrated View of Aristolochic Acid Nephropathy: Update of the Literature.* Int J.Mol Sci., 2017. **18**(2).

8. Jelakovic, B., et al., *Balkan Endemic Nephropathy and the Causative Role of Aristolochic Acid.* Semin.Nephrol., 2019. **39**(3): p. 284-296.

9. Panizo, S., et al., *Fibrosis in Chronic Kidney Disease: Pathogenesis and Consequences.* Int J Mol Sci, 2021. **22**(1).

10. Djudjaj, S. and P. Boor, *Cellular and molecular mechanisms of kidney fibrosis.* Mol Aspects Med, 2019. **65**: p. 16-36.

11. Liu, Y., *Cellular and molecular mechanisms of renal fibrosis.* Nat Rev Nephrol, 2011. **7**(12): p. 684-96.

12. Miao, H., et al., *Deciphering the cellular mechanisms underlying fibrosis-associated diseases and therapeutic avenues.* Pharmacol Res, 2021. **163**: p. 105316.

13. Ovadya, Y. and V. Krizhanovsky, *A new Twist in kidney fibrosis.* Nat Med, 2015. **21**(9): p. 975-7.

14. Wang, N., et al., *Novel Mechanism of the Pericyte-Myofibroblast Transition in Renal Interstitial Fibrosis: Core Fucosylation Regulation.* Sci Rep, 2017. **7**(1): p. 16914.

15. Piersma, B., R.A. Bank, and M. Boersema, *Signaling in Fibrosis: TGF-beta, WNT, and YAP/TAZ Converge.* Front Med (Lausanne), 2015. **2**: p. 59.

16. Isaka, Y., *Targeting TGF-beta Signaling in Kidney Fibrosis.* Int J Mol Sci, 2018. **19**(9).

17. Tan, R.J., et al., *Wnt/beta-catenin signaling and kidney fibrosis.* Kidney Int Suppl (2011), 2014. **4**(1): p. 84-90.

18. Zhou, D., et al., *Wnt/beta-catenin signaling in kidney injury and repair: a double-edged sword.* Lab Invest, 2016. **96**(2): p. 156-67.

19. Zuo, Y. and Y. Liu, *New insights into the role and mechanism of Wnt/beta-catenin signalling in kidney fibrosis.* Nephrology (Carlton), 2018. **23 Suppl 4**: p. 38-43.

20. He, W., et al., *Wnt/beta-catenin signaling promotes renal interstitial fibrosis.* J Am Soc Nephrol, 2009. **20**(4): p. 765-76.

21. Bruno, S., et al., *The Role of Extracellular Vesicles as Paracrine Effectors in Stem Cell-Based Therapies.* Adv Exp Med Biol, 2019. **1201**: p. 175-193.

22. Raposo, G. and P.D. Stahl, *Extracellular vesicles: a new communication paradigm?* Nat Rev Mol Cell Biol, 2019. **20**(9): p. 509-510.

23. van Niel, G., G. D'Angelo, and G. Raposo, *Shedding light on the cell biology of extracellular vesicles.* Nat Rev Mol Cell Biol, 2018. **19**(4): p. 213-228.

24. Valadi, H., et al., *Exosome-mediated transfer of mRNAs and microRNAs is a novel mechanism of genetic exchange between cells.* Nat.Cell Biol., 2007. **9**(6): p. 654-659.

25. Burrello, J., et al., *Stem Cell-Derived Extracellular Vesicles and Immune-Modulation.* Front Cell Dev Biol, 2016. **4**: p. 83.

26. Grange, C., et al., *Stem Cell-Derived Extracellular Vesicles and Kidney Regeneration.* Cells, 2019. **8**(10).

27. Jafarinia, M., et al., *Mesenchymal Stem Cell-Derived Extracellular Vesicles: A Novel Cell-Free Therapy.* Immunol Invest, 2020. **49**(7): p. 758-780.

28. Bruno, S., et al., *Mesenchymal stem cell-derived microvesicles protect against acute tubular injury.* J Am Soc Nephrol, 2009. **20**(5): p. 1053-67.

29. Alzahrani, F.A., *Melatonin improves therapeutic potential of mesenchymal stem cells-derived exosomes against renal ischemia-reperfusion injury in rats.* Am J Transl Res, 2019. **11**(5): p. 2887-2907.

30. Bruno, S., et al., *Microvesicles derived from mesenchymal stem cells enhance survival in a lethal model of acute kidney injury.* PLoS.One., 2012. **7**(3): p. e33115.

31. Grange, C., et al., *Stem cell-derived extracellular vesicles inhibit and revert fibrosis progression in a mouse model of diabetic nephropathy.* Sci.Rep., 2019. **9**(1): p. 4468.

32. He, J., et al., *Bone marrow stem cells-derived microvesicles protect against renal injury in the mouse remnant kidney model.* Nephrology (Carlton), 2012. **17**(5): p. 493-500.

33. He, J., et al., *Micro-vesicles derived from bone marrow stem cells protect the kidney both in vivo and in vitro by microRNA-dependent repairing.* Nephrology.(Carlton.), 2015. **20**(9): p. 591-600.

34. Herrera, M.B., et al., *Isolation and characterization of a stem cell population from adult human liver.* Stem Cells, 2006. **24**(12): p. 2840-50.

35. Herrera, M.B., et al., *Human liver stem cells improve liver injury in a model of fulminant liver failure.* Hepatology, 2013. **57**(1): p. 311-9.

36. Herrera Sanchez, M.B., et al., *Human liver stem cells and derived extracellular vesicles improve recovery in a murine model of acute kidney injury.* Stem Cell Res Ther, 2014. **5**(6): p. 124.

37. Grimwood, L. and R. Masterson, *Propagation and culture of renal fibroblasts.* Methods Mol Biol, 2009. **466**: p. 25-37.

38. Strutz, F., et al., *Identification and characterization of a fibroblast marker: FSP1.* J Cell Biol, 1995. **130**(2): p. 393-405.

39. Kowal, J., et al., *Proteomic comparison defines novel markers to characterize heterogeneous populations of extracellular vesicle subtypes.* Proc Natl Acad Sci U S A, 2016. **113**(8): p. E968-77.

40. Herrera Sanchez, M.B., et al., *Extracellular vesicles from human liver stem cells restore argininosuccinate synthase deficiency.* Stem Cell Res Ther, 2017. **8**(1): p. 176.

41. Schneider, C.A., W.S. Rasband, and K.W. Eliceiri, *NIH Image to ImageJ: 25 years of image analysis.* Nat.Methods, 2012. **9**(7): p. 671-675.

42. Dweep, H., N. Gretz, and C. Sticht, *miRWalk database for miRNA-target interactions.* Methods Mol Biol., 2014. **1182**: p. 289-305.

43. Thomas, P.D., et al., *PANTHER: a library of protein families and subfamilies indexed by function.* Genome Res, 2003. **13**(9): p. 2129-2141.

44. Koliha, N., et al., *A novel multiplex bead-based platform highlights the diversity of extracellular vesicles.* J.Extracell.Vesicles., 2016. **5**: p. 29975.

45. Wiklander, O.P.B., et al., *Systematic Methodological Evaluation of a Multiplex Bead-Based Flow Cytometry Assay for Detection of Extracellular Vesicle Surface Signatures.* Front Immunol., 2018. **9**: p. 1326.

46. Chung, A.C. and H.Y. Lan, *MicroRNAs in renal fibrosis.* Front Physiol, 2015. **6**: p. 50.

47. Ratajczak, J., et al., *Embryonic stem cell-derived microvesicles reprogram hematopoietic progenitors: evidence for horizontal transfer of mRNA and protein delivery.* Leukemia, 2006. **20**(5): p. 847-856.

48. Deregibus, M.C., et al., *Endothelial progenitor cell derived microvesicles activate an angiogenic program in endothelial cells by a horizontal transfer of mRNA.* Blood, 2007. **110**(7): p. 2440-2448.

49. Eirin, A., et al., *Mesenchymal stem cell-derived extracellular vesicles attenuate kidney inflammation.* Kidney Int, 2017. **92**(1): p. 114-124.

50. Jiang, Z.Z., et al., *Exosomes secreted by human urine-derived stem cells could prevent kidney complications from type I diabetes in rats.* Stem Cell Res Ther, 2016. **7**: p. 24.

51. Nagaishi, K., et al., *Mesenchymal stem cell therapy ameliorates diabetic nephropathy via the paracrine effect of renal trophic factors including exosomes.* Sci.Rep., 2016. **6**: p. 34842.

52. Zhou, L., et al., *Mechanism of chronic aristolochic acid nephropathy: role of Smad3.* Am.J.Physiol Renal Physiol, 2010. **298**(4): p. F1006-F1017.

53. Huang, L., et al., *Development of a chronic kidney disease model in C57BL/6 mice with relevance to human pathology.* Nephron Extra., 2013. **3**(1): p. 12-29.

54. Yuan, S.Y., et al., *Comparative nephrotoxicity of aristolochic acid and tetrandrine in vitro and in vivo.* Int J.Toxicol., 2011. **30**(1): p. 35-46.

55. Black, L.M., J.M. Lever, and A. Agarwal, *Renal Inflammation and Fibrosis: A Double-edged Sword.* J.Histochem.Cytochem., 2019. **67**(9): p. 663-681.

56. Lo, S.H., et al., *Aristolochic acid nephropathy complicating a patient with focal segmental glomerulosclerosis.* Nephrol.Dial.Transplant., 2004. **19**(7): p. 1913-1915.

57. Yang, L., X. Li, and H. Wang, *Possible mechanisms explaining the tendency towards interstitial fibrosis in aristolochic acid-induced acute tubular necrosis.* Nephrol.Dial.Transplant., 2007. **22**(2): p. 445-456.

58. Yang, L., et al., *Aristolochic acid nephropathy: variation in presentation and prognosis.* Nephrol.Dial.Transplant., 2012. **27**(1): p. 292-298.

59. Sato, Y. and M. Yanagita, *Resident fibroblasts in the kidney: a major driver of fibrosis and inflammation.* Inflamm.Regen., 2017. **37**: p. 17.

60. Pozdzik, A.A., et al., *Aristolochic acid induces proximal tubule apoptosis and epithelial to mesenchymal transformation.* Kidney Int, 2008. **73**(5): p. 595-607.

61. Shultz, L.D., et al., *Human lymphoid and myeloid cell development in NOD/LtSz-scid IL2R gamma null mice engrafted with mobilized human hemopoietic stem cells.* J Immunol, 2005. **174**(10): p. 6477-89.

62. Kholia, S., et al., *Human Liver Stem Cell-Derived Extracellular Vesicles Prevent Aristolochic Acid-Induced Kidney Fibrosis.* Front Immunol., 2018. **9**: p. 1639.

63. Pozdzik, A.A., et al., *Patterns of interstitial inflammation during the evolution of renal injury in experimental aristolochic acid nephropathy.* Nephrol.Dial.Transplant., 2008. **23**(8): p. 2480-2491.

64. Wang, Y., et al., *TGF-beta1/Smad7 signaling stimulates renal tubulointerstitial fibrosis induced by AAI.* J.Recept.Signal.Transduct.Res, 2008. **28**(4): p. 413-428.

65. Ignarski, M., R. Islam, and R.U. Muller, *Long Non-Coding RNAs in Kidney Disease.* Int J.Mol Sci., 2019. **20**(13).

66. Trionfini, P., A. Benigni, and G. Remuzzi, *MicroRNAs in kidney physiology and disease.* Nat.Rev.Nephrol., 2015. **11**(1): p. 23-33.

67. Thum, T., et al., *MicroRNA-21 contributes to myocardial disease by stimulating MAP kinase signalling in fibroblasts.* Nature, 2008. **456**(7224): p. 980-984.

68. Liu, G., et al., *miR-21 mediates fibrogenic activation of pulmonary fibroblasts and lung fibrosis.* J.Exp.Med., 2010. **207**(8): p. 1589-1597.

69. Denby, L., et al., *miR-21 and miR-214 are consistently modulated during renal injury in rodent models.* Am.J.Pathol., 2011. **179**(2): p. 661-672.

70. Zhou, Y., et al., *Secreted fibroblast-derived miR-34a induces tubular cell apoptosis in fibrotic kidney.* J.Cell Sci., 2014. **127**(Pt 20): p. 4494-4506.

71. Bijkerk, R., et al., *Silencing of microRNA-132 reduces renal fibrosis by selectively inhibiting myofibroblast proliferation.* Kidney Int, 2016. **89**(6): p. 1268-1280.

72. Denby, L., et al., *MicroRNA-214 antagonism protects against renal fibrosis.* J.Am.Soc.Nephrol., 2014. **25**(1): p. 65-80.

73. Liu, Y., et al., *MicroRNA-34a Promotes Renal Fibrosis by Downregulation of Klotho in Tubular Epithelial Cells.* Mol Ther, 2019. **27**(5): p. 1051-1065.

74. Collino, F., et al., *AKI Recovery Induced by Mesenchymal Stromal Cell-Derived Extracellular Vesicles Carrying MicroRNAs.* J Am Soc Nephrol, 2015. **26**(10): p. 2349-60.

75. Collino, F., et al., *Exosome and Microvesicle-Enriched Fractions Isolated from Mesenchymal Stem Cells by Gradient Separation Showed Different Molecular Signatures and Functions on Renal Tubular Epithelial Cells.* Stem Cell Rev Rep, 2017. **13**(2): p. 226-243.

76. Zhou, Y., et al., *Exosomes released by human umbilical cord mesenchymal stem cells protect against cisplatin-induced renal oxidative stress and apoptosis in vivo and in vitro.* Stem Cell Res Ther, 2013. **4**(2): p. 34.

77. Burger, D., et al., *Human endothelial colony-forming cells protect against acute kidney injury: role of exosomes.* Am J Pathol, 2015. **185**(8): p. 2309-23.

78. Grange, C., C. Iampietro, and B. Bussolati, *Stem cell extracellular vesicles and kidney injury.* Stem Cell Investig, 2017. **4**: p. 90.

79. Gatti, S., et al., *Microvesicles derived from human adult mesenchymal stem cells protect against ischaemia-reperfusion-induced acute and*

chronic kidney injury. Nephrol Dial Transplant, 2011. **26**(5): p. 1474-83.

80. Zou, X., et al., *Microvesicles derived from human Wharton's Jelly mesenchymal stromal cells ameliorate renal ischemia-reperfusion injury in rats by suppressing CX3CL1.* Stem Cell Res Ther, 2014. **5**(2): p. 40.

81. Nagaishi, K., et al., *Mesenchymal stem cell therapy ameliorates diabetic nephropathy via the paracrine effect of renal trophic factors including exosomes.* Sci Rep, 2016. **6**: p. 34842.

82. Decleves, A.E., et al., *Protective effect of nitric oxide in aristolochic acid-induced toxic acute kidney injury: an old friend with new assets.* Exp Physiol, 2016. **101**(1): p. 193-206.

83. Depierreux, M., et al., *Pathologic aspects of a newly described nephropathy related to the prolonged use of Chinese herbs.* Am J Kidney Dis, 1994. **24**(2): p. 172-80.

84. Pozdzik, A.A., et al., *Aristolochic acid nephropathy revisited: a place for innate and adaptive immunity?* Histopathology, 2010. **56**(4): p. 449-63.

85. Huang, L., et al., *Development of a chronic kidney disease model in C57BL/6 mice with relevance to human pathology.* Nephron Extra, 2013. **3**(1): p. 12-29.

86. Debelle, F.D., et al., *Aristolochic acids induce chronic renal failure with interstitial fibrosis in salt-depleted rats.* J Am Soc Nephrol, 2002. **13**(2): p. 431-6.

87. Debelle, F.D., J.L. Vanherweghem, and J.L. Nortier, *Aristolochic acid nephropathy: a worldwide problem.* Kidney Int, 2008. **74**(2): p. 158-69.

88. Wang, Y., et al., *TGF-beta1/Smad7 signaling stimulates renal tubulointerstitial fibrosis induced by AAI.* J Recept Signal Transduct Res, 2008. **28**(4): p. 413-28.

89. Moore, B.B., et al., *The role of CCL12 in the recruitment of fibrocytes and lung fibrosis.* Am J Respir Cell Mol Biol, 2006. **35**(2): p. 175-81.

90. Kitagawa, K., et al., *Blockade of CCR2 ameliorates progressive fibrosis in kidney.* Am J Pathol, 2004. **165**(1): p. 237-46.

91. Simon-Tillaux, N. and A. Hertig, *Snail and kidney fibrosis.* Nephrol Dial Transplant, 2017. **32**(2): p. 224-233.

92. Ohnuki, K., et al., *Expression of transcription factor Snai1 and tubulointerstitial fibrosis in progressive nephropathy.* J Nephrol, 2012. **25**(2): p. 233-9.

93. Schlotzer-Schrehardt, U., et al., *Role of transforming growth factor-beta1 and its latent form binding protein in pseudoexfoliation syndrome.* Exp Eye Res, 2001. **73**(6): p. 765-80.

94. Lepparanta, O., et al., *Regulation of TGF-beta storage and activation in the human idiopathic pulmonary fibrosis lung.* Cell Tissue Res, 2012. **348**(3): p. 491-503.

95. O'Reilly, S., *MicroRNAs in fibrosis: opportunities and challenges.* Arthritis Res Ther, 2016. **18**: p. 11.

96. Lee, S.B. and R. Kalluri, *Mechanistic connection between inflammation and fibrosis.* Kidney Int Suppl, 2010(119): p. S22-6.

97. Liu, M., et al., *Signalling pathways involved in hypoxia-induced renal fibrosis.* J Cell Mol Med, 2017. **21**(7): p. 1248-1259.

98. Dai, C., et al., *Wnt/beta-catenin signaling promotes podocyte dysfunction and albuminuria.* J Am Soc Nephrol, 2009. **20**(9): p. 1997-2008.

99. Surendran, K., S. Schiavi, and K.A. Hruska, *Wnt-dependent beta-catenin signaling is activated after unilateral ureteral obstruction, and recombinant secreted frizzled-related protein 4 alters the progression of renal fibrosis.* J Am Soc Nephrol, 2005. **16**(8): p. 2373-84.

100. Cao, H., et al., *Inhibition of Wnt/beta-catenin signaling suppresses myofibroblast differentiation of lung resident mesenchymal stem cells and pulmonary fibrosis.* Sci Rep, 2018. **8**(1): p. 13644.

101. Jeon, K.I., et al., *Antifibrotic Actions of Peroxisome Proliferator-Activated Receptor gamma Ligands in Corneal Fibroblasts Are Mediated by beta-Catenin-Regulated Pathways.* Am J Pathol, 2017. **187**(8): p. 1660-1669.

102. O'Brien, J., et al., *Overview of MicroRNA Biogenesis, Mechanisms of Actions, and Circulation.* Front Endocrinol (Lausanne), 2018. **9**: p. 402.

103. Sakuma, H., et al., *Potential Targeting of Renal Fibrosis in Diabetic Kidney Disease Using MicroRNAs.* Front Pharmacol, 2020. **11**: p. 587689.

104. Kriegel, A.J., et al., *The miR-29 family: genomics, cell biology, and relevance to renal and cardiovascular injury.* Physiol Genomics, 2012. **44**(4): p. 237-44.

105. Xiao, J., et al., *miR-29 inhibits bleomycin-induced pulmonary fibrosis in mice.* Mol Ther, 2012. **20**(6): p. 1251-60.

106. Qin, W., et al., *TGF-beta/Smad3 signaling promotes renal fibrosis by inhibiting miR-29.* J Am Soc Nephrol, 2011. **22**(8): p. 1462-74.

107. Fan, Y., et al., *Emerging role of miRNAs in renal fibrosis.* RNA Biol, 2020. **17**(1): p. 1-12.

108. Huang, H., et al., *The MicroRNA MiR-29c Alleviates Renal Fibrosis via TPM1-Mediated Suppression of the Wnt/beta-Catenin Pathway.* Front Physiol, 2020. **11**: p. 331.